Novel Neural Interfaces For Upper-Limb Motor Rehabilitation After Stroke

Dissertation

zur Erlangung des Grades eines
Doktors der Naturwissenschaften

der Mathematisch-Naturwissenschaftlichen Fakultät
und
der Medizinischen Fakultät
der Eberhard-Karls-Universität Tübingen

vorgelegt
von

Andrea Sarasola Sanz

aus San Sebastian, Spanien
März - 2019

Tag der mündlichen Prüfung	3. Juni 2019
Dekan der Math.-Nat. Fakultät:	Prof. Dr. W. Rosenstiel
Dekan der Medizinischen Fakultät:	Prof. Dr. I. B. Autenrieth
1. Berichterstatter:	Prof. Dr. Dr. hc. mult. Niels Birbaumer
2. Berichterstatter:	Prof. Dr. Ulf Ziemann
Prüfungskommission:	Prof. Dr. Dr. hc. mult. Niels Birbaumer Prof. Dr. Ulf Ziemann Prof. Dr. Christoph Braun Prof. Dr. Martin Giese

I hereby declare that I have produced the work entitled: **"Novel neural interfaces for upper-limb motor rehabilitation after stroke"**, submitted for the award of a doctorate, on my own (without external help), have used only the sources and aids indicated and have marked passages included from other works, whether verbatim or in content, as such. I swear upon oath that these statements are true and that I have not concealed anything. I am aware that making a false declaration under oath is punishable by a term of imprisonment of up to three years or by a fine.

City, Date	Signature

To my parents Ama and Aita, my sister Lucia, my "Tübingen family",
and my adventure partner David Lee

Acknowledgments

I would like to thank Dr. Ander Ramos-Murguialday and Prof. Niels Birbaumer for inviting me to join his lab, for introducing me into this exciting field of research and for teaching me so many valuable things for my professional career. Thanks a lot for all the opportunities, hours, help and advice you have given to me.

I thank my closest colleague and friend Nerea Irastorza Landa for being so patient with me, for all the great moments we have shared in and out of the lab and especially, for all those extremely useful hints to improve my awful presentations. I wouldn't have achieved this goal without your unconditional help and support. I would also like to thank my colleagues at the Institute, who have helped me move forward on this long PhD path. Especial thanks to Eduardo Lopez Larraz, Andreas Ray and Farid Shiman.

I would also like to thank all my friends in Tübingen for becoming my second family. Thanks for all those fun "jumping nights" and amazing times that made the intense PhD life much easier and memorable.

Very special thanks to my Aita, my Ama and my sister Lucia for their true love, support and advice. Thank you so much for being always "there" for me. I couldn't be more grateful to have this family.

Last but not least, I would like to thank my very special friend David Lee Butkiewicus for walking together with me along this path, for his encouragement and deep love, for opening my mind and making me grow personally. Thanks a lot for this unforgettable adventure, Dave!

List of abbreviations

MI	Myoelectric interface
BMI	Brain-machine interface
hBMI	Hybrid brain-machine interface
EMG	Electromyography
EEG	Electroencephalography
DoF	Degree of freedom
CNS	Central nervous system

Abstract

Stroke is the third most common cause of death and the main cause of acquired adult disability in developed countries. The most common consequence of stroke is motor impairment, which becomes chronic in 56% of stroke survivors. However, reorganization of brain networks can occur in response to sensory input, experience and learning. Although several post-stroke neurorehabilitation techniques have been investigated, there is no standardized therapy for severely impaired chronic stroke patients except for brain-machine interfaces (BMIs), which have shown positive results but still fail to elicit full motor function restoration. This work presents novel neural interfaces that aim to improve the existing rehabilitation therapies and to offer an alternative treatment to severely paralyzed stroke patients. First, we propose a novel myoelectric interface (MI) that is calibrated with electromyographic (EMG) data from the healthy limb, mirrored and used as a reference model for the paretic arm in order to reshape the pathological muscle synergy organization of stroke patients. A 4-session motor training with this mirror MI sufficed to induce motor learning in 10 healthy participants, suggesting that it might be a potential tool for the correction of maladaptive muscle activations and by extension, for the subsequent motor rehabilitation after stroke. Second, although significant positive results have been achieved with non-invasive BMIs based on electroencephalographic (EEG) activity, the functional motor recovery induced by such therapies still remains modest mainly due to poor decoding performance. Here, we explored the possibility of using novel algorithms to increase the performance of multi-class EEG-decoding of movements from the same limb, showing encouraging but still limited results. Finally, we propose integrating the novel mirror MI into a cortico-muscular hybrid BMI that combines brain and residual muscle activity to increase decoding accuracy and hence, allow a more natural and dexterous control of the interface, facilitating neuroplasticity and motor recovery. The system was validated in a healthy participant and a stroke patient, setting the premise for its application in a clinical setup.

Keywords: Chronic stroke, motor rehabilitation, neural interfaces, MI, BMI, hBMI.

Contents

Acknowledgements iv
List of abbreviations v
Abstract vi

1 Synopsis **1**
1.1 Introduction 1
1.1.1 Motor impairment as a consequence of stroke 1
1.1.2 Neuroplasticity and neurorehabilitation 2
1.1.3 Neural interfaces for upper-limb motor rehabilitation after stroke 4
1.2 Objectives 9
1.3 Results and Discussion 11
1.3.1 Myoelectric interfaces 11
1.3.2 Brain-machine interfaces 14
1.3.3 Hybrid brain-machine interfaces 15
1.4 Conclusions 17
1.5 Outlook 19
1.6 List of papers 21
1.7 Statement of Contributions 23
1.7.1 EMG-based multi-joint kinematics decoding for robot-aided rehabilitation therapies 23
1.7.2 Design and effectiveness evaluation of mirror myoelectric interfaces: a novel method to restore movement in hemiplegic patients 24
1.7.3 Motor learning with a multi-degree-of-freedom mirror myoelectric interface during functional task training 25
1.7.4 An EEG-based brain-machine interface to control a 7-degrees of freedom exoskeleton for stroke rehabilitation 26
1.7.5 Classification of different reaching movements from the same limb using EEG 27

1.7.6 A Hybrid Brain-Machine Interface based on EEG and EMG activity for the Motor Rehabilitation of Stroke Patients . . . 28

2 Chapter 2: EMG-based multi-joint kinematics decoding for robot-aided rehabilitation therapies 29
2.1 Abstract . . . 29
2.2 Introduction . . . 30
2.3 Methods . . . 31
2.3.1 Experimental Protocol . . . 31
2.3.2 Data Collection . . . 33
2.3.3 Data processing . . . 34
2.3.4 Algorithms . . . 34
2.3.5 Decoding schemes . . . 36
2.3.6 Cross-validation . . . 36
2.3.7 Performance evaluation . . . 37
2.4 Results . . . 38
2.5 Discussion . . . 40
2.6 Conclusion . . . 42
2.7 Acknowledgements . . . 43

3 Chapter 3: Design and effectiveness evaluation of mirror myoelectric interfaces: a novel method to restore movement in hemiplegic patients 44
3.1 Abstract . . . 44
3.2 Introduction . . . 45
3.3 Methods . . . 48
3.3.1 Novel rehabilitation paradigm . . . 48
3.3.2 Study design . . . 49
3.3.3 Experimental Protocol . . . 51
3.3.4 Healthy participants . . . 54
3.3.5 Stroke patients . . . 55
3.3.6 Data collection and processing . . . 55
3.3.7 Decoding schemes and algorithm . . . 57
3.3.8 Statistics . . . 59
3.4 Results . . . 60
3.5 Discussion . . . 65
3.6 Acknowledgements . . . 69

4 Chapter 4: Motor learning with a multi-degree-of-freedom mirror myoelectric interface during functional task training 70
4.1 Abstract . . . 70

4.2 Introduction . . . 71
4.3 Methods . . . 73
4.3.1 Subjects . . . 73
4.3.2 Experimental setup and protocol . . . 73
4.3.3 Data acquisition and processing . . . 77
4.3.4 Feature extraction and decoder calibration . . . 77
4.3.5 Myoelectric control paradigm . . . 78
4.3.6 Performance metrics . . . 79
4.3.7 Analyses . . . 80
4.4 Results . . . 83
4.5 Discussion . . . 89
4.6 Acknowledgements . . . 93
4.7 Supplementary material . . . 93

5 Chapter 5: An EEG-based brain-machine interface to control a 7-degrees of freedom exoskeleton for stroke rehabilitation 96
5.1 Abstract . . . 96
5.2 Introduction . . . 96
5.3 Methods . . . 97
5.3.1 Experimental protocol . . . 97
5.3.2 Data collection and processing . . . 98
5.3.3 Real-time decoding and operation of the exoskeleton . . . 99
5.4 Results . . . 100
5.5 Discussion and conclusions . . . 100

6 Chapter 6: Classification of different reaching movements from the same limb using EEG 102
6.1 Abstract . . . 102
6.2 Introduction . . . 103
6.3 Materials and Methods . . . 106
6.3.1 Participants . . . 106
6.3.2 Experimental Setup . . . 106
6.3.3 IS-MORE Robotic Exoskeleton . . . 106
6.3.4 Experimental Paradigm . . . 107
6.3.5 Data acquisition . . . 108
6.3.6 Data Analysis . . . 108
6.4 Results . . . 115
6.5 Discussion . . . 120
6.6 Conclusion . . . 125
6.7 Acknowledgements . . . 125

7 Chapter 7: A Hybrid Brain-Machine Interface based on EEG and EMG activity for the Motor Rehabilitation of Stroke Patients 126
7.1 Abstract . . . 126
7.2 Introduction . . . 127
7.3 Methods . . . 128
7.3.1 Experimental design . . . 128
7.3.2 Data acquisition and processing . . . 131
7.3.3 hBMI calibration . . . 132
7.3.4 hBMI operation . . . 133
7.3.5 Performance evaluation . . . 134
7.4 Results . . . 136
7.5 Discussion . . . 139
7.6 Conclusion . . . 141
7.7 Acknowledgements . . . 141

8 References 142

1. Synopsis

1.1 Introduction

1.1.1 Motor impairment as a consequence of stroke

Stroke is the third most common cause of death and the main cause of acquired adult disability in developed countries [1]. The World Health Organization (WHO) states that the incidence of stroke worldwide is around 200 cases per 100.000 inhabitants/year, although this value varies across countries [2]. A stroke occurs when the blood flow to the brain is interrupted because a blood vessel is blocked by a clot (ischemic) or because it bursts (hemorrhagic). As a result, there is a cutoff of nutrients and oxygen to the brain that can cause the death of brain cells.

The effects of stroke are various and depend mainly on the location and severity of the damage. Among the survivors, the most common consequence of stroke is motor impairment due to an injury in the motor cortex, premotor cortex, motor tracts or related tracks in the cerebellum and cerebrum. It can be explained as a loss or limitation of movement control that typically affects the extremities on the side opposite to the injured hemisphere. From all stroke survivors showing no active upper limb motion at hospital admission, 14% show complete recovery, 30% show partial recovery and 56% show no recovery, but the grand majority retain sensory function [3].

Spasticity, which is increased, involuntary and uncontrolled muscle tone that especially affects flexor muscles, represents one of the handicaps that stroke patients need to overcome in order to produce the desired movements. Hence, most impaired muscles can usually elicit, if any, very weak or uncontrolled (spastic)

electromyographic (EMG) activity. In addition, movement dysfunction in chronic (minimum of six months after stroke) stroke patients is often characterized by abnormal patterns of muscle activations or muscle synergies [4–6], which may result from maladaptive compensatory strategies and are thought to be encoded at the spinal or brainstem level [7–10]. After stroke, cortical damage interferes with the flow of descending signals to the spinal cord, which leads to the creation of abnormal patterns of muscle activations. It has been found that the preservation of muscle synergies has a positive correlation with hand functionality in severely paralyzed patients with intact sensorimotor cortex and only subcortical lesions [5]. It follows that this abnormal movement coordination might constitute the primary source of movement dysfunction (spasticity and muscle weakness being secondary [11]) and that the recovery of normal synergies may be to some extent, linked to the improvement of the upper limb motor function. Therefore, voluntary muscle contraction and relaxation in chronic severely impaired patients is either not feasible or accompanied by abnormal muscle synergies. These factors lead to a reduction in the muscle use, to muscle atrophy and to abnormal attitudes of the limbs such as the "claw hand" or the "foot drop".

Since most of the chronic stroke patients are not able to perform activities of daily living by themselves, they require the assistance of a caregiver or a family member. This affects the quality of life of patients and their families and their integration in society, and entails a serious global health-care problem due to the high costs associated to life-time care. Therefore, several stroke rehabilitation strategies for the upper limb have been investigated that attempt to achieve the recovery of the lost motor function by inducing neuroplastic changes.

1.1.2 Neuroplasticity and neurorehabilitation

Neuroplasticity refers to the ability of the brain and other parts of the central nervous system (CNS) to reorganize themselves and encompasses both structural and functional changes. Among others, well-known Hebbian mechanisms, initiated by coincident activation of presynaptic and postsynaptic neurons, might play a fundamental role in generating activity-dependent plasticity. More specifically, neuroplastic changes involve the alteration and/or creation of new synapses, the

sprouting of dendrites and the production of neurochemicals, which are necessary to create compensatory circuits that allow regaining the lost motor function [12]. Motor recovery is associated with the recruitment of intact cortical motor structures adjacent to the injury, which generate commands to the compromised muscles that are relevant for the task [13]. This implies certain redundancy in regions of the motor cortex and the uncovering of pre-existing cortico-cortical connections [14]. It has been demonstrated that this reorganization of brain networks occurs in response to sensory input, experience and learning [15]. Hence, most of the motor therapies designed for rehabilitation are based on motor learning principles.

Physical therapy is the traditionally accepted method of rehabilitation for chronic stroke patients. Methods such as mirror therapy and constraint induced movement therapy have also been extensively used to complement traditional physiotherapy. However, there is evidence suggesting that the more repetitive, intensive and engaging the practice the greater the induced plastic changes and the longer the retention and generalization of the learned skills [13,16]. As a result, in the last decade post stroke neurorehabilitation therapies have turned the focus towards the use of robots that enable repetitive and intensive training, requiring less time and effort from clinicians.

Many upper-limb robots (e.g., the MIT-MANUS, the ARM-GUIDE, the MIME, the InMotion Shoulder-Elbow Robot) have been tested in randomized clinical trials [17–22]. The most commonly used paradigms to control such devices have been: passive, in which the robot moves the paretic arm of the patient; active-assistive, in which the patient has to actively try to perform the movement while the robot provides the patient with "assistance as needed"; active-resistive, in which the robot exerts resistance to the patient′s movement; and bilateral, in which the healthy arm motion is mirrored to move the paretic arm in a symmetric fashion.

Although the results from these studies suggest that robot-assisted therapies may improve motor control [22,23], there is not consistent evidence of the positive effect on functional abilities (i.e. ability to perform a movement or activity) and neither of the long-term effects of such therapies [24]. Moreover, most severely

affected stroke patients are not eligible for these rehabilitation therapies, as they lack residual movement of the upper-limb. These limitations opened the way for the development of alternative neurorehabilitation therapies based on residual EMG activity, such as myoelectric interfaces (MIs) or brain activity, such as brain-machine interfaces (BMIs).

1.1.3 Neural interfaces for upper-limb motor rehabilitation after stroke

Recovery of the motor function after stroke requires reorganization of the motor structures of the CNS through neuroplastic changes. These changes can be artificially facilitated by using three stimulation paradigms: repetitive stimulation, paired stimulation, and closed-loop stimulation [25]. Neural interfaces are optimal tools to implement a closed-loop stimulation paradigm that associates volition and action, exciting the motor network and reinforcing its synaptic connections. More specifically, neural interfaces such as MIs or BMIs record, decode and translate muscle or brain activity into an effector action. For instance, the information decoded from the muscle or brain activity while the patients are trying to move their paretic limb, can be translated into control commands to a robotic or prosthetic device that moves their paralyzed limb, exciting their afferent pathways. Therefore, these neural interfaces establish a consistent timing of the afferent feedback relative to the efferent electrophysiological signals, inducing Hebbian plasticity and by extension, eliciting motor function restoration. Additionally, unlike many other therapies that require residual movement in the affected arm, one of the advantages of MIs and BMIs is that they can be used by completely paralyzed patients or by patients with decodable residual EMG that is not strong enough to elicit any movement.

Myoelectric interfaces

EMG activity has been recently proposed as an assessment tool to provide a more objective and finer measurement of the patient′s motor function than standard clinical scales such as Fugl-Meyer [26], Wolf test [27], Action Research Arm

Test (ARAT) [28], Motor Activity Log (MAL) [29], Ashworth test [30] and Goal Attainment Scaling [31]. Furthermore, EMG has been extensively explored for the control of prostheses, rehabilitation exoskeletons or functional electrical stimulation systems, as it provides a direct measurement of the user′s motion intention.

Myoelectric interfaces (MIs) are systems that decode the motion intention of patients from the electromyographic (EMG) signal of their paretic limb and send control commands to a body actuator (e.g., wearable robot or prosthesis) attached to their impaired limb to reproduce the decoded movement. MIs can impose a persistent causal relationship between presynaptic and postsynaptic activity by timing the visual and proprioceptive stimulation from the body actuator at one site relative to endogenous muscle activity recorded and decoded at a second site.

Among the existing control strategies, the simplest ones use threshold-based or proportional controllers that trigger a predefined movement when the EMG activity amplitude reaches certain values. More complex myoelectric control paradigms have been implemented by decoding the movement intention of the patient from EMG signals with an algorithm based on classification or continuous trajectory-decoding techniques. This however, raises the question of whether it is possible to accurately decode the EMG activity of hemiplegic patients of any impairment level. Previous studies reported a decoding accuracy between 36.7% and 96.1% with 4-20 movement classes using the EMG of the paretic upper limb in mild to severely impaired stroke patients [32–34]. Recently, in a study by Ramos-Murguialday et al. that included 41 severe stroke patients, decodable EMG activity (accuracy >65%) was found in 46% of the enrolled patients, even in the absence of movement of the paretic arm [35]. These results suggest that rehabilitation techniques based on EMG-decoding could be applicable even to a good amount of severely affected stroke patients, who cannot benefit from many other rehabilitation techniques, in which minimal movement of the paretic limb is necessary.

Classification techniques have been largely investigated for post-stroke rehabilitation showing encouraging but still limited results [32–34, 36]. On the other hand, continuous trajectory-decoding strategies offer a more intuitive, natural and

finer myoelectric control and thus, a better training [37–46]. However, most of these studies are limited to healthy participants or to the simultaneous control of up to 3 degrees of freedom (DoFs) of a cursor on a screen [44], a virtual reality interface [43] or a simple wrist or shoulder exoskeleton [45]. This prevents the training of functional movements involving proximal (shoulder and elbow) and distal joints (wrist and fingers) of the upper limb simultaneously, which has been demonstrated to be a potential rehabilitation strategy for stroke patients, since the activation of the less affected proximal muscles could facilitate the activation of the more compromised distal muscles [47].

Myoelectric training paradigms for rehabilitation aim at activating neuroplastic mechanisms that reshape the pathological muscle activity present in most chronic stroke patients leading to motor learning and eventually, to motor function restoration. However, it could be argued that using a myoelectric decoder calibrated with paretic EMG data (i.e. an ipsilateral myoelectric decoder), could indeed reinforce the existence and maintenance of pathological muscle synergies (i.e. promote "bad" neuroplasticity). Cesqui et al. [34] tackled this problem by building a model of healthy muscle patterns from data collected on 9 healthy participants and using it to classify the paretic EMG of stroke patients into reaching movements towards 4 different positions. Although this is the only approach designed to enhance the recovery of healthy muscle activations, it is limited by: i) the necessity of forming a large database of EMG activity from healthy subjects to generalize to the specific anatomical and neurophysiological characteristics of each patient, and ii) the fact that the decoder was confined to the classification of the EMG activity into four discrete movements, involving only proximal joints. Therefore, the development of a MI that can offer dexterous control of a multi-DoF body actuator while correcting the pathological muscle synergy structure of stroke patients is the next step to be taken.

Brain-machine interfaces

Brain-machine interfaces (BMIs) for stroke rehabilitation are systems that measure and decode the brain activity related to motor intention and bypass the lesion

by translating this intention into the real movement of the patient′s paretic limb through a body actuator. This enables patients to generate volitional movement through the normal cortico-spinal pathways and provides them with contingent feedback (e.g., proprioceptive and visual feedback) about their neural activations, hence establishing a closed-loop system that promotes learning.

Brain electrophysiological activity can be recorded with non-invasive techniques (e.g., electroencephalography (EEG), magnetoencephalography (MEG)) or invasive techniques (e.g., electrocorticography (ECoG) and intracortical arrays). Non-invasive recordings are lower cost and safer than invasive signals while the latter are much more precise and offer higher resolution, and therefore, more dexterous BMI control in more DoFs simultaneously.

From the first BMI study in which Birbaumer et al. [48] effectively linked brain information acquired through EEG with functional electrical stimulation of the muscles, several studies have explored the use of non-invasive BMIs for stroke rehabilitation showing positive results. Ramos-Murguialday and colleagues [49] demonstrated that contingently pairing the efferent motion intention decoded from EEG activity with the afferent visual and proprioceptive feedback provided by the movement of an orthosis could lead to partial motor recovery in severely impaired chronic stroke patients. This study has been successfully replicated demonstrating the potential of non-invasive BMIs for neurorehabilitation, even in the chronic state [50, 51]. Nevertheless, although progress has been recently made in the classification of different motor tasks from EEG activity [52, 53], non-invasive BMI performance is still far from providing natural and skilled control.

Invasive BMIs have been widely used to investigate neuroprosthetic control and motor learning in primates. It was demonstrated that primates can achieve skillful control of a BMI with intracortical neural activity and that this learning reshapes cortical networks producing larger scale modifications in the primate brain [54, 55]. Invasive BMIs have been recently used in human studies as assistive technologies [56–58] and are currently being explored for rehabilitation applications, as they can offer more natural, intuitive and skillful control over more DoFs,

therefore boosting the potential of traditional non-invasive BMIs to elicit motor rehabilitation.

Hybrid brain-machine interfaces as optimized tools for motor recovery

Although even severely impaired patients can achieve skillful control of BMI systems [49, 50, 59, 60], big improvements are still needed in order to evoke clear positive functional outcomes in stroke rehabilitation. The inclusion of additional non-physiological information such as kinematics, may improve BMI performance. However, kinematic signals are not a direct link to the nervous system and might be less efficient producing functional neuroplasticity in a rehabilitative framework. On the other hand, EMG can offer valuable additional information of the motion intention of patients, as demonstrated in MI studies. However, factors such as muscle fatigue or the absence of residual EMG in patients with high severity levels hinder the rehabilitative potential of MIs.

Combining BMI technology with supplementary information from EMG activity of the muscles has led to the formulation of optimized BMIs referred to as cortico-muscular hybrid BMIs (hBMIs). Cortico-muscular hBMIs integrate brain and muscle activity as input control signals achieving higher decoding accuracy [61–66] over more DoFs [67] than BMIs or MIs alone and thus, allowing a richer and smoother control that involves central and peripheral structures of the nervous system. Therefore, hBMIs build on the advantages and alleviate the limitations of BMIs and MIs, boosting the rehabilitation potential of neural interfaces.

The method to integrate brain and EMG signals in the control of a body actuator varies among applications and is not trivial, as patients could tend to rely only on one type of signal to control the interface if the integration formula was not appropriately defined. Little research has been done about the way both input signals should be processed (e.g., sequentially, simultaneously) and fused (e.g., Bayesian algorithms, equally balanced weights to both inputs), and further investigation is needed to find optimal hybrid control strategies for stroke rehabilitation.

1.2 Objectives

This thesis is divided into 6 studies that present the work done with different neural interfaces for stroke motor rehabilitation. The main objective of this thesis was to develop a myoelectric decoding algorithm that could be integrated within a closed-loop rehabilitation system to control a multi-DoF exoskeleton and eventually, within a cortico-muscular hBMI that would act at both central and peripheral levels of the nervous system to elicit motor recovery in severely impaired chronic stroke patients. More specifically, the objectives of each study are the following:

1. Study 1: EMG-based multi-joint kinematics decoding for robot-aided rehabilitation therapies [68].

   In this study surface EMG activity from the upper limb of 8 healthy participants was recorded during functional tasks performed with a 7-DoF exoskeleton. As there were no previous studies that could continuously map EMG activity into the speed and direction of a multiple-DoF wearable exoskeleton during complex tasks, the objective of this work was to compare the offline performance of two linear algorithms that could offer such multi-DoF myoelectric control with acceptable accuracy.

2. Study 2: Design and effectiveness evaluation of mirror myoelectric interfaces: a novel method to restore movement in hemiplegic patients [69].

   Most studies involving MIs for rehabilitation overlooked the presence of pathological synergies in chronic stroke patients. Thus, the objective of this study was to propose and validate a novel myoelectric decoding method that would focus on the restoration of healthy and natural muscle synergies. To this end, EMG activity was recorded from both arms in 8 healthy participants and 2 chronic stroke patients and the knowledge learned from Study 1 was used. We evaluated if a decoder trained with the EMG and kinematics of one arm could be mirrored and used as a reference model for the opposite arm to learn the encoded healthy EMG-to-kinematics mapping during multiple tasks, which could eventually reshape the abnormal muscle synergy structure in stroke patients.

3. Study 3: Motor learning with a multi-degree-of-freedom mirror myoelectric interface during functional task training.

   The objective of this study was twofold:

   First, to integrate the mirror myoelectric decoder of Study 2 within a rehabilitation platform and validate its use with 10 healthy participants controlling a 7-DoF exoskeleton in real-time during functional tasks.

   Second, to investigate whether training with this mirror myoelectric interface during 4 sessions could elicit EMG activity adaptation and motor learning in healthy participants, establishing the premise for its clinical test in stroke patients.

4. Study 4: An EEG-based brain-machine interface to control a 7-degrees of freedom exoskeleton for stroke rehabilitation [70].

   In this study, an EEG-decoding method proven to induce significant motor recovery [49] was integrated in the rehabilitation platform of Studies 1-3 and its use was validated with 6 subjects and a chronic stroke patient, who controlled the BMI in real-time during a functional task, involving 7 DOFs of the arm, wrist and hand. This was a step forward towards the implementation of an hBMI for rehabilitation.

5. Study 5: Classification of different reaching movements from the same limb using EEG [53].

   The objective of this work was to improve the state of the art EEG-decoding algorithms by classifying brain activity from healthy participants into different reaching movements of the same limb, and thus increasing the decoding accuracy and control possibilities of existing BMIs.

6. Study 6: A Hybrid Brain-Machine Interface based on EEG and EMG activity for the Motor Rehabilitation of Stroke Patients [71].

   The existing non-invasive cortico-muscular hBMIs are limited to one DoF or to offline tests. This work combined the work done in Studies 1-4 to implement and validate the first cortico-muscular hBMI that could be used to control a 7-DoF exoskeleton in real-time during a functional task involving

proximal and distal joints of the upper-limb. As a proof of concept, we aimed to demonstrate that one healthy participant and one chronic severely paralyzed stroke patient could successfully control this hBMI.

1.3 Results and Discussion

The results of the studies of this thesis are organized into three main topics and summarized here. Their implication in the motor rehabilitation of stroke patients is also discussed.

1.3.1 Myoelectric interfaces

It has recently been demonstrated that residual EMG of stroke patients, even in a severe impairment level, can be decoded with acceptable (>65%) accuracy [35]. This has stressed the potential of MIs for the rehabilitation of this population and has led to the investigation of several EMG-decoding methods and training protocols. However, there are several factors that have prevented them from becoming an established clinical or "at home" rehabilitation method.

A significant effort has been invested in the development of EMG-decoding algorithms that enable natural and skillful control of MIs. Most studies have used algorithms that decode EMG signals into different movement classes [32,72]. However, these approaches fail to offer natural and smooth control of a trajectory and to generalize to untrained movements. On the other hand, algorithms that map EMG activity into a continuous velocity profile could lead to more intuitive and natural control of the interface. However, the existing continuous decoding algorithms are limited to the offline decoding of simple movements involving only a few DoFs of the arm, wrist or hand [42, 73–78]. Another limiting factor in the use of MIs is the non-stationary nature of EMG signals. Adaptive algorithms or recalibration protocols have been proposed to address this problem.

In Study 1 [68], we evaluated the offline performance of two algorithms (the Kalman filter and the ridge regression) for the continuous decoding of EMG activity. We tested these algorithms for the simultaneous decoding of multiple DoFs

(upper arm, forearm, wrist and hand) of the upper limb during functional tasks, which has not been achieved before. Moreover, we implemented various decoding schemes (within-session, across-session and recalibrated across-session) to analyze how susceptible they are to non-stationarities across-days. The results show that although the Kalman filter has been more widely used in MI applications, the ridge regression outperformed the former and could successfully be used for the simultaneous control of 7 DoFs (proximal and distal) of the upper limb. The regularization implicit in the ridge regression algorithm can prevent overfitting and makes the model more robust to across-session non-stationarities. Furthermore, the results show that including a short recalibration phase at the beginning of each session could offer a much more accurate EMG-decoding and control. Nevertheless, the benefits and disadvantages of including a daily re-calibration phase should be carefully considered in order to choose the most suitable approach for each particular scenario.

Rehabilitation therapies based on MIs aim to activate neuroplastic mechanisms that can correct compensatory muscle activation patterns developed after stroke, resulting in functional improvements. However, Cesqui et al. [34] argued that all existing MIs were calibrated with EMG from the paretic arm and that using this as a reference model during motor training could in fact reinforce the pathological muscle activity. Hence, Cesqui et al. proposed building a model of healthy muscle activity from a pool of healthy participants that could be utilized to enhance the correction of abnormal muscle synergies in stroke patients. Although this was a promising approach, it had two main limitations: data from a large number of subjects was needed to generalize to the neurophysiological characteristics of each patient, and the decoding was restricted to the classification of four movements involving proximal joints only.

In Study 2 [71], we proposed a novel myoelectric decoding method that could reshape the abnormal muscle synergy structure after stroke. Since previous evidence [79, 80] indicates that there are no substantial inter-limb differences in the synergy structure of healthy individuals, we proposed and tested a myoelectric interface calibrated with EMG activity of one arm, which was mirrored to be

used as a reference model for the opposite arm. The proposed mirror decoder showed performance values comparable or even higher to those of ipsilateral decoders tested across sessions (calibrated and tested in the same arm in different days). This demonstrates that the inter-limb variability of the EMG patterns is not big enough to produce a significant drop in the decoding performance and so, confirms the validity of our mirror decoder approach.

Additionally, we evaluated the generalization ability of the ridge regression algorithm to untrained tasks, which is a relevant factor for rehabilitation therapies during which, the trained tasks and range of motion vary according to the evolution of the patient. We compared a task-specific decoder, trained with a specific task only, and a general decoder trained with various tasks. The results show lower decoding errors for the general decoder than the task-specific decoder, especially when tested in untrained tasks. Therefore, a general decoder would perform better when decoding new tasks or different ranges of motion and would avoid the need of switching between decoders depending on the task being trained.

In Study 3 [69], the mirror decoder was tested in a real-time control paradigm with healthy participants proving that they could successfully control the mirror MI. More relevant is that a 4-day training with the mirror MI induced motor learning, reflected in significantly less time spent to reach the target and higher number of accomplished trials over sessions. Although long-term changes in the muscle activation patterns of healthy subjects could not be demonstrated, this study shows evidence that the users adapted their EMG activity to achieve smoother and more skillful control of the exoskeleton. This finding is very relevant for post-stroke rehabilitation, as reorganization of the motor networks occurs in response to sensory input, experience and learning [15], implying that a longer training with this mirror MI might induce the reorganization of brain and lower structures of the CNS, eventually reshaping the pathological muscle synergy structure and leading to motor recovery.

Another relevant finding of Study 3 is the degrading control of the distal DoFs observed along the experiment. Conversely, there was an improvement in the prox-

imal DoFs control over the sessions. One reason that could explain this difference is that the decoding accuracy for the distal DoFs is in general poorer than for the proximal DoFs, as individual finger movements are finer and more difficult to discriminate from surface EMG than proximal joint movements [68]. In addition, the task completion condition was based only on the proximal DoF position, although participants were not told about it. They could control and receive feedback on the distal DoFs but they were never informed whether they reached the target position on those DoFs (i.e., they never got a reward related to the distal DoFs). This lack of information might have impeded the occurrence of a learning process based on reinforcement learning (i.e., on reward), which would have been reflected in a more accurate control of the distal DoFs over time. This supports the importance of receiving not only contingent sensory feedback but also reward (e.g., beep indicating task completion) of the DoFs being controlled for motor control and learning [49, 81, 82].

1.3.2 Brain-machine interfaces

Despite the limitations of EEG technology and the moderated performance of EEG-decoding methods, several studies [49–51, 83] have demonstrated the potential of EEG-based BMIs as a tool for post-stroke rehabilitation. In Study 4 [70], we implemented and tested an EEG-based decoding algorithm, whose effectiveness for eliciting partial recovery was already proved, within a closed-loop rehabilitation platform with a 7-DoF exoskeleton. Eight healthy participants and a chronic stroke patient could successfully control the BMI in real-time by modulating their sensorimotor rhythms (SMR rhythms) from 2-3 motor cortex channels, during a functional task involving proximal and distal segments of the upper limb. The validated system constituted a potential rehabilitation platform, as it established a contingent link between motion intention and movement of the paralyzed limb, it provided a suitable setup for the training of functional tasks including the interaction with objects, and it opened the doors for the integration of additional neurophysiological signals in the control of the interface.

Neural populations modulate movements of the arm in different directions [84],

which can be decoded from brain activity with invasive techniques [57, 85]. The EEG-based BMI of Study 4 allowed the binary control of the interface, triggering or stopping a pre-programmed movement including several DoFs. Although this approach established a contingent connection between motion volition and action activating neuroplastic mechanisms that lead to motor recovery, we believed that discriminating different movements within the same limb would allow more intuitive and natural control of the neural interface. Upper limb and especially hand movement decoding from EEG activity is still challenging mainly due to poor signal to noise ratio and spatial resolution. Recent studies have classified EEG activity into up to 3 movement classes of the same limb [52, 86–88], although they are still far from providing natural and skillful control. In Study 5 [53], we went a step further and proved that the Filter Bank Common Spatial Pattern (FBCSP) algorithm could classify EEG activity into 6 different movements (reaching towards four different targets, rest and backwards movement from the targets) with a mean decoding accuracy above 50%. Mean performance raises to 69% and 62% when the number of classes is reduced to 3 and 4, respectively.

Motor execution of reaching movements of the same limb activates regions with very close representation on the motor cortex [89]. This spatial proximity, EEG volume conducting effects, limited spatial resolution and signal to noise ratio and electrical and neurophysiological artefacts hinders classification of such movements. Furthermore, this problem gets magnified when attempting to classify reaching movements towards close-by targets, as our results suggest [53]. Adding more features such as motor related cortical potentials, using longer time windows for the decoding, having higher density of electrodes over the motor cortex or including other neurophysiological signal in the control (i.e., hybrid BMIs) could improve these results. Nevertheless, this study sets the basis of multi-directional EEG-decoding for BMI rehabilitation applications.

1.3.3 Hybrid brain-machine interfaces

Non-invasive BMIs have been proven to induce partial motor recovery post-stroke. However, the limitations of non-invasive recording techniques and the fact that

BMIs directly target brain networks only, prevent them from becoming fully effective tools for motor rehabilitation. On the other hand, decoding of arm, wrist and individual fingers movements from EMG activity is feasible [36, 68, 72, 90] and has been utilized in MIs for the control of body actuators [91]. However, accurate decoding of EMG activity in stroke patients is challenging and might not be possible in some severely paralyzed cases. Therefore, cortico-muscular hBMIs that merge brain and residual EMG in the control of the interface, have recently arisen as optimized systems that overcome some of the limitations of BMIs and MIs alone.

The MI and the BMI validated throughout Studies 1-4 were integrated into a cortico-muscular hBMI tested in Study 6 [71]. This hBMI required the active participation of both central (brain) and peripheral (muscles) structures in a biologically-inspired hierarchical control, which mimicked the natural motor command flow. One healthy subject and one stroke patient received contingent visual and proprioceptive feedback about their EEG and EMG activity in the form of velocity modulation of an exoskeleton during functional task training.

No evidence of motor learning was found due to the short length of the training in Study 6. However, both the healthy participant and the stroke patient were able to modulate their SMR rhythms and their EMG activity to successfully operate the hBMI. The stroke patient presented less stable desynchronization of SMR rhythms during the trial time than the healthy subject, which can be caused by periods of attention deficit often occurring in this population. Initially, longer latency periods prior to the movement onset and smaller amount of movement time during the trial periods were observed in the patient. However, the patient achieved better control of the hBMI over the course of the session. Similarly, EMG decoding values were poorer in the stroke patient than in the healthy participant, due to the existence of muscle weakness and abnormal activation patterns. However, both were able to modulate their EMG activity to bring the exoskeleton to the target position in 3-5 attempts.

The control of the hBMI in Study 6 followed the natural human motor command flow. In healthy individuals, motor commands are initiated at the brain,

travelling through the spinal cord to reach the peripheral nerves and eventually the muscles. Thus, it seems natural to think that an effective hBMI control strategy should constantly require an initial command from the brain to later on transfer the control to the muscles. In this way, the active participation of both the brain and the muscles is necessary, which prevents patients from remaining passive and tackles various problems generally present after stroke, such as muscle weakness or maladaptive muscle activation patterns. Moreover, stroke patients without residual EMG could initially train with the BMI only, until they recovered enough EMG to be decoded and introduced in the control of the hBMI. Despite the encouraging results, more research is needed to evaluate whether this type of hierarchical hBMI control is adequate not only to achieve higher decoding accuracy and more dexterous and smoother control of the exoskeleton, but also to activate neuroplastic mechanisms and induce a joint brain and muscle rehabilitation process.

1.4 Conclusions

The conclusions and implications for stroke rehabilitation that can be drawn from the presented studies are the following:

- A simple linear algorithm such as the ridge regression can offer accurate continuous EMG control of 7-DoF trajectories with an arm, wrist and hand exoskeleton. This allows the training of functional tasks involving simultaneous and coordinated proximal and distal DoF movements of the upper limb in a synergistic fashion, which might facilitate the translation of the re-learned motor skills to activities of daily living [5, 6].

- A myoelectric decoder based on the ridge regression algorithm and calibrated with various tasks would perform well if new (untrained) tasks or movements with wider ranges of motion were included in the therapy, as patients′ severity stage varied in the course of the treatment.

- A mirror myoelectric decoder calibrated with data from the healthy arm could be used as a reference model for the paretic arm to reshape the pathological muscle synergy structure in stroke patients, as there are no substantial

inter-limb differences in the muscle synergy organization of healthy individuals [79, 80] and the decoding performance of mirror decoders (across arms) does not differ significantly from ipsilateral (within arm) decoders.

- Training of functional tasks with a mirror myoelectric interface that establishes a contingent link between the EMG activity of the arm and the movement of a multi-DoF upper limb exoskeleton can induce motor learning in healthy individuals. If the healthy population can adapt their muscle activations and learn the imposed EMG-to-kinematics mapping, this myoelectric interface might be a potential tool for the correction of the pathological synergy structure and eventually, for the motor rehabilitation of stroke patients.

- Simple EEG-decoding algorithms such as linear discriminant analysis, proven to induce partial motor recovery in BMI training therapies [49], can be used to control more complex body actuators involving simultaneous and coordinated movements of several DoFs of the upper limb.

- Three, four and six-class EEG-decoding of reaching movements of the same limb is possible with the Filter Bank Common Spatial Pattern algorithm, achieving mean performances of 50%, 62% and 69% respectively in healthy participants. Although this is a step further in the multi-class decoding of EEG signals, higher accuracy is necessary to allow more natural and skillful control of body actuators and thus, boost the potential of BMI therapies for post-stroke rehabilitation.

- Cortico-muscular hybrid BMIs are systems designed to build on the advantages and alleviate the limitations of BMIs and MIs alone, resulting in more robust interfaces that aim to boost motor recovery by acting at both central (brain) and peripheral (muscle) structures. Successful operation of a multi-DoF exoskeleton with an hBMI that follows a top-down hierarchical control flow (i.e., continuous EEG gating EMG control) has been demonstrated. Nevertheless, the advantages of hBMIs over regular BMIs or MIs should be directly compared and the effects of hBMI training in the motor rehabilitation of stroke should be investigated.

1.5 Outlook

Neural interfaces have provided us with the possibility to interact directly with the human nervous system and to understand some neuroplastic mechanisms that play a key role in motor learning and recovery. There is evidence that closed-loop systems such as BMIs or MIs that establish a contingent link between motion volition decoded from neurophysiological signals and afferent visual and proprioceptive feedback can induce partial motor recovery in severely impaired chronic stroke patients. However, neural interfaces have not yet been fully effective for motor rehabilitation due to several factors.

The huge heterogeneity of brain lesions due to stroke and the subsequent motor disorders hampers the use of standard neural interfaces and the generalization of the learned knowledge to every other patient. Moreover, the fundamental singularity of cortical patterns in each individual, derives in diverse neural activity among patients performing the same task [92–95]. Up to know this issue has been mitigated by customizing neural interfaces and therapies for the specific anatomical and neurophysiological characteristics of each patient with daily re-calibrations or adaptive algorithms, which are sometimes time-consuming processes. Reducing this calibration process to the minimum in order to achieve optimized subject-dependent training strategies or finding new methods effective for various patients would facilitate the standardized use of neural interfaces for stroke rehabilitation.

Another limitation of neural interfaces is the decoding accuracy that can be achieved with non-invasive techniques. EEG-decoding algorithms still fail to accurately decode several DoFs of the arm due to low signal to noise ratio and spatial resolution constraints. Invasive techniques can offer higher decoding performance over several DoFs of the upper limb [57, 85] but acceptance of invasive BMIs is still low, due to the risks associated with the surgical intervention. On the other hand, myoelectric decoders using surface EMG signals have demonstrated acceptable performance for the decoding of arm, wrist and individual finger movements, especially when employing high-density electrode arrays [36, 42, 69, 74, 96]. However, the correction of the pathological synergy organization of stroke patients

has been ignored and accurate decoding of coordinated and simultaneous movements of several DoFs still remains a challenge, due to signal non-stationarities and the across-session variability of factors such as electrode position and arm posture. Cortico-muscular hBMIs might offer an alternative to this issue by combining brain and residual EMG activity in the control of the interface and so, improving the decoding accuracy and allowing more natural and dexterous control. Nevertheless, hBMIs are still in an early stage of development and further clinical research is needed to evaluate their influence in motor rehabilitation.

Providing patients with somatosensory afferent feedback related to their neural activations is a key component of neural interfaces for motor control and learning, as most stroke patients preserve their afferent pathways intact [97]. Furthermore, this feedback should be contingent to the generated motion volition to elicit motor recovery [49]. Stimulation of central or peripheral structures of the nervous system through electrical or magnetic stimulation could also be a reactivation method to excite neural networks and facilitate plasticity, boosting the effects of BMI therapies and accelerating the recovery process [98,99]. Nevertheless, a better understanding of the behavior of the neural networks associated with sensorimotor integration and neuroplastic processes would allow the design of more effective stimulation and rehabilitation paradigms.

Finally, most of the current studies in stroke patients apply their proposed rehabilitation paradigm during periods shorter than a month. While this might be long enough to demonstrate the potential of the proposed method, the limited duration of the treatment often prevents them from achieving relevant and long-term effects on the motor recovery process of their patients. Longer practices that would adapt the therapy according to the patient′s evolution may lead to significant functional changes and have a real impact on the patient′s quality of life.

1.6 List of papers

1. **EMG-based multi-joint kinematics decoding for robot-aided rehabilitation therapies**
   Sarasola-Sanz, A., Irastorza-Landa, N., Shiman, F., López-Larraz, E., Spüler, M., Birbaumer, N., Ramos-Murguialday, A.

2. **Design and effectiveness evaluation of mirror myoelectric interfaces: a novel method to restore movement in hemiplegic patients**
   Sarasola-Sanz, A., Irastorza-Landa, N., López-Larraz, E., Shiman, F., Spüler, M., Birbaumer, N., Ramos-Murguialday, A.

3. **Motor learning with a multi-degree-of-freedom mirror myoelectric interface during functional task training**
   Sarasola-Sanz, A., López-Larraz, E., Irastorza-Landa, N., Rossi, G., Figueiredo, T., McIntyre, J., Birbaumer, N., Ramos-Murguialday, A.

4. **An EEG-based brain-machine interface to control a 7-degrees of freedom exoskeleton for stroke rehabilitation**
   Sarasola-Sanz, A., López-Larraz, E., Irastorza-Landa, N., Klein, J., Valencia, D., Belloso, A., Morin, F.O., Spüler, M., Birbaumer, N., Ramos-Murguialday, A.

5. **Classification of different reaching movements from the same limb using EEG**
   Shiman, F., López-Larraz, E., Sarasola-Sanz, A., Irastorza-Landa, N., Spüler, M., Birbaumer, N., Ramos-Murguialday, A.

6. **A Hybrid Brain-Machine Interface based on EEG and EMG activity for the Motor Rehabilitation of Stroke Patients**

   Sarasola-Sanz, A., Irastorza-Landa, N., López-Larraz, E., Bibián, C., Helmhold, F., Broetz, D., Birbaumer, N., Ramos-Murguialday, A.

1.7 Statement of Contributions

1.7.1 EMG-based multi-joint kinematics decoding for robot-aided rehabilitation therapies

Andrea Sarasola-Sanz	Protocol design Setup and experiment preparation Data collection and analysis Manuscript writing
Nerea Irastorza-Landa	Protocol design Setup and experiment preparation Data collection Manuscript review
Farid Shiman	Protocol design Experiment preparation Data collection
Eduardo López-Larraz	Data collection
Martin Spüler	Data analysis Manuscript review
Niels Birbaumer	Protocol design Manuscript review
Ander Ramos-Murguialday	Protocol design Data analysis Manuscript review

1.7.2 Design and effectiveness evaluation of mirror myoelectric interfaces: a novel method to restore movement in hemiplegic patients

Andrea Sarasola-Sanz	Protocol design Setup and experiment preparation Data collection and analysis Manuscript writing
Nerea Irastorza-Landa	Protocol design Setup and experiment preparation Data collection Manuscript review
Eduardo López-Larraz	Protocol design Data analysis Manuscript review
Farid Shiman	Protocol design Experiment preparation Data collection
Martin Spüler	Data analysis
Niels Birbaumer	Protocol design Manuscript review
Ander Ramos-Murguialday	Protocol design Data analysis Manuscript review

1.7.3 Motor learning with a multi-degree-of-freedom mirror myoelectric interface during functional task training

Andrea Sarasola-Sanz	Protocol design Setup and experiment preparation Data collection and analysis Manuscript writing
Eduardo López-Larraz	Protocol design Data collection and analysis Manuscript review
Nerea Irastorza-Landa	Protocol design Setup and experiment preparation
Giulia Rossi	Setup and experiment preparation Data collection
Thiago Figueiredo	Data analysis
Joseph McIntyre	Data analysis Manuscript review
Niels Birbaumer	Protocol design Manuscript review
Ander Ramos-Murguialday	Protocol design Data analysis Manuscript review

1.7.4 An EEG-based brain-machine interface to control a 7-degrees of freedom exoskeleton for stroke rehabilitation

Andrea Sarasola-Sanz	Protocol design Setup and experiment preparation Data collection and analysis Manuscript writing
Eduardo López-Larraz	Protocol design Data analysis Manuscript review
Nerea Irastorza-Landa	Protocol design Setup and experiment preparation Data collection Manuscript review
Julius Klein	Exoskeleton development and maintenance
David Valencia	Exoskeleton development and maintenance
Fabrice O. Morin	Exoskeleton development and maintenance
Martin Spüler	Data analysis
Niels Birbaumer	Protocol design
Ander Ramos-Murguialday	Protocol design Data analysis Manuscript review

1.7.5 Classification of different reaching movements from the same limb using EEG

Farid Shiman	Protocol design Experiment preparation Data collection and analysis Manuscript writing
Eduardo López-Larraz	Data analysis Manuscript review
Andrea Sarasola-Sanz	Protocol design Setup and experiment preparation Data collection Manuscript review
Nerea Irastorza-Landa	Protocol design Setup and experiment preparation Data collection Manuscript review
Martin Spüler	Data analysis Manuscript review
Niels Birbaumer	Protocol design Manuscript review
Ander Ramos-Murguialday	Protocol design Data analysis Manuscript review

1.7.6 A Hybrid Brain-Machine Interface based on EEG and EMG activity for the Motor Rehabilitation of Stroke Patients

Andrea Sarasola-Sanz	Protocol design Setup and experiment preparation Data collection and analysis Manuscript writing
Nerea Irastorza-Landa	Protocol design Setup and experiment preparation Data collection Manuscript review
Eduardo López-Larraz	Data analysis Manuscript review
Carlos Bibián	Data collection
Florian Helmhold	Data collection
Doris Broetz	Patient recruitment Patient care and physiotherapy
Niels Birbaumer	Protocol design
Ander Ramos-Murguialday	Protocol design Data analysis Manuscript review

2. Chapter 2: EMG-based multi-joint kinematics decoding for robot-aided rehabilitation therapies

This manuscript has been published as [68].

2.1 Abstract

In recent years, a significant effort has been invested in the development of kinematics-decoding models from electromyographic (EMG) signals to achieve more natural control interfaces for rehabilitation therapies. However, the development of a dexterous EMG-based control interface including multiple degrees of freedom (DOFs) of the upper limb still remains a challenge. Another persistent issue in surface myoelectric control is the non-stationarity of EMG signals across sessions. In this work, the decoding of 7 distal and proximal DOFs' kinematics during coordinated upper-arm, fore-arm and hand movements was performed. The influence of the EMG non-stationarity was tested by training a continuous EMG decoder in three different scenarios. Moreover, the generalization characteristics of two algorithms (ridge regression and Kalman filter) were compared in the aforementioned scenarios. Eight healthy participants underwent EMG and kinematics recordings while performing three functional tasks. We demonstrated that ridge regression significantly outperformed the Kalman filter, indicating a superior generalization ability. Furthermore, we proved that the performance drop caused by the session-to-session non-stationarities could be significantly mitigated by including a short re-calibration phase. Although further tests should be performed, these prelim-

inary findings constitute a step forward towards the non-invasive control of the next generation of upper limb rehabilitation robotics.

2.2 Introduction

In recent years, several studies have been carried out in the field of myoelectric control for applications such as teleoperation of robots, prosthesis for amputees and rehabilitation of patients with paralyzed limbs [32, 35, 42, 72–78]. However, the development of dexterous and natural myoelectric control interfaces with multiple degrees of freedom still remains a challenge.

Most of the studies in this field have emphasized the use of EMG signals for the classification of different movement classes [32, 72]. However, these approaches have limited success when natural and smooth control of the trajectory is necessary. A decoder that maps EMG signals into a continuous profile of upper limb kinematics could overcome this limitation. Studies developing such decoders have already been performed, although most of them are limited to simple movements of either distal [42, 73, 75] or proximal [76–78] degrees of freedom (DOFs) of the upper limb. To the best of our knowledge, the only study that reported decoding of several distal and proximal DOFs of the upper limb [74] was not focused on rehabilitation approaches. Moreover, in that study target-specific and object-specific models were built for the decoding of reach-to-grasp movements, which led to high error values.

A ubiquitous issue in the field of EMG control interfaces is the non-stationarity of EMG signals that occurs across multiple sessions. Factors such as sweat, fatigue, varying upper limb configurations, electrode shift and impedance changes, could change the EMG signal distribution. This change is referred to as covariate shift and could notably affect the performance of the decoder.

In this study we aimed to decode the motion of seven DOFs (distal and proximal) of the upper limb from surface EMG signals, while participants performed dif-

ferent functional tasks of increasing complexity. Three different decoding schemes were implemented: within-session decoder (WS), session-to-session decoder (SS) and re-calibrated session-to-session decoder (RSS). As re-calibration was shown to improve decoding performance (e.g. by classifier adaptation [100]), a re-calibration phase using data from the beginning of the subsequent session was used to compensate for the negative effects of the session-to-session covariate shift. The performance of these three decoders was compared in order to assess the influence of the EMG non-stationarity on the decoding accuracy. Furthermore, this analysis was performed using two different algorithms, namely, ridge regression [101] and Kalman filter (KF) [102]. Up to this point, Kalman filter has been the most widely used algorithm for these applications [73,76,77]. However, the ridge regression technique is often underestimated and has been included in very few recent studies [42] for the decoding of EMG signals. Nevertheless, we hypothesized that, due to regularization (i.e. penalizing model complexity by imposing a constraint to the coefficients to prevent overfitting), the ridge regression technique could have a better generalization ability than the KF (i.e. predict kinematics under variable conditions more accurately).

2.3 Methods

2.3.1 Experimental Protocol

Eight healthy participants (3 females, 5 males, age 20-28, all right-handed) participated in this study. None of them had any neuromuscular disorder and all of them gave written consent to the procedures as approved by the ethics committee of the Faculty of Medicine of the University of Tübingen, Germany. Participants performed three different tasks while sitting and wearing a 7-DOF exoskeleton (Tecnalia, San Sebastian, Spain) on their right upper limb placed over a 70×50 cm mat. The exoskeleton allowed movements in 7 DOFs (see Fig. 2.1): displacement and rotation of the forearm in a 2D horizontal plane parallel to the mat's plane (3 proximal DOFs: (i) p_x position; (ii) p_y position; (iii) θ_{xy} orientation angle), pronation and supination of the wrist (1 distal DOF: (iv) ϕ_{wrist} angle) flexion and extension of the thumb, index and the group of middle, ring and pinky fingers

measured as the angle of rotation with respect to the metacarpophalangeal joints (3 distal DOFs: (v) δ_{thumb}; (vi) ψ_{index}; (vii) $\alpha_{3fingers}$).

All the participants underwent two sessions that were separated by 2-9 days. During these sessions they were instructed, by means of imperative auditory cues, to perform three different tasks that always started and ended at a predefined rest position.

1) The first task consisted of reaching movements (hand relaxed) towards one of the four different targets around the mat.

2) In the second task, participants were asked to reach and point to two different targets with his/her index finger, moving towards the first target from the rest position and towards the second target immediately after reaching the first target.

3) In the third task, three objects of different shapes and sizes were located in one of the four target positions. Participants had to reach a target, grab the object placed in that position, move it to another target and then come back to the rest position. It should be noted that each of the objects required a different grasp type, which were: pinch grip, key grasp and cylindrical grasp.

Each of the tasks was divided in 5 blocks, which consisted of a set of 10-40 trials depending on the task type (40 for task 1; 10 for task 2; 22 for task 3). Resting intervals of 1-5 minutes were included between blocks in order to avoid fatigue. Participants were asked to perform the movements at their own pace and were given 4 seconds to complete task 1 trials and 6 seconds for task 2 and task 3 trials. This makes a total of approximately 30 min (task 1), 7 min (task 2) and 15 min (task 3) of recorded data per participant in each of the two sessions. It should be pointed out that, although participants performed the trials at their own pace, the aforementioned trial durations (task 1: 4 sec; task 2 and task 3: 6 sec) implied that they had to keep a rapid pace in order to accomplish the trials within the given time limits.

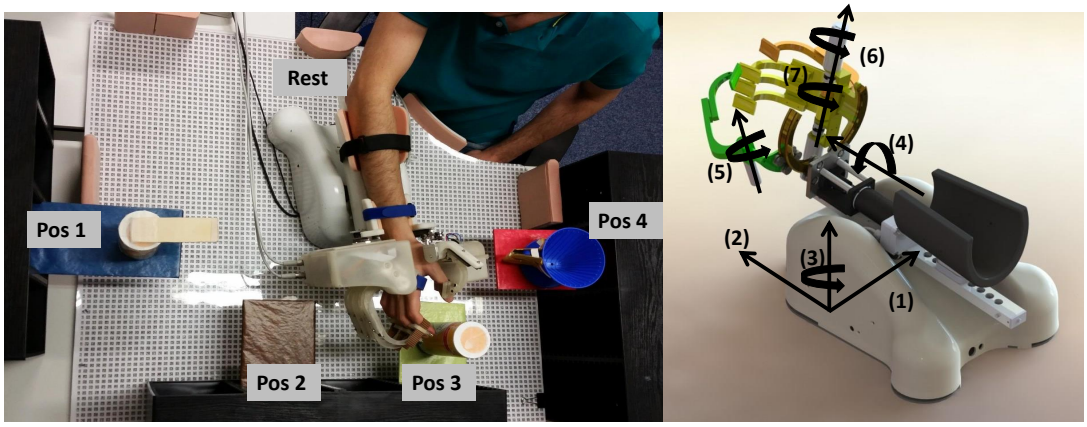

Figure 2.1: *(Left): Workspace where the experiments were performed. Pos1, Pos2, Pos3 and Pos4 correspond to the four targets and Rest was the predefined rest position where all the trials started and ended. (Right): Schematic of the 7 DOFs of the exoskeleton: (1)* p_x*; (2)* p_y*; (3)* θ_{xy}*; (4)* ϕ_{wrist}*; (5)* δ_{thumb}*; (6)* ψ_{index}*; (7)* $\alpha_{3fingers}$

2.3.2 Data Collection

Surface EMG activity from 10 disposable bipolar electrodes (Myotronics-Noromed, Tukwila, WA, USA) over the upper-arm and fore-arm was acquired at 2500Hz using a bipolar amplifier (Brain Products GmbH, Gilching, Germany). The electrodes were placed over: 1) the abductor pollicis longus, 2) the extensor carpi ulnaris, 3) the extensor digitorium, 4) the flexor carpi radialis, palmaris longus and flexor carpi ulnaris, 5) the pronator teres, 6) the long head of biceps, 7) the external head of triceps, 8) the anterior portion of deltoid, 9) the lateral portion of deltoid and 10) the posterior portion of deltoid over the teres minor and infraespinatus muscles. The ground monopolar electrode was placed over the right clavicle. Kinematic activity of the above mentioned DOFs was recorded at 18Hz and synchronized offline with the EMG signals. The kinematics of the fore-arm DOFs, namely, p_x, p_y and θ_{xy}, were collected with a camera attached to the bottom of the exoskeleton, which tracked the movements by using an optical symbol recognition system (more details in [103]). The prono-supination angle ϕ_{wrist} was captured from a motor encoder and the fingers' angles δ_{thumb}, ψ_{index} and $\alpha_{3fingers}$ were acquired using potentiometers. Nevertheless, all the kinematic data was acquired with the same software and at the same frequency. Therefore, only the synchronization of

the kinematics with the EMG signal had to be done. For this purpose, the EMG recording was initiated first. At the beginning of each block, along with the initiation of the kinematics recordings, a step signal was generated and fed into the EMG recording so that both signals could be synchronized offline.

2.3.3 Data processing

EMG data was filtered using a 4^{th} order Butterworth band-pass filter (10-500 Hz) to remove movement artifacts and high frequency noise. In addition, a 50 Hz comb filter was utilized in order to remove power line noise and its harmonics. Kinematic data was low-pass filtered with a 4^{th} order Butterworth filter (f_c = 1.5 Hz). The derivation of the positions and angles with respect to time was computed in order to obtain linear and angular velocity profiles, which were the variables to be predicted from EMG signals. The kinematic signal predicted from the decoder was filtered using a moving average with a backwards time window of 180 ms to improve movement smoothness towards online robot control.

Seven time-domain features typically used for myoelectric interfaces (Mean of absolute values, Variance, Waveform Length, Root-mean-square error, Willison Amplitude (WAMP), Zero crossing (ZC) and Slope sign changes (SSC)) [104] were extracted from each of the 10 EMG channels in 200 ms windows, resulting in a 70-element EMG feature set (7 features x 10 channels). The thresholds for the last three features were empirically selected and fixed to the same values for all the participants (TH_{WAMP} = 30 μV; TH_{ZC} = 30 μV; TH_{SSC} = 700 μV). Each of the EMG features of the generated set was normalized to zero mean and unit variance before being fed to the decoder. The testing data was normalized using the mean and standard deviation computed on the training dataset.

2.3.4 Algorithms

1) *Kalman filter*

A Kalman filter models the system by the state transition equation:

$$x_{t+1} = A_t x_t + w_t \tag{2.1}$$

Where x_t is the state at time t, A_t is the state transition matrix and w_t is the model white noise $\sim \mathcal{N}(0, Q)$.

The observations of the state are made through a measurement system which can be represented by the following linear equation:

$$y_t = C_t x_t + v_t \tag{2.2}$$

Where y_t is the observation or measurement at time t, x_t is the state at time t, C_t is the measurement matrix and v_t is additive measurement noise $\sim \mathcal{N}(0, R)$.

2) *Ridge regression*

The relationship between the dependent variable of length n, $y \in \Re^{1\times n}$, in this case velocity, and the independent variable, a p-dimensional EMG feature set $X \in \Re^{pxn}$, is modeled as follows:

$$y = \beta^T X + \beta_0 \quad \text{s.t.} \quad \sum_{j=1}^{p} \beta_j^2 \leq s \tag{2.3}$$

With $\beta^T \in \Re^{px1}$ being the vector of coefficients and β_0 the intercept term. The regularization consists of constraining the sum of squared coefficients with some value $s > 0$.

The solution is the one that minimizes the penalized residual sum of squares, which is expressed as:

$$\sum_{i=1}^{n}(y_i - \sum_{j=1}^{p} x_{ij}\beta_j)^2 + \lambda \sum_{j=1}^{p} \beta_j^2 \tag{2.4}$$

With λ being the regularization parameter. Since the penalized residual sum of squares in equation 2.4 is convex, it has a unique solution given by:

$$\beta_{ridge} = (X^T X + \lambda I_p)^{-1} X^T y \tag{2.5}$$

2.3.5 Decoding schemes

Three decoding schemes were implemented by using different training and testing conditions:

- *Within-session decoder* (WS): This decoder was trained and tested with data from the same session. It was implemented in order to have a metric of how good our decoder could work. Since we collected data during two sessions, we developed two types of decoders: one using only data from the first session S1 (WS1) and the other one only with data from the second session S2 (WS2).
- *Session-to-session decoder* (SS): This decoder was trained and validated in the first session S1 and tested in the next session S2. A performance drop due to the session-to-session transfer was expected when comparing its performance to the one of the WS decoder.
- *Re-calibrated session-to-session decoder* (RSS): This decoder was similar to the SS decoder explained above with the difference that a few minutes of data were collected at the beginning of S2 in order to re-calibrate the decoder. This was useful in order to check if this re-calibration phase could compensate for the expected performance drop due to the session-to-session transfer.

2.3.6 Cross-validation

All three of the decoding schemes were implemented for each task and DOF separately. The data from each session, task and DOF was divided into 5 blocks, each of them containing trials of all the trajectory types. These five blocks were divided into the training and test sets as follows:

For the WS decoding scheme, a 5-fold cross-validation (CV) was applied using only data from either S1 (for WS1) or S2 (for WS2). The values obtained from

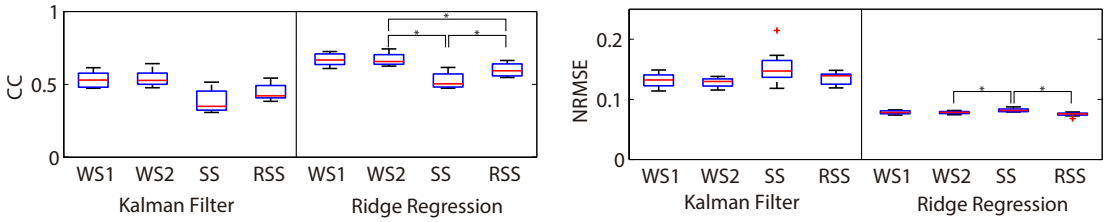

Figure 2.2: *Correlation coefficient (left) and normalized root mean squared error (right) for each combination of decoding scheme (WS1, WS2, SS or RSS) and algorithm (Kalman filter or ridge regression) after averaging over all subjects, tasks and involved DOFs. The median and the* 25^{th} *and* 75^{th} *percentiles are shown. Significant differences found between the decoding schemes using ridge regression are marked with an asterisk.*

the testing phase of each CV-fold were averaged to compute the reported final performance. The SS decoding scheme, instead, consisted of a training phase with all 5 blocks of S1 and a testing phase with all 5 blocks of S2. For the RSS decoding scheme, all 5 blocks of S1 and the first block of S2 were included in the training set in order to re-calibrate the decoder. The remaining 4 blocks of S2 were assigned to the test set.

It should be mentioned that in the case of ridge regression, a nested CV was applied in all the decoding schemes because an optimum value for the regularization parameter had to be found. In each fold of the inner CV-loop, one of the blocks from the training set was employed as validation data in order to find the optimum regularization parameter. A grid search of values in the range $[10^{-7} - 10^{7}]$ was utilized to find the best parameter. After this, the decoder was once again trained with this optimized parameter and tested in the outer loop.

2.3.7 Performance evaluation

The correlation coefficient (CC) and the normalized root mean squared error (NRMSE) were employed as performance metrics. The reported performance values for each combination of decoding scheme and algorithm were computed as the average over the three tasks and the 8 participants. Each task's performance was in turn computed as the mean performance of the DOFs involved (i.e. actively

used) in the corresponding task only.

Both for the CC and NRMSE values the following tests were applied:

Data was assumed to be normally distributed and a 2-way repeated measures Analysis of Variance (ANOVA) test with two factors (Algorithm and Decoding Scheme) was performed. The algorithm factor was comprised of two levels: Kalman filter and ridge regression while the decoding scheme factor consisted of three levels: WS2, SS and RSS.

This first test was used in order to find out which algorithm performed better overall and if that difference in performance was significant. Subsequent tests were then limited to the best algorithm. Secondly, a one-way repeated measures ANOVA was performed to test the effect of the decoding scheme factor only for the best algorithm. Post-hoc pairwise comparisons of the three decoding schemes were performed and controlled for multiple comparisons using Bonferroni correction.

For the best algorithm, a paired t-test comparing WS1 and WS2 decoding performance was also carried out in order to analyze the performance stability of the WS decoder and by extension, the reliability of session S1 and S2 data.

2.4 Results

For both metrics, the ANOVA resulted in a significant effect for both the algorithm (CC: $p = 10^{-6}$; NRMSE: $p = 10^{-5}$) and decoding scheme (CC: $p = 10^{-6}$; NRMSE: $p = 0.011$) factors while the interaction turned out to be non-significant (CC: $p = 0.075$; NRMSE: $p = 0.070$). The ridge regression algorithm performed significantly better than the Kalman filter and thereby, the subsequent tests were reduced to the comparison of the different decoding schemes using only ridge regression.

With the factor algorithm fixed at ridge regression, the one-way ANOVA test

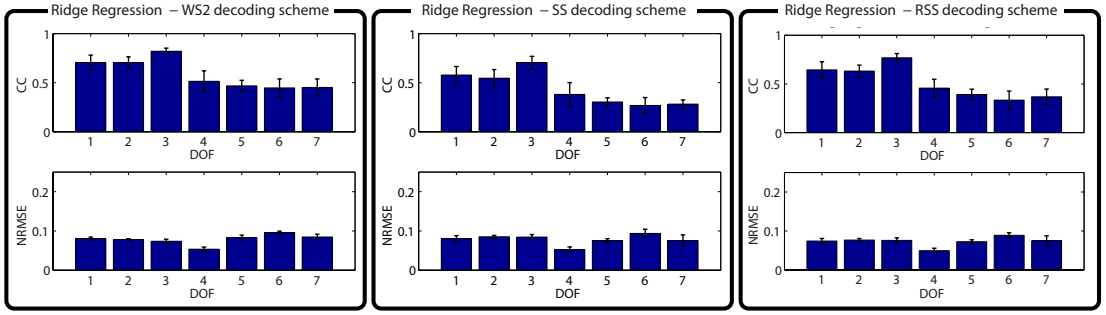

Figure 2.3: *Mean and standard deviation values of correlation coefficient (top) and normalized root mean squared error (bottom) for the decoded linear or angular velocities in each individual DOF, obtained with the WS2 (left), SS (middle) and RSS (right) decoding schemes. DOFs 1-2 correspond to linear velocities of: (1) p_x, (2) p_y; and DOFs 3-7 correspond to angular velocities of: (3) θ_{xy}; (4) ϕ_{wrist}; (5) δ_{thumb}; (6) ψ_{index}; (7) $\alpha_{3fingers}$.*

resulted in a significant decoding scheme effect in both cases (CC: $p < 10^{-6}$; NRMSE: $p = 10^{-5}$). Post-hoc Bonferroni corrected test results differed for each metric (see Fig. 2.2). For the CC, post-hoc tests revealed significant differences between the three decoding schemes. (WS2 vs SS: $p < 10^{-6}$; SS vs RSS: $p = 2.1 \cdot 10^{-4}$; WS2 vs RSS: $p = 3.1 \cdot 10^{-5}$). However, for the NRMSE metric, significant differences were found for the comparisons WS2 vs SS ($p = 4.5 \cdot 10^{-3}$) and SS vs RSS ($p = 7.5 \cdot 10^{-4}$) while the comparison WS2 vs RSS showed no significant difference ($p = 0.129$).

The paired t-test comparing WS1 and WS2 decoding schemes performance showed no significant difference for both CC ($p = 0.918$) and NRMSE ($p = 0.859$).

Additionally, for each of the three decoding schemes based on the ridge regression algorithm, the performance values (CC and NRMSE) for each of the DOFs separately were computed (see Fig. 2.3 and values in Table 2.1). The performance values obtained for each DOF were consistent across decoding schemes. A significantly ($p = 10^{-6}$) lower CC for the distal DOFs (mean CC = 0.39) compared to the proximal DOFs (mean CC = 0.68) can be seen. However, the NRMSE stayed stable at a mean value of 0.077 (7.7%) for all the DOFs.

Table 2.1: *Mean and std values of cc and nrmse for each dof and decoding schemes using only ridge regression*

DOF	CC			NRMSE		
	WS2	SS	RSS	WS2	SS	RSS
1	0.70 (± 0.08)	0.58 (± 0.09)	0.64 (± 0.08)	0.081 (± 0.004)	0.080 (± 0.008)	0.074 (± 0.007)
2	0.70 (± 0.06)	0.55 (± 0.09)	0.63 (± 0.06)	0.078 (± 0.002)	0.085 (± 0.003)	0.077 (± 0.004)
3	0.82 (± 0.03)	0.70 (± 0.06)	0.77 (± 0.04)	0.074 (± 0.005)	0.084 (± 0.007)	0.076 (± 0.007)
4	0.51 (± 0.11)	0.38 (± 0.12)	0.46 (± 0.09)	0.054 (± 0.006)	0.053 (± 0.007)	0.049 (± 0.007)
5	0.47 (± 0.06)	0.30 (± 0.04)	0.39 (± 0.06)	0.083 (± 0.006)	0.076 (± 0.005)	0.072 (± 0.005)
6	0.45 (± 0.09)	0.27 (± 0.08)	0.33 (± 0.09)	0.096 (± 0.004)	0.094 (± 0.011)	0.089 (± 0.007)
7	0.45 (± 0.08)	0.28 (± 0.04)	0.37 (± 0.08)	0.085 (± 0.007)	0.075 (± 0.015)	0.074 (± 0.013)

2.5 Discussion

In this study, multiple decoding schemes and algorithms for the continuous mapping of EMG signals into upper limb kinematics were tested. The analysis included the decoding of distal and proximal DOFs during complex functional movements involving coordinated upper-arm and fore-arm muscle activity. Kalman filter and ridge regression techniques were compared across different decoding scenarios in order to test their ability to overcome the EMG non-stationarity as well as the variability in the performed movements. All these aspects are of great importance and have a direct impact on the clinical applications of EMG decoding.

The Kalman filter model has been extensively used before for myoelectric control applications. However, simple algorithms like ridge regression are often underestimated and therefore excluded from EMG decoding studies. Regularization methods impose a constraint to the model coefficients (i.e. control how large the coefficients are). This introduces the advantage of preventing overfitting and thus, of having a model with good generalization characteristics. This is highly desirable, especially in situations in which the decoder should be able to generalize to movements from which sufficient training data is not available. The results of the work presented here confirm our hypothesis that ridge regression generalizes to new EMG data better than the Kalman filter. Therefore, ridge regression constitutes a desirable algorithm for the continuous EMG decoding of upper limb kinematics.

Factors such as external interference, electrode shift and lift, electrode impedance changes, muscle fatigue, sweat and varying upper-limb positions alter the EMG signal distribution. Sources of variation like external interference can be mostly suppressed by filtering or electromagnetic shielding techniques. However, the remaining sources constitute a persistent issue in clinical practice and severely affect the performance of myoelectric decoders. In fact, we believe that in this particular study, one of the main factors affecting the performance stability could have been the variable positioning of the EMG electrodes from session-to-session since they were just placed within the general vicinity. A daily re-calibration phase was proposed as a solution to alleviate the effects of such non-stationarities. The additional time of re-calibrating the decoder and the cost of recording new data at the beginning of each session could be a concern for certain applications. Nevertheless, the performance comparisons between the three developed decoding schemes showed that there was a significant improvement in performance (a 14% increase in CC and a 8% reduction in NRMSE with respect to SS) when a re-calibration of the decoder was carried out. Moreover, the NRMSE values of the re-calibrated decoder were not significantly different from those achieved when training and testing the decoder with data from the same session (WS2 decoder). This implies that a re-calibration phase could reduce the error to the extent that the values would be just as low as if the decoder was trained using a larger amount of data only from the current session. It should also be mentioned that the calibration data length was 5 min, 1.5 min and 3 min for each task respectively and that it took a negligible amount of time to build the decoding model and choose the optimal regularization parameter, as opposed to other more complex algorithms. Therefore, the proposed approach was not very time and computationally demanding and served to significantly raise the performance. Nonetheless, the benefits and disadvantages of including a daily re-calibration phase should be carefully considered in order to choose the most suitable approach for each particular scenario.

The majority of recent studies in the field of myoelectric control interfaces are constrained to the decoding of a few distal or proximal DOFs. These devices could be employed for those cases in which impaired function of a few specific DOFs is present. However, the ability for interfaces to control multiple DOFs of the up-

per limb during dexterous and functional movements is necessary, especially for patients who are undergoing rehabilitation therapies for motor impairment of an entire extremity. Our protocol included the decoding of coordinated multi-joint movements. While the NRMSE was stable at a very low value for all the DOFs, the lower CC values achieved for the distal DOFs might be due to the limited number of electrodes used for the decoding of distal DOFs. Extensors and flexor muscles of the forearm are often more difficult to target and it is usually hard to isolate the EMG activity from each recorded muscle. This makes the discrimination and decoding of individual finger movements more challenging. The minimum number of electrodes on the forearm that are necessary to attain an accurate decoding of distal DOF movements has been extensively investigated before [**?**, 42, 72, 105]. From the results presented in these previous studies, it can be concluded that a minimum of 12-16 electrodes are necessary to distinguish between multiple individual finger and wrist movements. Therefore, future studies should be performed with additional electrodes placed over the fore-arm in order to improve the decoding accuracy of distal DOFs.

2.6 Conclusion

This study addressed important aspects for the use of myoelectric control interfaces in clinical practice, which were: (*i*) the choice of a decoding algorithm with good generalization characteristics; (*ii*) the training procedure to follow in order to develop a decoder, which is robust to non-stationarities; and (*iii*) the decoding of coordinated distal and proximal DOF movements during complex functional tasks. From the results presented here, we concluded that a simple regularized algorithm such as ridge regression has good generalization characteristics for the EMG-based continuous decoding of multiple DOFs of the upper limb. Moreover, we demonstrated that by introducing a daily re-calibration phase the effects of the session-to-session non-stationarities could be significantly mitigated. Further studies including additional electrodes over the fore-arm should be performed in order to more accurately discriminate individual finger movements. Nevertheless, this pilot study is an important step towards the development of a robust myo-

electric interface for the online control of coordinated multi-joint movements in robot-aided rehabilitation therapies.

2.7 Acknowledgements

This study was funded by the Baden-Württemberg Stiftung (GRUENS), the Indian-European collaborative research and technological development projects (INDIGO-DTB2-051), the Natural Science Fundation of China (NSFC 31450110072), EU COST action TD1006, Deutsche Forschungsgemeinschaft (DFG, Koselleck), Eva und Horst Köhler Stiftung, Volkswagen Stiftung and Bundes Ministerium für Bildung und Forschung BMBF MOTOR-BIC (FKZ 13GW0053). A. Sarasola-Sanz's work is supported by La Caixa-DAAD scholarship, E. López-Larraz's work by the Spanish projects HYPER-CSD2009-00067 and DGA-FSE (grupo T04) and N. Irastorza-Landa's work by the Basque Government and IKERBASQUE, Basque Foundation for Science, Bilbao, Spain.

3. Chapter 3: Design and effectiveness evaluation of mirror myoelectric interfaces: a novel method to restore movement in hemiplegic patients

This manuscript has been published as [69].

3.1 Abstract

The motor impairment occurring after a stroke is characterized by pathological muscle activation patterns or synergies. However, while robot-aided myoelectric interfaces have been proposed for stroke rehabilitation, they do not address this issue, which might result in inefficient interventions. Here, we present a novel paradigm that relies on the correction of the pathological muscle activity as a way to elicit rehabilitation, even in patients with complete paralysis. Previous studies demonstrated that there are no substantial inter-limb differences in the muscle synergy organization of healthy individuals. We propose building a subject-specific model of muscle activity from the healthy limb and mirroring it to use it as a learning tool for the patient to reproduce the same healthy myoelectric patterns on the paretic limb during functional task training. Here, we aim at understanding how this myoelectric model, which translates muscle activity into continuous movements of a 7-degree of freedom upper limb exoskeleton, could transfer be-

tween sessions, arms and tasks. The experiments with 8 healthy individuals and 2 chronic stroke patients proved the feasibility and effectiveness of such myoelectric interface. We anticipate the proposed method to become an efficient strategy for the correction of maladaptive muscle activity and the rehabilitation of stroke patients.

3.2 Introduction

There is extensive evidence that the motor system coordinates muscle activations through a superposition of activations of different groups of muscles as single units (i.e. superposition of muscle synergies) that are specified at the spinal or brainstem level [7–9, 106]. Further investigation into the nature and characteristics of the electromyographic (EMG) activity of stroke patients has led to the discovery of abnormal patterns of muscle activations or synergies that may result from maladaptive compensatory strategies [5,6,107]. After a stroke, cortical and/or subcortical damage interferes with the flow of descending signals to the spinal cord, which yields a disrupted recruitment of muscle synergies and so, a pathological muscle coordination [79, 80]. Furthermore, it has been found that the preservation of muscle synergies has a positive correlation with hand functionality in severely paralyzed patients with intact sensorimotor cortex [5]. It follows that this abnormal movement coordination might constitute the primary source of movement dysfunction (spasticity and muscle weakness being secondary [11]) and that the recovery of healthy synergies may be to some extent, linked to the improvement of the upper limb motor function.

Physical therapy is the traditionally accepted rehabilitation method for stroke patients. However, in recent years, robot-aided training has become one of the most widely explored rehabilitation strategies for this type of patients. It allows repetitive, functional, meaningful, intensive and challenging training, which has been proven to promote neuroplasticity and motor learning [24, 108, 109]. Various control signals and strategies have been used for robot-aided rehabilitation therapies. Some devices adapt the provided assistance level based on participant́s

interaction forces [110–112]. Others allow free movements for a fixed time and then move the hand if the participant is not able to complete the task [20–22]. Myoelectric interfaces are often proposed in rehabilitation therapies for the control of body actuators such as wearable robots or prosthesis [74, 113].

A myoelectric interface is a system that decodes the intention of the patient from the electromyographic (EMG) activity of the paretic limb and sends the corresponding commands to the body actuator. This allows patients to generate volitional movement through their normal cortico-spinal pathways and provides them with feedback (e.g. proprioceptive and visual feedback), establishing a closed-loop system that promotes learning. These systems also encourage the active participation of the patient and they can improve muscle coordination and strength and reduce spasticity after training [114]. However, this raises the question of whether it is possible to find decodable EMG activity in hemiplegic patients of any impairment level. Some studies reported a decoding accuracy between 36.7% and 96.1% with 4-20 movement classes using the EMG of the paretic upper limb in mild to severely impaired stroke patients [32–34]. Recently, 46% of the 41 severe chronic stroke patients enrolled in a 1-month brain-machine interface (BMI) training study regained decodable EMG activity (accuracy >65%) [35]. Interestingly, in some cases, decodable EMG was found even in the absence of movement of the paretic arm. These results opened up the door of EMG-based rehabilitation therapies to severely affected stroke patients, who cannot benefit from many other rehabilitation techniques [115], in which residual movement of the paretic limb is necessary.

Among the existing EMG-based control strategies, a simple approach is to trigger a pre-programmed assistive movement when the EMG amplitude goes over a threshold [116]. Other controllers provide assistive forces proportional to the EMG amplitude of the impaired limb [114, 117, 118]. More complex myoelectric control interfaces are based on classification techniques (i.e. mapping the EMG into predefined discrete movements) or on continuous trajectory-decoding strategies (i.e. mapping the EMG into velocity of the movement). Classification techniques have been investigated for the post-stroke rehabilitation showing encouraging but still

limited results [32–34, 36]. On the other hand, continuous decoding strategies offer a more intuitive and natural myoelectric control, which allows for a richer therapy with a wider range of trained and untrained movements, and facilitates a less effortful and fine control, thus leading to a better training and probably by extension, to motor recovery too [37–46]. However, up to now very few studies used such methods to this end [43–45] and they are limited to neurologically intact subjects or allow the simultaneous control of up to 3 degrees of freedom (DoFs) of the upper limb through a virtual reality interface [43] or a cursor on a screen [44]. Liu et al. [45], also used an upper-limb exoskeleton to record EMG activity and kinematics and compute the offline decoding performance. However, their system allows the simultaneous control of 3 DoFs only (angle of the shoulder, angle of the elbow and wrist), which limits the possibility of performing a functional training including the hand joints. Therefore, the development of a rehabilitation system that allows a continuous (i.e. trajectory) and reliable myoelectric control of several proximal and distal DoFs of the upper limb simultaneously still remains a challenge.

Myoelectric interfaces for rehabilitation aim at activating neuroplastic mechanisms that reshape muscle activity and lead to motor learning, and eventually to motor function restoration. However, it could be argued that using a myoelectric decoder calibrated with paretic EMG data (i.e. an ipsilateral myoelectric decoder), could indeed reinforce the existence and maintenance of pathological synergies (i.e. promote "bad" neuroplasticity). Cesqui et al. [34] tackled this problem by building a model of healthy muscle patterns from data collected on 9 healthy participants and using it to classify the paretic EMG of stroke patients into reaching movements towards 4 different positions. Although this is the only approach designed to enhance the recovery of healthy activations, it is limited by: i) the necessity of forming a large database of EMG activity from healthy subjects to generalize to the specific anatomical and neurophysiological characteristics of each patient and ii) the fact that the decoder was confined to the classification of the EMG activity into four discrete movements, involving only proximal joints.

Here, we propose a new upper limb rehabilitation paradigm for stroke patients that overcomes the aforementioned limitations and puts special emphasis on the re-

covery of healthy and natural muscle activation patterns or synergies. We present a novel myoelectric interface that decodes the patient′s EMG into the direction and speed of a 7-DoF upper limb exoskeleton during functional tasks. Previous evidence [79,80] indicates that there are no substantial inter-limb differences in the synergy structure of healthy individuals. Hence, our myoelectric decoder, which we will refer to as the mirror myoelectric decoder, is calibrated with data mirrored from the healthy upper limb of the patient and serves as a reference model and a learning tool for him/her to reshape his/her muscle activation patterns. We present and evaluate the effectiveness of the proposed rehabilitation system in 8 healthy individuals and 2 chronic stroke patients.

3.3 Methods

3.3.1 Novel rehabilitation paradigm

Our novel motor rehabilitation paradigm is designed to reshape the muscle activation patterns of chronic stroke patients. It is intended to be used as part of a closed-loop rehabilitation system. In our setup, the IS-MORE 7-DoF robotic exoskeleton (Tecnalia, San Sebastian, Spain) acts as the body actuator that provides the patient with proprioceptive and visual feedback during functional task training.

The steps to build and utilize the rehabilitation system are summarized in Figure 3.1. First, EMG and kinematic data is acquired from the healthy upper limb of the hemiplegic patients while they perform a series of functional tasks with an exoskeleton. This data is utilized to build a subject-specific model of healthy EMG-to-kinematics mirrored to be used by the paretic arm (i.e. the DoFs that have opposite sign for left and right arms are flipped before building the model). Then, this model would be used to provide feedback about the EMG of the paretic upper limb. Thus, it would serve as a learning tool for the patient to reproduce the same correct healthy muscle activation patterns that have been mirrored to the paretic side. During the real-time operation, patients would try to perform similar functional tasks while wearing the exoskeleton and having EMG electrodes placed over the equivalent muscles on the impaired limb. In this phase, the myoelectric

Table 3.1: *Design of the two experiments. Differences and similarities between them.*

Sessions	**Experiment Healthy Participants**			**Experiment Healthy Participants**				**Experiment Stroke Patients**	
	S1	**S2**	**S3**	**S4**	**S5**	**S6**	**S7**	**S1**	**S2**
Purpose	1. Influence of the session-to-session and arm-to-arm transfers on the decoding performance 2. Generalization ability of mirror decoders			Compliance conditions for the calibration session				Preliminary tests of the effectiveness of the system in stroke patients	
Participants	8 healthy individuals			5 healthy individuals				2 chronic stroke patients	
Arm side	Right	Right	Left	Right	Left	Left	Right	Right (healthy)	Left (paretic)
Tasks	T1, T2, T3, T4 + Free movements			T1, T2, T3				T1, T2 (Patient 1); T1, T2, T3, T4 (Patient 2)	
Compliance	Active			Active	Active	Compliant	Compliant	Compliant	

interface would receive the paretic EMG signals as input and would predict the corresponding kinematics based on the mirror model. The predicted kinematics would determine the movement of the exoskeleton. In this way, this closed-loop system would provide the patient with visual, haptic and proprioceptive feedback about his/her muscle activations. For example, if the patient produces uncoordinated activation patterns the exoskeleton would deviate from the intended trajectory or move at a lower speed (depending on the control strategy). Hence, patients would have to modulate their EMG activity to produce the correct patterns that would bring the exoskeleton towards the target position. Thus, the purpose of this novel rehabilitation paradigm is to provide patients with feedback about the appropriate recruitment of their muscles, rather than only interpreting their motion intention independently of whether the EMG shows correct activation patterns for the intended movement or not.

3.3.2 Study design

One experiment in 8 able-bodied individuals and one proof of concept in 2 chronic stroke patients were performed to investigate the optimal parameters and validate the effectiveness of the system. Each of them was performed under slightly different conditions (see Table 3.1) and served to analyze various features of the system:

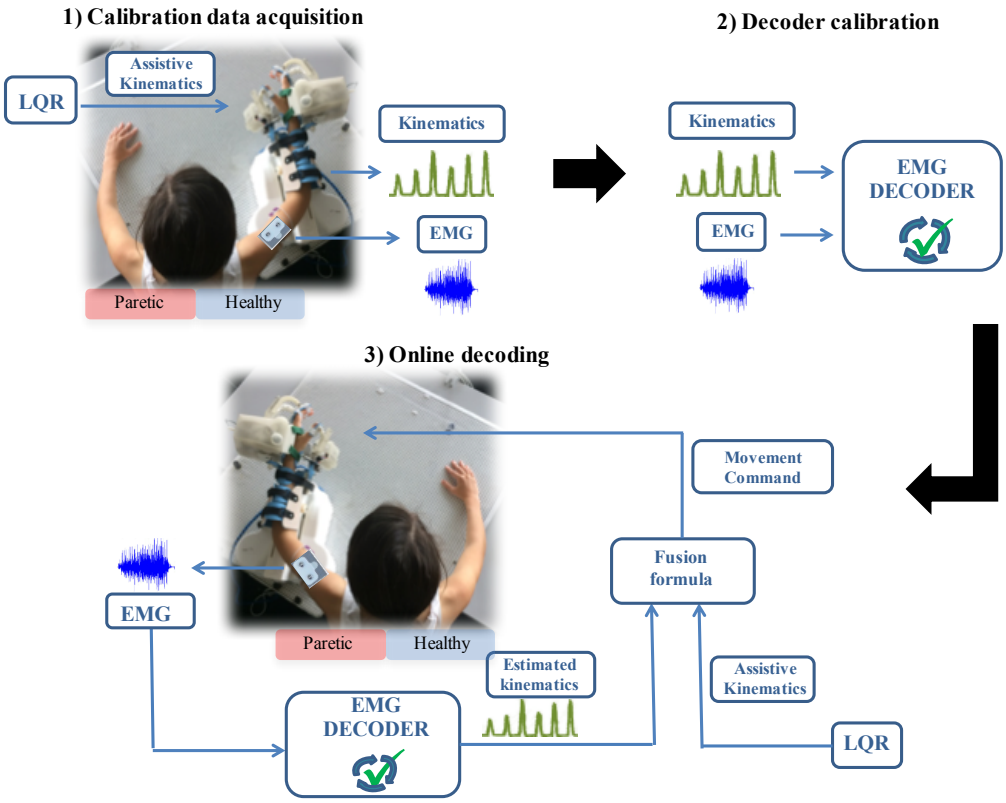

Figure 3.1: *Steps to follow to build and use a mirror myoelectric decoder: 1) Calibration session: EMG and kinematic data are recorded from the healthy upper limb during different functional movements with the exoskeleton. 2) The recorded data is used to calibrate a mirror EMG decoder (i.e. build a healthy EMG-kinematics mirror model). 3) The EMG activity recorded from the paretic limb during the real-time phase is fed to the mirror decoder. The latter is able to map the input EMG signal into the corresponding kinematics based on the mirror myoelectric model of healthy activity. The estimated kinematics are sent as control commands to the exoskeleton, which drives the movement of the paretic upper limb of the patient, providing him/her with visual and proprioceptive feedback.*

1) *Studying the influence of the session-to-session and arm-to-arm transfers on the decoding performance.* Factors such as varying upper limb positions, impedance changes, electrode shifts across days, and the EMG activity pattern disparity across arms might dramatically alter the decoding accuracy. We evaluated the influence of these factors on the performance of within- and across-sessions and -arms decoders.

2) *Generalization ability of the mirror decoder.* As new tasks or movement with bigger range of motion could be included during the therapy, we assessed the decoderś ability to decode untrained movements, which were not present in the calibration data. We compared several task-specific decoders with a single general decoder, considering properties such as practicality and accuracy.

3) *Optimal conditions for calibration data recording.* Two conditions were considered to record the calibration data: i) Active: the motors of the exoskeleton were off and users had to overcome the friction and weight of the robot (i.e., the robot was used as a kinematic sensing device only), ii) Compliant: the motors of the exoskeleton on, being the exoskeleton the one driving the fully-assistive movement. The users were explicitly asked to follow it trying to naturally activate their muscles and to avoid counteracting or forcing the movement of the exoskeleton.

4) *Proof of concept with chronic stroke patients.* This experiment was designed to test the offline performance of the general mirror decoder in chronic stroke patients.

3.3.3 Experimental Protocol

None of the healthy participants presented any neuromuscular disorder. All healthy participants and patients gave written informed consent to the procedures as approved by the ethics committee of the Faculty of Medicine of the University of Tübingen, Germany. All the experiments were performed according to the guidelines of the University of Tübingen and constitute a proof of concept for the clinical trial registered on the 5th of February of 2018 with the registration ID: DRKS00013926. Healthy participants and patients were asked to sit and perform

a series of functional tasks while wearing an upper limb exoskeleton either on their right or left arm (see Table 3.1). The IS-MORE exoskeleton allowed movements in 7 DoFs, including proximal (upper- and forearm) and distal (fingers and wrist) segments of the arm. The setup consisted of four coloured targets located on both sides and in front of the participant, and a 70 x 50 cm mat on top of which the exoskeleton was placed and the movements were executed (see Figure 3.2). Healthy participants and patients were instructed by means of auditory cues to perform up to four different functional tasks, which always started and ended at a predefined rest position that kept the arm and the hand in a relaxed configuration:

T1) Reaching task. This task 1 consisted of reaching movements from the rest position towards each of the four different targets and then back to the initial rest position.

T2) Static grasping task. Participants were asked to keep their arm still at the rest position while performing five different movements that involved finger and wrist joints: pinch grip, cylindrical grasp, pointing, supination and pronation of the wrist (see Figure 3.2).

T3) Double reaching + pointing task. First, participants had to reach one target while pointing at it, then move to another target while keeping the pointing gesture and finally come back to the initial rest position.

T4) Double reaching + object grasping task. Participants were instructed to reach a target, grab the object placed at that position, bring it to a different target position in which they had to deposit it and then come back to the initial rest position. Three objects of different sizes and shapes, which required performing a pinch grip, a key grip or a cylindrical grasp to take them, were presented to the participants.

Each of the four tasks was divided in 5 blocks of 40, 42, 10 and 22 trials, respectively. For the experiment with stroke patients, sessions were notably shorter ranging from 2-4 blocks depending on the self-reported fatigue and containing 8, 10, 6 and 6 trials each of the four tasks respectively. All participants could rest for a few minutes between blocks and inter-trial intervals of 2-3 secs were included

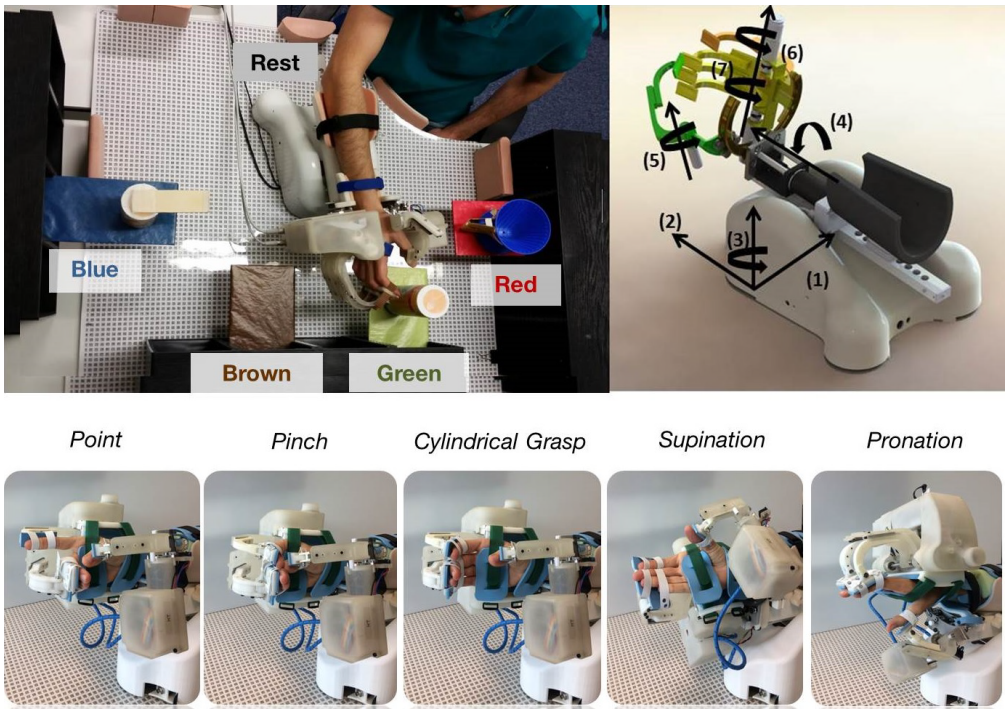

Figure 3.2: *Experimental setup and tasks performed: (a) Workspace where the tasks were performed. Pos 1-4 indicate the four colored targets and Rest the predefined rest position in which the trials started and ended. The three objects the participants had to interact with are also shown on top of the target shelves. (b) A model of the IS-MORE 7-DoF exoskeleton and the degrees of freedom on which it allows the movement: (1) and (2): translation of the forearm (2 DoFs); (3): rotation of the forearm (1 DoF); (4): wrist pronation-supination (1 DoF); (5): extension-flexion of the thumb (1 DoF), (6): the index (1 DoF) and (7): the group of middle-ring-pinky fingers (1 DoF). (c) Wrist and hand movements performed during the experiments.*

to avoid fatigue. Tasks T1-T4 were always performed in this order, completing all the blocks of each task before moving onto the blocks of the next task type.

3.3.4 Healthy participants

Eight healthy individuals (3 females, 5 males, age: 20-28, all right-handed) underwent three sessions (S1: right upper limb; S2: right upper limb; S3: left upper limb) on distinct days.

The four functional tasks explained above were included in this study. Additionally, at the end of each session subjects were asked to move their upper limb freely around the whole workspace (Free-Movement Task) during 3 minutes, without any time constraint, predefined task or trial structure. These three sessions S1-S3 were used to analyze the session-to-session and arm-to-arm influence on the decoding performance as well as the generalization ability of task-specific and general decoders (analyses 1 and 2).

It is important to emphasize that in these three sessions the exoskeleton was passive (i.e. Active condition from the user perspective, exoskeleton motors were off) and hence, subjects had to exert sufficient force to move the exoskeleton towards the required target position without any type of assistance.

In order to investigate the optimal way of recording the calibration data (analysis 3), five of the eight healthy participants (3 females, 2 males, age: 21-28, all right-handed) underwent four more sessions (S4: right upper limb; S5: left upper limb; S6: left upper limb; S7: right upper limb) on separate days. In these extra sessions S4-S7, the first three tasks of the set of functional tasks described above (T1, T2 and T3) were included. In sessions S4 and S5, just as in the previous S1-S3, no assistance was provided for the movement of the exoskeleton (i.e. Active condition). In sessions S6 and S7 participants performed the tasks with the exoskeleton actively moving their arm and participants following that exact movement (i.e. Compliant condition).

During the active condition sessions, participants could execute the movements

at their own pace but within a given time interval (5 secs for task 1 trials, 4 secs for task 2 trials, 8 secs for task 3 trials and 8 secs for task 4 trials). During the compliant sessions, instead, the direction and speed of the movement was predefined and customized for each participant according to their range of motion and kept constant among the various trials of each task.

3.3.5 Stroke patients

Two chronic stroke patients (2 males, Patient 1 (P1): age = 47 years, time since stroke = 5 years, moderate left hemiparesis according to [119], modified upper limb FMA = 87/114 and combined hand and arm FMA = 29/54; Patient 2 (P2): age = 62 years, time since stroke = 2 years, severe left hemiparesis, modified upper limb FMA = 59/114 and combined hand and arm FMA = 7/54) participated in this experiment consisting of two sessions (S1: healthy upper limb; S2: paretic upper limb) on different days. In both sessions, movements were executed under Compliant conditions. Regarding the tasks, P1 performed 4 blocks (healthy arm) and 1 block (paretic arm) of the first two functional tasks described above (T1-T2) while P2 carried out a training including 2 blocks (healthy and paretic arms) of the four tasks (T1-T4).

3.3.6 Data collection and processing

In healthy participants, EMG activity was recorded at 2500 Hz (Brain Products GmbH, Germany) from 10 standard bipolar electrodes with an inter-electrode distance of 2.2 cm (Myotronics-Noromed, USA) over: 1) the abductor pollicis longus, 2) the extensor carpi ulnaris, 3) the extensor digitorium, 4) the flexor carpi radialis, palmaris longus and flexor carpi ulnaris, 5) the pronator teres, 6) the long head of the biceps, 7) the external head of the triceps, 8) the anterior portion of the deltoid, 9) the lateral portion of the deltoid and 10) the posterior portion of the deltoid over the teres minor and infraespinatus muscles. Kinematics were recorded at 18Hz (details in [68, 103]).

EMG data was band-pass filtered at 10-500 Hz and power-line notch filtered at 50 Hz. Seven time-domain features (Mean of absolute values, Variance, Wave-

form Length, Root-mean-square value, Willison Amplitude (WAMP), Zero crossing (ZC) and Slope sign changes (SSC)) [46, 104] were extracted from each EMG channel in windows of 200 ms producing a set of 70 EMG features. This set of EMG features was down-sampled to 18 Hz and synchronized with the kinematic data, which was low-pass filtered at 1.5 Hz.

The EMG signal was normalized as in an online setup, using the mean and standard deviation computed in a 60sec-window of past samples. The estimated kinematics were smoothed with a weighted moving average filter (backwards window of 550 ms and linearly decreasing weights) to avoid a jerky and unstable control of the exoskeleton.

All the EMG channels were included in the control of each DoF, independently of them being directly, indirectly or not related at all to the movement of that specific DoF. Since this rehabilitation approach relies on the feedback given to the patients as a way of teaching them to recover healthy muscle activation patterns, including all the muscles in the control of each DoF could help them to avoid compensatory activations of non-related muscles.

For patients, EMG data was recorded at 1000 Hz. P2 used the same 10 bipolar electrodes as healthy participants. However, for the patient P1 the 5 bipolar electrodes over the extensor and flexor muscles of the forearm were substituted by two high-density arrays (Tecnalia, Spain) including 24 (6 x 4) monopolar electrodes each with an inter-electrode distance of 1.35 cm (horizontal) and 2 cm (vertical). These monopolar channels were bipolarized summing up to 100 channels and no dimensionality reduction was applied.

The three time-domain threshold-dependent features (i.e. WAMP, ZC and SSC) were removed from the processing to avoid any inaccuracies arising from the different EMG amplitude across arms. Instead, the logarithm of the variance was included as the fifth component of the feature set.

3.3.7 Decoding schemes and algorithm

We compare ipsilateral (within arm) and mirror (across arms) decoding schemes:

Ipsilateral decoding schemes:

- Within-session decoder (WS): This decoder was calibrated and tested with data from the same session and arm, following a 5-fold cross-validation [68].
- Session-to-session decoder (SS): This decoder was calibrated with data from one session and tested with data from a different session in which the movements were performed with the same arm.
- Re-calibrated session-to-session decoder (RSS): About 10 minutes of data collected at the beginning of the new session together with the data from the previous session were used to calibrate a new ("re-calibrated") session-to-session (SS) decoder [68]. The testing was performed on the remaining data of the new session.

Mirror decoding schemes:

- Task-specific arm-to-arm decoder (TSAA): This decoder was task specific and was calibrated with data from a specific task during a session(s) with one of the arms and tested during that same task from a different session using the other arm.
- General arm-to-arm decoder (GAA): This decoder was also calibrated and tested with data from different arms. However, this was the only decoder that gathered all the performed tasks in one decoder and thus, was not task-specific.

All the aforementioned ipsilateral and mirror decoders were subject-and DoF-specific. Figure 3.3 Illustrates all the variations of the decoding schemes that were analyzed in this study.

The ridge regression algorithm was selected to predict the output kinematics of each DoF from the input EMG features. Although this linear algorithm has several

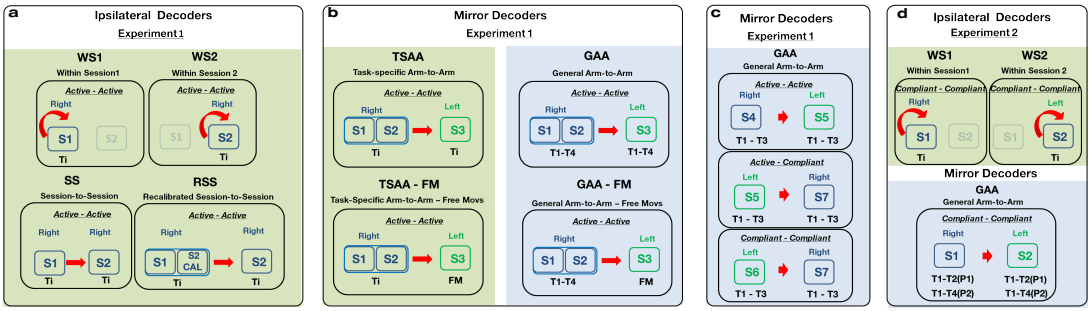

Figure 3.3: *Ipsilateral and mirror decoders built with data from the two experiments: (a) Ipsilateral and (b) mirror decoders from sessions S1-S3 of the experiment with healthy participants. (c) Mirror decoders from sessions S4-S7 of the experiment with healthy participants. (d) Ipsilateral and mirror decoders from the experiment with stroke patients. For the four diagrams, the information to the left of the red arrow refers to the calibration data and the one the arrow is pointing to, to the testing data. The green background color indicates that the decoders are task-specific, whereas the blue background color signifies that the decoders where general. The tasks that were used for calibrating and testing are displayed at the bottom left and right of the squared box of each decoder respectively. For the task-specific decoders, Ti indicates that a separate decoder was built for each of the four tasks Ti, i = 1-4. For the general decoders, Tk-Tj means that all the tasks from k to j were used for calibrating and/or testing a decoder. FM stands for the free movement task. The mirror decoder of the experiment with stroke patients specifies the tasks employed for each of the patients P1 and P2. The "Left" and "Right" labels specify which limb the participants wore the exoskeleton on during that session. Finally, the "Active-Active", "Active-Compliant" and "Compliant-Compliant"labels inform about the compliance conditions under which the "calibration- testing" data was recorded.*

limitations (e.g. various activation patterns could lead to the same kinematics), it allows the simultaneous and proportional control over multiple DoFs, it was also proven to outperform other methods such as the regular Kalman filter [68] and to perform similar to non-linear regression methods online [120], and it penalizes the co-activation of agonist-antagonist pairs, which is an important aspect for stroke rehabilitation. The optimum value of the regularization parameter λ for the WS schemes was found in a nested cross-validation loop using a grid search of values in the range $[10^{-7}, 10^{7}]$. However, for the rest of the decoding schemes λ was fixed at 10^{4}, chosen experimentally [71].

3.3.8 Statistics

The EMG-decoding was computed offline in a pseudo-online manner (i.e. streaming the data into the decoder as in a real-time scenario). The decoding performance was measured by comparing the smoothed kinematics predicted from the EMG activity and the smoothed kinematics recorded with the exoskeleton. The Pearson correlation coefficient (CC) and the normalized root-mean-square error (NRMSE) were used as performance metrics. The overall performance of each decoder was computed as the average over the 7-DoFs, all the tasks and all the participants of each experiment. The α -level for all the statistical tests was set to 0.05.

The statistical tests applied to the four analyses described above are:

1) After checking for the normality of the data distribution, all the ipsilateral and mirror decoders utilized to study the session and arm transfer influence (Figure 3.3a and 3.3b) were compared with a one-factor repeated measures analysis of variance (ANOVA), being the factor the decoding scheme. Significant results were followed by post-hoc pairwise comparisons using paired t-tests with Bonferroni correction.

2) A paired t-test was computed to compare the generalization ability of the mirror decoders tested only in the unrestricted free movements (FM) (i.e. TSAA-FM vs. GAA-FM of Figure 3.3b).

3) The performance of the general decoders calibrated and tested under Active or Compliant conditions (Figure 3.3c), were compared with a 1-factor (com-

pliance condition) ANOVA test, followed by Bonferroni-corrected post-hoc comparisons.

4) Finally, the general mirror decoder was tested in stroke patients (Figure 3.3d) and its performance was reported for each patient separately.

3.4 Results

Session-to-session and arm-to-arm transfers' influence

The session-to-session and arm-to-arm transfer influence due to factors such as electrode shift and inter-limb variability was assessed by comparing the performance of ipsilateral and mirror decoders (Figure 3.3a and 3.3b). The performance for each of them is presented in Figure 3.4. The ANOVA showed significant differences between these decoders for both the CC ($p < 10^{-6}$) and NRMSE ($p = 4.0 \cdot 10^{-6}$). Subsequent Bonferroni-corrected pairwise comparisons (see Table 3.2) showed that the within-session and recalibrated decoders (WS1, WS2 and RSS) outperformed the other three (SS, TSAA and GAA) in terms of CC. However, no significant difference was found between the CC values of the session-to-session (SS) and the two mirror (TSAA and GAA) decoders. The error of the general arm-to-arm decoder (GAA) was significantly lower than all the others except the within-session decoder of session S2 (WS2).

Generalization ability of the mirror decoding schemes

Table 3.2 shows the lower error ($p = 1.7 \cdot 10^{-5}$) of the general mirror decoder GAA compared to the equivalent task-specific one TSAA, when tested in tasks T1-T4 that were included in the calibration set. Additionally, these two mirror decoders were tested during free movements (TSAA-FM and GAA-FM) and their comparison confirms the significantly better generalization ability of the general decoder compared to the task-specific one (CC: $p = 0.012$; NRMSE: $p = 0.017$) (see Figure 3.5).

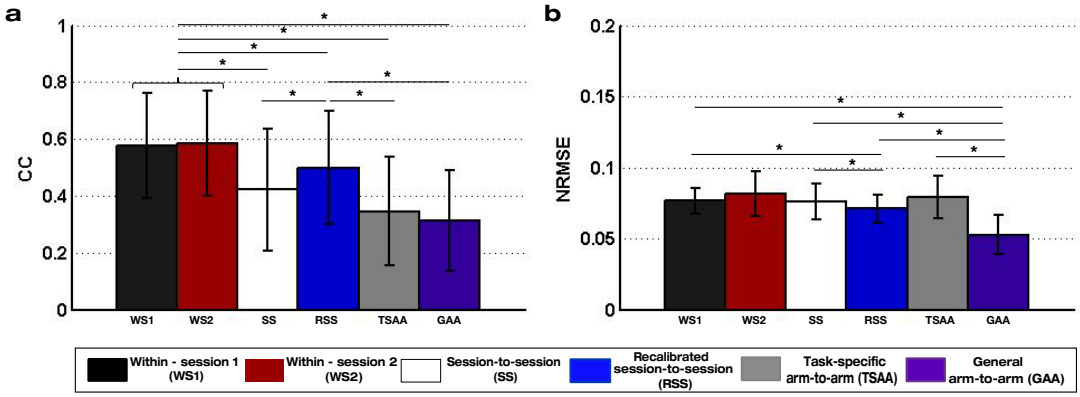

Figure 3.4: *Performance values of the ipsilateral and mirror decoders from sessions S1-S3 of the experiment with healthy participants: (a) Correlation coefficient (CC) and (b) normalized root-mean-square error (NRMSE) mean and standard deviation values of the ipsilateral decoders: within-session (WS1 and WS2), session-to-session (SS) and recalibrated session-to-session (RSS); and the mirror decoders: task-specific arm-to-arm (TSAA) and general arm-to-arm (GAA) decoders of the experiment with healthy participants. The asterisks show significant ($p < 0.05$) differences between decoders.*

Table 3.2: *Bonferroni corrected p-values of the ANOVA test comparing the correlation coefficient (CC) and normalized root-mean-square error (NRMSE) of the decoders from sessions S1-S3 of the experiment with healthy participants. In bold all p-values < 0.05 (significance level).*

	Within-session 2 (WS2)	**Session-to-session (SS)**	**Recalibrated session-to-session (RSS)**	**Task-specific arm-to-arm (TSAA)**	**General arm-to-arm (GAA)**
WS1	p_{CC} = 1.000 p_{NRMSE} = 1.000	**$p_{CC} = 3.2 \cdot 10^{-4}$ ($CC_{WS1} > CC_{SS}$) p_{NRMSE}** = 1.000	**$p_{CC} = 0.005$ ($CC_{WS1} > CC_{RSS}$) $p_{NRMSE} = 0.032$ ($NRMSE_{WS1} > NRMSE_{RSS}$)**	**$p_{CC} = 1.0 \cdot 10^{-5}$ ($CC_{WS1} > CC_{TSAA}$)** p_{NRMSE} = 1.000	**$p_{CC} = 1.7 \cdot 10^{-5}$ ($CC_{WS1} > CC_{GAA}$) $p_{NRMSE} = 2.1 \cdot 10^{-5}$ ($NRMSE_{WS1} > NRMSE_{GAA}$)**
WS2		**$p_{CC} = 1.5 \cdot 10^{-5}$ ($CC_{WS2} > CC_{SS}$)** p_{NRMSE} = 1.000	**$p_{CC} = 4.7 \cdot 10^{-4}$ ($CC_{WS2} > CC_{RSS}$)** p_{NRMSE} = 1.000	**$p_{CC} = 2.5 \cdot 10^{-5}$ ($CC_{WS2} > CC_{TSAA}$)** p_{NRMSE} = 1.000	**$p_{CC} = 9.2 \cdot 10^{-5}$ ($CC_{WS2} > CC_{GAA}$)** p_{NRMSE} = 0.157
SS			**$p_{CC} = 0.003$ ($CC_{SS} < CC_{RSS}$) $p_{NRMSE} = 0.023$ ($NRMSE_{SS} > NRMSE_{RSS}$)**	p_{CC} = 0.057 p_{NRMSE} = 1.000	p_{CC} = 0.05 **$p_{NRMSE} = 7.2 \cdot 10^{-4}$ ($NRMSE_{SS} > NRMSE_{GAA}$)**
RSS				**$p_{CC} = 1.1 \cdot 10^{-4}$ ($CC_{RSS} > CC_{TSAA}$) p_{NRMSE} = 0.207**	**$p_{CC} = 4.2 \cdot 10^{-4}$ ($CC_{RSS} > CC_{GAA}$) $p_{NRMSE} = 0.002$ ($NRMSE_{RSS} > NRMSE_{GAA}$)**
TSAA					p_{CC} = 0.139 **$p_{NRMSE} = 1.7 \cdot 10^{-5}$ ($NRMSE_{TSAA} > NRMSE_{GAA}$)**

In bold all p-values < 0.05 (significance level).

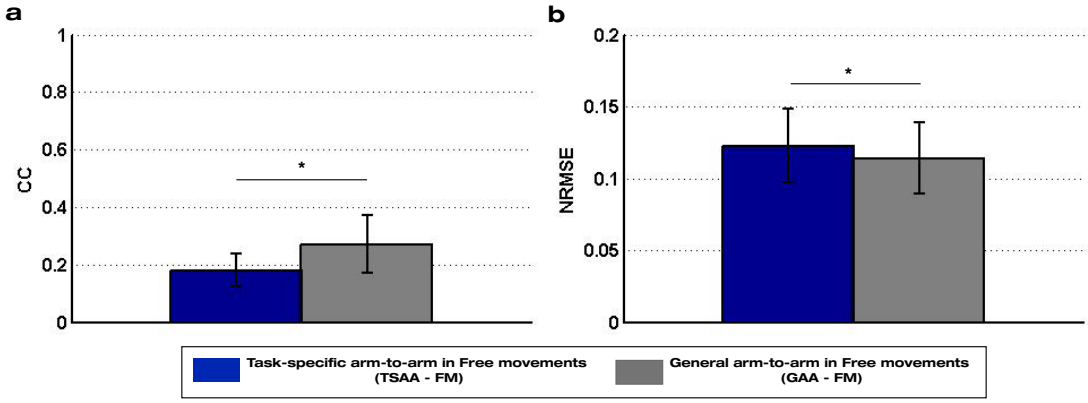

Figure 3.5: *Performance values of the mirror decoders from sessions S1-S3 of the experiment with healthy participants tested on free movements: (a) Correlation coefficient (CC) and (b) normalized root-mean-square error (NRMSE) mean and standard deviation values of the task-specific arm-to-arm (TSAA-FM) and general arm-to-arm (GAA-FM) decoders tested on the three minutes of free movements of the experiment with healthy participants. The asterisks show significant ($p < 0.05$) differences between decoders.*

Optimal conditions for calibration data recording

Three variants of the general mirror decoder were built (Active-Active; Active-Compliant; Compliant-Compliant), which differed in the active or compliant condition of the calibration and testing datasets (see Figure 3.3c). No significant differences between the CC values of the three decoders were found ($p = 0.089$). However, the Active-Active decoder outperformed the other two cases in terms of NRMSE (Active-Compliant: $p = 0.002$; Compliant-Compliant: $p = 0.005$). The error of the Compliant-Compliant case was also significantly ($p = 0.049$) lower than that of the Active-Compliant decoder (See Figure 3.6).

Proof of concept with chronic stroke patients

The effectiveness of the mirror decoder was evaluated in two chronic patients with moderate and severe paralysis. Both patients reported a good acceptance of the system, the exoskeleton ergonomics and mobility as well as the speed and complexity of the movements. Ipsilateral within-session decoders were also evaluated

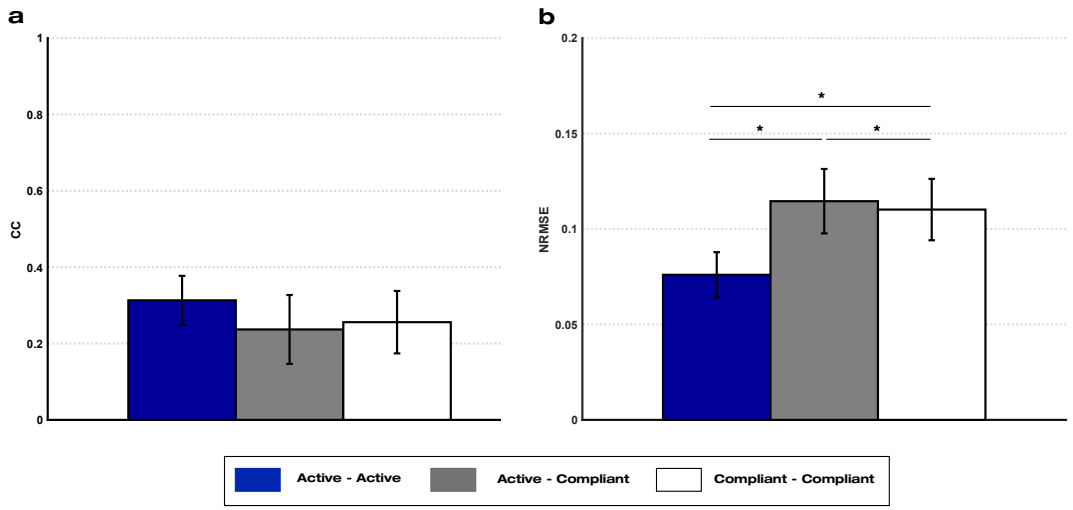

Figure 3.6: *Performance values of the mirror decoders from sessions S4-S7 of the experiment with healthy participants: (a) Correlation coefficient (CC) and (b) normalized root-mean-square error (NRMSE) mean and standard deviation values of the general arm-to-arm (GAA) decoder with different compliance conditions for the calibration and testing data. The asterisks show significant ($p < 0.05$) differences between decoders.*

both for the healthy and paretic arms of each patient. Figure 3.7 illustrates the performance of the ipsilateral and mirror decoders for patients P1 (left; moderate impairment) and P2 (right; severe impairment). As expected, the within-session decoder WS1 of the healthy arm shows the highest performance values for both patients. We found variable and poor decoding performance for the within-session decoders WS2 of the paretic arm, as paretic EMG patterns are highly variable and abnormal. Moreover, it should be noticed that for P1 patient only 1 block of data of tasks T1 and T2 was recorded and thus, the 5-fold cross validation of WS2 was computed with little data. The values of the general arm-to-arm decoder (GAA) reflect a performance drop compared to WS1, due to the transfer across arms and the pathological EMG activity of stroke patients. Since the performance metrics show how similar the kinematics decoded from the paretic EMG are to the real kinematics determined by the assister, pathological EMG activity produces kinematics that deviate from the ideal trajectory and thus, lead to poor performance values. There is also a rather variable performance across DoFs for P1 compared

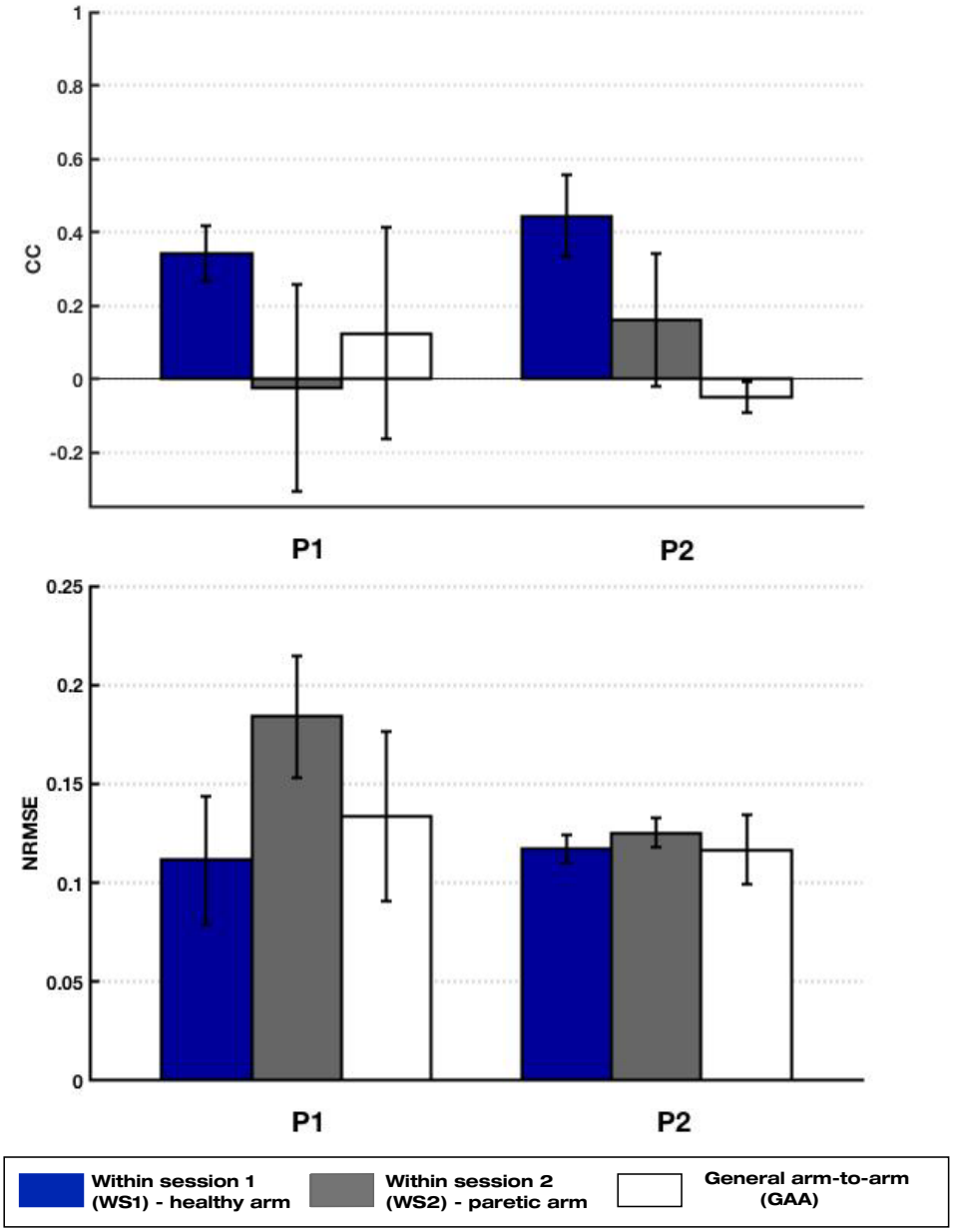

Figure 3.7: *Performance values of the ipsilateral and mirror decoder from the experiment with chronic patients: (a) Correlation coefficient (CC) and (b) normalized root-mean-square error (NRMSE) mean and standard deviation values of the within-session decoder WS1 of the healthy arm (blue), the within-session decoder WS2 of the paretic arm (grey) and the general arm-to-arm GAA decoder (white) for P1 (left) and P2 (right) patients.*

to P2, as reflected in the larger standard deviation values. The correlation coefficient of patient P2 reached negative values due to the severe impairment and the existence of pathological muscle activations. However, these values are expected to raise as the patient learns the mirror mapping and the impairment level is reduced, as inferred from the higher CC values of patient P1 with moderate impairment. The mean error plot shows highest error values for the WS2 of the paretic arm and comparable values for the WS1 and GAA decoders for both patients.

3.5 Discussion

In this study, we presented a novel rehabilitative concept that turns the focus of the existing myoelectric interfaces by enhancing the recovery of healthy muscle activation patterns. Furthermore, we tested and validated it on 8 healthy participants and 2 chronic stroke patients.

The significant performance difference between the within-session and the session-to-session decoders confirms that variables such as electrode position shift and impedance changes can affect the decoding accuracy. On the other hand, the difference between the session-to-session (SS) and the mirror decoders (TSAA and GAA) was not significant. This implies that the inter-limb variability of the EMG patterns is not big enough to produce a significant drop in the decoding performance, as suggested by previous studies [79, 80]. This supports the use of the mirror decoder as a reference model for the paretic limb in the rehabilitation of stroke hemiplegic patients. Although a recalibrated decoder with data from the paretic arm could raise the decoding accuracy, this option was not considered since the aim of the mirror decoding paradigm is to impose the model of healthy activity on the paretic arm so that they can correct their pathological activity, instead of using it to decode their motion intention as accurately as possible.

The generalization analysis shows that the general decoder outperforms the task-specific one, especially when decoding EMG data from untrained tasks (TSAA-FM vs. GAA-FM). Utilizing a general decoder would avoid the need of switching

between decoders depending on the task being executed at that moment. In addition, the general decoder would be advantageous to decode new tasks included in the course of the intervention or movements with a bigger range of motion, as the patient recovered certain motor function. On top of that, less data would be needed to calibrate a single general decoder than several task-specific decoders, as demonstrated by the analysis with equally balanced calibration datasets (TSAA-FM vs. GAA-FM). Therefore, it would be more practical and accurate to build a general decoder than various task-specific decoders. This knowledge was applied to further develop, optimize and test our platform in the experiment with stroke patients.

The decoder calibrated and tested under Active conditions (i.e. Active-Active) performed better than the other two cases. However, it should be noticed that the Active-Active decoder was trained with data from the fourth session of training with the dominant arm (S4) while the other decoders were trained with the first (S5) or second session (S6) of the non-dominant arm, which might have biased the results. Despite the higher performance of the Active-Active decoder, the possibility of employing such methodology with severely paralyzed patients is doubtful, as most of them would not be able to move the exoskeleton by themselves. Hence, considering patients′ impairment with a weak or atrophied musculature, the operation of the myoelectric interface with the paretic limb would have to be done under compliant conditions. Moreover, the movement of the exoskeleton is intended to be used as feedback for the patients to correct their paretic activity patterns. Therefore, the question is whether to calibrate the system with data from active (Active-Compliant case) or compliant movements (Compliant-Compliant case) with the healthy upper limb. On one hand, following and adapting to the pace and trajectory of the exoskeleton during a compliant movement may be challenging and the risk that the patients remain passive exists. That is why EMG should be continuously tracked and participants should be repetitively reminded that the movement had to be followed actively and as naturally as possible. The results show a lower error achieved by the Compliant-Compliant case over the Active-Compliant approach, indicating that if the conditions of the calibration and testing sessions are the same (Compliant-Compliant) the activation patterns

might be more similar to each other. Moreover, performing the tasks with the healthy arm under compliant conditions may help the patient to get used to the pace and velocity profiles of the exoskeleton movements before the operation phase starts. Therefore, we propose using Compliant conditions during the calibration phase as a novel and optimal method to collect data to train a myoelectric decoder for rehabilitation therapies with stroke patients.

The presence of pathological muscle activity in chronic stroke patients is reflected in the poor correlation and large error values between the real recorded kinematics and the ones predicted from the EMG activity (Figure 3.7, GAA decoder). As expected, the within-session decoder WS1 of the healthy arm of patients was the most accurate one, as this represents how good the decoder could estimate the kinematics without arm-to-arm, session-to-session or task-to-task variability. The transfer across arms, sessions and tasks, and the existence of pathological EMG activity resulted in a performance drop for the mirror decoder GAA. Although the number of channels for patient P1 was notably larger than for P2, the decoding performance of WS1 was lower for P1 than for P2, implying that the lower performance of the mirror decoder GAA for P2 compared to P1 might be mainly influenced by the severity of the impairment, measured by the clinical scales. Therefore, the higher the paresis and the spasticity level, the lower the EMG decoding performance values and the poorer the control. The lower performance achieved by the patients compared to the healthy participants supports this conclusion too (see Figures 3.4 and 3.7). From these results, one could infer that the modular organization of the muscle activity of the patient with moderate paralysis (P1) may resemble more that of a healthy individual, whereas rather pathological patterns could probably be found when looking at the EMG activity of patient P2, with severe paralysis. We anticipate that in a longitudinal study with severe patients, the initial performance will be poor and the real-time control unskilled. Alternatively, those patients with poor or no decodable muscle activity could initially train with an EEG-brain-machine-interface (EEG-BMI) [49, 50, 59, 60, 83] or a hybrid BMI [61, 66, 71] until they recovered sufficient EMG activity to benefit from a myoelectric therapy. We foresee that as patients train with this mirror myoelectric interface, the modular organization of the EMG activity will resem-

ble more that of their healthy upper limb. Thus, the decoding performance and control of the exoskeleton would become more skillful and accurate, eventually leading to the recovery of certain degree of motor function. Nonetheless, in order to demonstrate such hypothesis, a longitudinal study including the assessment of the muscle synergy structure evolution and the functional impairment level along the intervention would be needed.

Overall, the proposed rehabilitation paradigm brings in several assets. First of all, it offers a well-founded [79,80] method to promote the reintegration of healthy muscle activation patterns on the paretic limb of stroke patients, by utilizing the synergy structure of their intact upper limb as reference. Furthermore, this system is the first one that allows the simultaneous and continuous (direction and speed) myoelectric control of 7 DoFs of the upper limb, involving proximal and distal joints. This enables the training of functional multi-DoF movements of the upper limb in a synergistic fashion, which facilitates the translation of the re-learned motor skills to activities of daily living [6,47]. Additionally, it includes several features that are of paramount importance for the activation of neuroplastic mechanisms such as, closed-loop control with online contingent visual and proprioceptive feedback [49, 59, 60], improved perception and constant active participation and engagement of the patient in the task [121, 122]. Lastly, the majority of the stroke population could benefit from this type of therapy, since the only requirement is the presence of decodable EMG activity even in the complete absence of movement of the paretic limb, which has been found even in severely impaired patients [35]. The results presented here aided in the definition of certain aspects such as the calibration data conditions, and validated the effectiveness of the system in chronic stroke patients. Therefore, we envisage this approach to be a potential rehabilitation method to elicit the recovery of healthy muscle recruitment patterns in stroke patients of a wide range of impairment levels. Nonetheless, further developments such as the implementation of synergy-based algorithms that have been reported reliable and robust [123, 124] could be implemented to boost the decoding performance and to ensure that different muscle activation patterns do not lead to the same kinematics. In the future, a longitudinal study that includes the real-time operation of the interface by stroke patients should be carried out in order to assess

the rehabilitation effects of the proposed method.

3.6 Acknowledgements

This study was funded by the Baden-Württemberg Stiftung (GRUENS ROB-1), the Deutsche Forschungsgemeinschaft (DFG, Koselleck), the Fortüne-Program of the University of Tübingen (2422-0-0), and the Bundes Ministerium für Bildung und Forschung BMBF MOTORBIC (FKZ 13GW0053), AMORSA (FKZ 16SV7754), Gipuzkoa Regional Government (INKRATEK), Ministry of Science of the Basque Country (Elkartek: EXOTEK). A. Sarasola-Sanz′s work was supported by La Caixa-DAAD scholarship and N. Irastorza-Landa′s work by the Basque Government and IKERBASQUE, Basque Foundation for Science, Bilbao, Spain.

4. Chapter 4: Motor learning with a multi-degree-of-freedom mirror myoelectric interface during functional task training

4.1 Abstract

After stroke, the generation of motor commands and/or their descent to the spinal cord are often compromised. This leads to pathological muscle activation patterns (pathological muscle synergies) in the limb contralateral to the brain lesion. However, sensory input, experience and learning can induce reorganization of sensorimotor circuits. Hence, motor learning mediated by motor training has been explored for the correction of abnormal muscle synergies and functional recovery in motor impaired patients. Myoelectric interfaces together with rehabilitation exoskeletons allow stroke patients to train motor tasks with their paretic limb and receive real-time feedback about their muscle activity. However, the number of degrees of freedom that can be simultaneously controlled is still limited, which hinders the training of functional tasks and the effectiveness of the rehabilitation therapy. We developed a myoelectric system that allows multi-degree-of-freedom control of an exoskeleton simultaneously involving arm, wrist and hand joints, with an eye toward using this tool for rehabilitation. We hypothesize that controlling an exoskeleton with EMG signals from a stroke patient′s paretic limb, based on such a decoder trained with EMG from the healthy arm, will foster learning of natural EMG patterns and hence, recovery of motor function. In this study,

we first validated the effectiveness of the myoelectric decoder; we showed that 10 healthy participants could learn to control the system trained on the contralateral arm, within the span of a five-session experiment. We then showed evidence that subjects modulated EMG patterns to fit the mirror model, as reflected by a significant decrease in the time to execute trials and an increase in the percentage of successful trials. These results are the necessary precursor to evaluate if this system could also elicit motor learning in stroke patients and whether this process is accompanied by rectification of pathological synergies leading to motor recovery.

4.2 Introduction

A voluntary movement is the result of complex mechanisms in which the central nervous system recruits groups of muscles in a coordinated way (i.e., muscle synergies). These muscle synergies have different activation patterns and temporal profiles and are encoded at the spinal or brainstem levels [7, 9, 125–134]. Local brain damage due to stroke frequently affects the initiation of motor commands and/or their descending flow to the spinal cord. This leads to a disrupted recruitment or to an abnormal development of muscle synergies and so, to pathological muscle coordination in the limbs opposite to the injured hemisphere. Motor recovery after stroke is characterized by neuroplastic changes involving a structural and functional reorganization of the brain [135]. This implies the recruitment of intact cortical motor structures adjacent to the injury, which generate commands to the compromised muscles that are relevant for the intended task [13]. However, the brain networks involved in motor learning and recovery processes and the underlying neural mechanisms are not yet well understood [136–140]. Nonetheless, there is evidence that the brain and the lower sensorimotor circuitry can change or reorganize itself in response to sensory input, experience and learning [15, 16]. A remaining challenge, however, is how to foster the relearning of natural muscle synergies in order to achieve effective motor recovery.

Motor leaning is a complex process that comprises motor adaptation and skill acquisition [13, 141–143]. Motor adaptation occurs implicitly, presumably in a

short period and as a response to the error between what the brain predicts and the observed outcome. Motor skill acquisition is instead related to the ability to accurately execute the movement and may need of a more extensive training period to occur [144]. The relationship of motor skill acquisition and adaptation to motor recovery is still unclear. Several studies have confirmed that functional recovery mediated by motor training entails a learning process in patients with motor impairment [13, 15, 145–149]. However, training paradigms still need to be optimized to become truly effective [13, 146]. In recent years, technological advances and rehabilitation strategies have explored methods to elicit learning as a means to achieve motor recovery. For instance, rehabilitation robots allow intense task training, precise control of timing and the use of visual and proprioceptive feedback, which enhances motor learning [24, 108, 109, 150, 151].

Electromyographic (EMG) signals have been widely explored for the control of rehabilitation robots, as they offer a direct measurement of the motion intention of a person [46, 114, 124, 152–154]. However, several factors have hindered the exploitation of myoelectric interfaces and held up its transfer to commercial applications [155]. One of the main problems is the lack of systems that can simultaneously control several degrees of freedom (DoFs) in real-time. In the last few years, some studies have expanded from simple cursor control [156, 157] to the simultaneous control of multi-DoF external (non-wearable) robots in real-time [124, 158–160]. However, the control of wearable prostheses or exoskeletons adds one more level of complexity, since human motor control mechanisms are difficult to model and mechanical constraints and dynamics of the robot might hinder control proficiency [161]. For these reasons, myoelectric interfaces for controlling wearable robots have only been validated with up to 2 DoFs simultaneously [41, 162–164].

Another concern in myoelectric applications is that most systems are usually validated in one single session, or those with longer paradigms are focused on recalibrating or adapting the mapping every new session as a way to optimize the learning process. However, Ison and colleagues recently demonstrated that using a fixed mapping between the EMG and the output control command could induce

learning and the creation of novel muscles synergies in healthy individuals. Moreover, these synergies were retained after one week, facilitating the generalization to new tasks and the increase in performance over time without the need of recalibrating the decoder (i.e., changing the mapping) [159,165,166]. This implies that the utilization of dynamic mappings may not be as critical as suggested in recent research. Based on these studies, we believe that hemiplegic stroke patients could reshape the pathological synergy structure of their paretic limb by learning a fixed mapping or model built with EMG activity of their healthy upper limb (i.e., a mirror myoelectric decoder), as suggested in [69]. The potential of this paradigm for the continuous decoding of multi-DoF functional movements was already proved offline [68,69,71].

In this study, we investigated the viability of using a novel EMG decoding strategy to control an upper limb multi-joint exoskeleton in real-time during functional tasks, based on a mirror model from the contralateral arm [69]. Moreover, we evaluated if the proposed system can be used to elicit motor learning in 10 healthy participants and to adapt their muscle activity according to the imposed mirror EMG-to-kinematics map. Additionally, with a view toward optimizing such a system in a patient-centered approach to stroke recovery, we queried participants in the experiments about their perceptions of different features of the system.

4.3 Methods

4.3.1 Subjects

Ten able-bodied volunteers (5 females and 5 males, age: 20-33, all right-handed) without any known neuromuscular impairment participated in this study. All of them gave written consent to the procedures as approved by the ethics committee of the Faculty of Medicine of the University of Tübingen, Germany.

4.3.2 Experimental setup and protocol

The IS-MORE robotic exoskeleton (Tecnalia, San Sebastian, Spain) is a 7-DoF robotic exoskeleton for the proximal (upper and forearm) and the distal (wrist

and fingers) segments of the upper limb (more details in [68]). The exoskeleton lies on a 70 x 50cm mat on top of which the user performs gravity-compensated movements. Four shelves of different color placed around the mat define the four targets that the participants have to reach (see Figure 4.1(b) and supplementary video).

Volunteers were asked to sit on a chair in front of the workspace and wear the exoskeleton on their right or left upper limb for a single decoder calibration session and for four closed-loop control sessions, respectively (see below). For each participant, a posture in which they could keep their arm relaxed was selected at the beginning of the calibration session and defined as the "Rest" position. Similarly, four target poses (i.e., the position and orientation of the arm around each target and the angle of the wrist and the fingers) were also defined according to each subjectś range of motion.

All the participants underwent five sessions on five consecutive days: the calibration session (S1) used to train an EMG decoder with the right arm, and four closed-loop control sessions (S2-S5) in which subjects performed targeted movements controlling the robot with EMG activity of the left arm interpreted by the mirror decoder obtained in S1.

In the calibration session (S1) participants performed 5 blocks of "compliant movements" with the exoskeleton on their right arm, during which they had to follow the movement driven by the exoskeleton in an active and natural way. They were constantly reminded to adhere to the pace and trajectory of the exoskeleton without counteracting the movement. These blocks of compliant movements with the right arm were referred to as calibration blocks (CBs) (see Figure 4.1(a)). Each block was comprised of 8 trials, each consisting of an outward (towards the target) and an inward (towards the "Rest" position) movement. Subjects were instructed to supinate the wrist and open their hand while approaching the target, and to pronate the wrist and close their hand while going back to the "Rest" position. The beginning and end of each movement were marked by auditory cues. An inter-trial rest interval of 3 seconds was included to avoid muscle fatigue and to allow the

participants to prepare for the next trial. The data recorded during S1 was used to calibrate the myoelectric decoder.

In sessions S2-S5, participants performed 2 reference blocks (RBs), one at the beginning and one at the end of the session, and 5 training blocks (TBs) with their left arm. The RBs included compliant movements and served to help participants to get a reference of the trajectory the exoskeleton should ideally follow, and to assess the adaptation of their EMG activity patterns as a result of the training within each session and along the intervention. In the TBs, the movement of the exoskeleton was determined by the weighted sum of two components (see Equation 4.1: a component based on the EMG activity of the subject, and an assistive component that would always redirect the exoskeleton towards the required position. From the 8 trials included in each training block, 6 were randomly set to an assistance level of 30% (i.e. 70% of the velocity of the exoskeleton was based on EMG activity and 30% on assistive target directed velocities). The remaining 2 were catch trials assigned to assistance levels of 10% and 60% and randomly placed within the block of 8. The three different levels of assistance (catch trials plus main trials) served to evaluate the influence of the amount of assistance on the myoelectric control.

In every outward or inward movement, subjects were given 30 seconds to move as far as they could in the required direction. If they were unable to reach the target or the "Rest" position after the timeout, they would be presented with the next target. As a way of motivation, a piece of classical music with increasing intensity over time was played during each movement. Since the movements of the distal DoFs were finer and it was found that they were more difficult to control than the proximal DoFs [68], the trials were considered to be completed when the target position of the 3 proximal DoFs (i.e., position and orientation of the arm) was reached, independent of the angle of the wrist and the fingers. Nonetheless, even though the task accomplishment depended solely on the proximal DoFs′ position, participants were not informed of this fact. Subjects could control the movement in the 7-DoFs and received feedback in all of them. Therefore, in these training blocks, participants received visual and proprioceptive feedback of their EMG ac-

tivity by means of the velocity modulation of the 7 DoFs of the exoskeleton and an auditory reward if the target was reached.

After each trial, subjects were asked to rate the difficulty of the previous movement on a scale from 0-10, with 0 representing the lowest difficulty and 10 the highest. Similarly, the opinion of the participants regarding several aspects of the platform, such as the comfort of the setup, the difficulty of the task, the quality of the control and the functioning of the exoskeleton, was collected with a feedback questionnaire that they were asked to fill out at the end of each session.

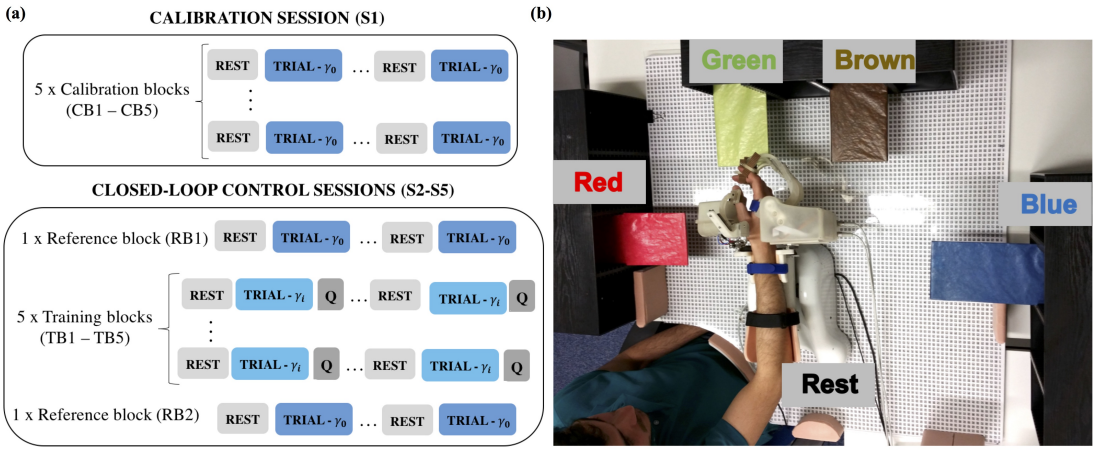

Figure 4.1: *Panel (a): Block structure of the calibration (S1) and closed-loop control sessions (S2-S5). The calibration session consisted of 5 calibration blocks (CBs) of compliant movements ($\gamma_0 = 0$, control independent of EMG, 100% assistance). Each of the four closed-loop control sessions comprised one initial reference block (RB1) of compliant movements ($\gamma_0 = 0$, 100% assistance), 5 training blocks (TB1-TB5) in which the myoelectric control was on, and a final reference block (RB2) with 100% assistance. The training blocks included 8 trials, each with a movement towards a target and back to the initial rest position: six trials with medium assistance level (30% assistance, $\gamma_i = 0.7$), one with high assistance (60% assistance, $\gamma_i = 0.4$) and another one with low assistance (10% assistance, $\gamma_i = 0.9$). After each trial, participants were asked to rate how difficult they found it, (indicated by the Q letter), followed by rest intervals of 2-3 seconds; Panel (b): Experimental setup indicating the four targets and the rest position, as well as the robotic exoskeleton.*

4.3.3 Data acquisition and processing

Two high-density arrays of 24 channels each (Tecnalia-Serbia, Belgrade, Serbia) were placed over the extensor and flexor muscles of the forearm to record the muscular activity with high spatial resolution. Differential signals were computed from each closest-neighbor pair of electrodes along the diagonals and straight directions, resulting in a total of 110 bipolar channels collected from the forearm muscles. In addition, six standard bipolar electrodes (Myotronics-Noromed, USA) were used to record the EMG activity from the Abductor Pollicis Longus, the Biceps, the Triceps, and the Frontal, Middle and Posterior Portions of the Deltoid. The reference and ground electrodes were located over the olecranon and the clavicle, respectively. The location of the electrodes on the left and right upper limbs was symmetrical, and the positions on the left arm were marked with permanent markers to mitigate the effects of varying electrode positions across sessions.

The EMG activity was acquired at 1000Hz (Brain Products GmbH, Germany), band-pass filtered (10-450Hz) and comb-filtered (50Hz and harmonics). Kinematics of the 7-DoFs were collected at 20Hz and low-pass filtered (1.5Hz).

4.3.4 Feature extraction and decoder calibration

Five time-domain features (mean of absolute value, variance, waveform length, root-mean-square error and the logarithm of the variance) were extracted from each EMG channel in windows of 200ms. The resulting matrix of features was normalized to zero mean and unit variance using the mean and standard deviation computed from the whole calibration data set. During the closed-loop control the normalizing factors were continuously updated by computing the mean and standard deviation over the previous minute of EMG data.

A channel selection process was applied to the high-density EMG channels to reduce the dimensionality of the feature input set. We followed an iterative cross-validation process [71] to select a set of 10-50 channels. Once the channels were selected and the features extracted, a myoelectric decoder was calibrated with

these features and the kinematics collected during the calibration session and then kept fixed throughout the subsequent closed-loop control sessions. The decoding algorithm was a ridge regression, which has proven to outperform other linear algorithms for myoelectric applications [68]. The regularization parameter λ was fixed at 10^4, a value that was empirically found to attain a good bias-variance tradeoff. Thanks to this regularization, the algorithm could capture the regularities present in the calibration data set while at the same time was able to generalize well to unseen data.

4.3.5 Myoelectric control paradigm

During the myoelectric control, the features extracted from the produced EMG in real-time were normalized based on the previous minute of data and fed to the myoelectric decoder, which predicted the velocity of each DoF. This output velocity was smoothed with a recursive filter that contained the last ten outputs and gave more relevance to the most recent ones (i.e., linearly increasing weights from the past to the most recent outputs). This filtering step ensured a smoother control of the exoskeleton and prevented unwanted jerky movements due to noise or non-stationarities in the EMG signal.

We implemented a partially assisted control scheme to avoid initial frustration due to the complexity of the task. Hence, the velocity for each DoF that was sent to the exoskeleton and that described its movement during the trial periods was determined by the following formula:

$$V_{net} = (1 - \gamma) * V_{assist} + \gamma * V_{EMG} \tag{4.1}$$

Where V_{net} is the velocity sent to the exoskeleton; V_{assist} is the assistive component that redirects the exoskeleton towards the target (computed with a Linear Quadratic Regulator); V_{EMG} is the velocity predicted by the mirror decoder from the EMG activity exerted by the left arm; and $\gamma \in [0, 1]$ is the weight determining the influence of each component on the net velocity command sent to the exoskeleton (e.g. $\gamma = 0.7$ during the trials with 30% of assistance). Therefore,

the closed-loop control was established by linking the movement volition detected from the EMG signals with the actual movement of the exoskeleton attached to their left limb. Subjects were continuously provided with information about their EMG muscle activations in the form of velocity modulation. Hence, they had to understand and learn the mapping between their EMG activity and the changes in the trajectory and speed of the movement. Based on this visual and proprioceptive feedback, they had to produce EMG patterns similar to those encoded in the reference model, mirrored from the opposite arm, in order to bring the exoskeleton towards the target position as quickly and as smoothly as possible.

4.3.6 Performance metrics

The following five metrics were selected to evaluate different aspects of the EMG-decoding and of the participants′ performance during the myoelectric control:

- *Execution time (percentage)*: represents the percentage of the total time allowed per movement (i.e. 30 seconds) that the participants took to reach the target.
- *Timeouts (percentage)*: represents the percentage of trials that were not accomplished because the participants ran out of time before they reached the target.
- *Spectral Arc Length (SPARC)*: measures the smoothness of the movement in each DoF [167]; the closer to zero, the smoother the trajectory.
- *Correlation coefficient (CC)*: reflects the coherence of the assistive and the EMG velocity components of the command to the exoskeleton.
- *Normalized root-mean-square-error (NRMSE)*: measures the difference between the assistive velocity component and the EMG-based predicted velocity component.

Although SPARC, CC and NRMSE were computed for each DoF individually, they were analyzed in three different ways, i.e. by averaging: (1) across all the DoFs (*_all); (2) across the DoFs of the upper arm and forearm only (*_proximal); and

(3) across the DoFs of the wrist and the hand only (*_distal). Assessing the performance of the proximal and the distal DoFs separately allowed us to investigate whether the fact that the task completion was dependent only on the proximal DoFs influenced the learning process and the control over the different segments of the arm, i.e. reinforcement and instrumental learning effects.

The first three metrics (i.e., Execution time, Timeouts, and SPARC) are behavioral metrics and represent the ability of the participants to control the exoskeleton with their EMG activity, while we considered the last two to be electrophysiological metrics (i.e., CC and NRMSE) that measure the ability of the subjects to match the movement template of the assistive control via the EMG decoder (i.e. to modulate their EMG activity patterns to produce kinematics that are aligned with the assistive component). Note that since the movements during the RBs were fully-assisted and predefined (i.e., the myoelectric control was not active), the participants did not have any influence on the execution time nor on the path smoothness and so, the first three metrics were not computed for this type of blocks.

4.3.7 Analyses

Using the aforementioned metrics, we performed four analyses to study the effectiveness, usability and acceptability of the system:

1) Motor learning

   We hypothesized that the subjects would be able to learn the EMG-to-kinematics model and achieve a more dexterous control of the exoskeleton, reflected in a positive evolution of the performance over time. During the TBs, we could analyze the online muscle activity adaptation to the exoskeleton motor control, which would reflect sensorimotor adaptation based on afferent information (visual, proprioceptive and haptic) about the ability to reach the target. On the other hand, during RBs we could analyze the generalization and retention of the newly learned EMG-to-kinematics map

during the training, as participants were instructed to actively follow the exoskeleton movements even if their EMG activity had no influence on the exoskeleton kinematics during these trials. We therefore studied the motor learning process occurring across and within sessions separately for TBs and RBs.

For the across session analysis, the performance values achieved in the TBs or RBs of the four closed-loop control sessions were concatenated, and a multivariate linear model was fitted with two variables: one indicating the block number (TBs: 1-20; RBs: 1-8), and the other one the session number. The intercept determined the initial performance and the slope defined the learning rate. Positive learning rate values indicate an increase in performance over time for all the metrics except for the NRMSE, for which it means a decrease.

Similarly, we investigated the occurrence of a motor learning process within sessions. We averaged the performance of each TB or RB across the closed-loop control sessions (i.e., averaging all the first blocks of the four sessions, all the second blocks, etc.). The evolution of the performance during the TBs was modeled with a first order univariate polynomial, where the variable represented the block number (1-5). The mean performance of the two RBs within session were compared with a Wilcoxon non-parametric test.

2) Perception

In this analysis, we studied the correlation between the ratings of the subjects about the difficulty of each trial and their ability to control the exoskeleton during that trial (i.e., with the first three performance metrics: Execution Time, Timeouts and SPARC). Thus, for each subject, we computed the three performance metrics on a trial-by-trial basis and looked for a correlation with the corresponding ratings (Kendall tau correlation). Finally, after checking for normality, we applied a one-way repeated measures analysis of variance (ANOVA) to compare the correlation values across all the performance met-

rics and hence, evaluated which metric was perceived as a better indicator of performance by the participants.

In addition, we investigated whether the participants perceived the different assistance levels, despite the fact that they were not informed about their existence. We computed the mean rating of all the trials with the same assistance level (low = 10%, medium = 30% or high = 60%) for each session and compared these values with a two-way repeated measures ANOVA (Factors: assistance level (low, medium and high) and session (S2-S5)). We performed post-hoc pairwise comparisons between the significant sub-factors and controlled for multiple comparisons using the Bonferroni correction.

3) Assistance level - performance relationship

We evaluated the variability of the performance as a function of the assistance level. We expected that a higher level of assistance would facilitate the control of the exoskeleton, which would be reflected in a shorter execution time and a smoother trajectory. We used the first three metrics (i.e., Execution time, Timeouts, and SPARC) to measure the ability of the subject to control the exoskeleton during each closed-loop control session (S2-S5) and for each assistance level (i.e., low = 10%, medium = 30% and high assistance = 60%). We compared these values with a two-way repeated measures ANOVA (Factors: assistance level (low, medium and high) and session (S2-S5)). We performed post-hoc pairwise comparisons and corrected them using the Bonferroni method.

4) Feedback questionnaire

The responses to the feedback questionnaire were numeric, on a range from 0 (most negative value) to 10 (most positive value). In order to simplify the analysis, the questions were classified into the following groups:

A) *Exoskeleton functioning*: evaluated whether the exoskeleton moved smoothly and at a comfortable speed.

B) *Exoskeleton hardware*: comprised questions about how comfortable it was to wear and operate the exoskeleton.

C) *Ease of controlling the exoskeleton (subdivided into proximal and distal DoFs)*: participants were asked to rate how difficult it was for them to control the movement of the exoskeleton over the proximal and distal DoFs with their EMG activity.

D) *Feedback accuracy*: evaluated the perception of the participants about the feedback provided (i.e., whether they felt that the exoskeleton assisted the movement or instead, it moved against their will).

E) *Protocol design, pauses and rest periods*: looked for the opinion of the participants regarding how tired they were after the training, whether the pauses were long enough, etc.

The average of the responses of all the participants was calculated for each closed-loop control session (S2-S5) to study their general perception about the listed features of the system and the experimental protocol.

4.4 Results

All participants could control the 7-DoFs of the exoskeleton in real-time with the muscle activity of their left arm (see video in supplementary material), with an average of 92,2% of movements accomplished within the 30-second time limit. Additionally, we analyzed the existence of a motor learning process, as this system aims not only at overcoming the challenge of achieving multi-DoF myoelectric control but also at eliciting motor learning and rehabilitation in stroke patients.

1) Motor learning

We investigated the occurrence of a motor learning process both across and within sessions. These two analyses were applied separately to the TBs and the RBs.

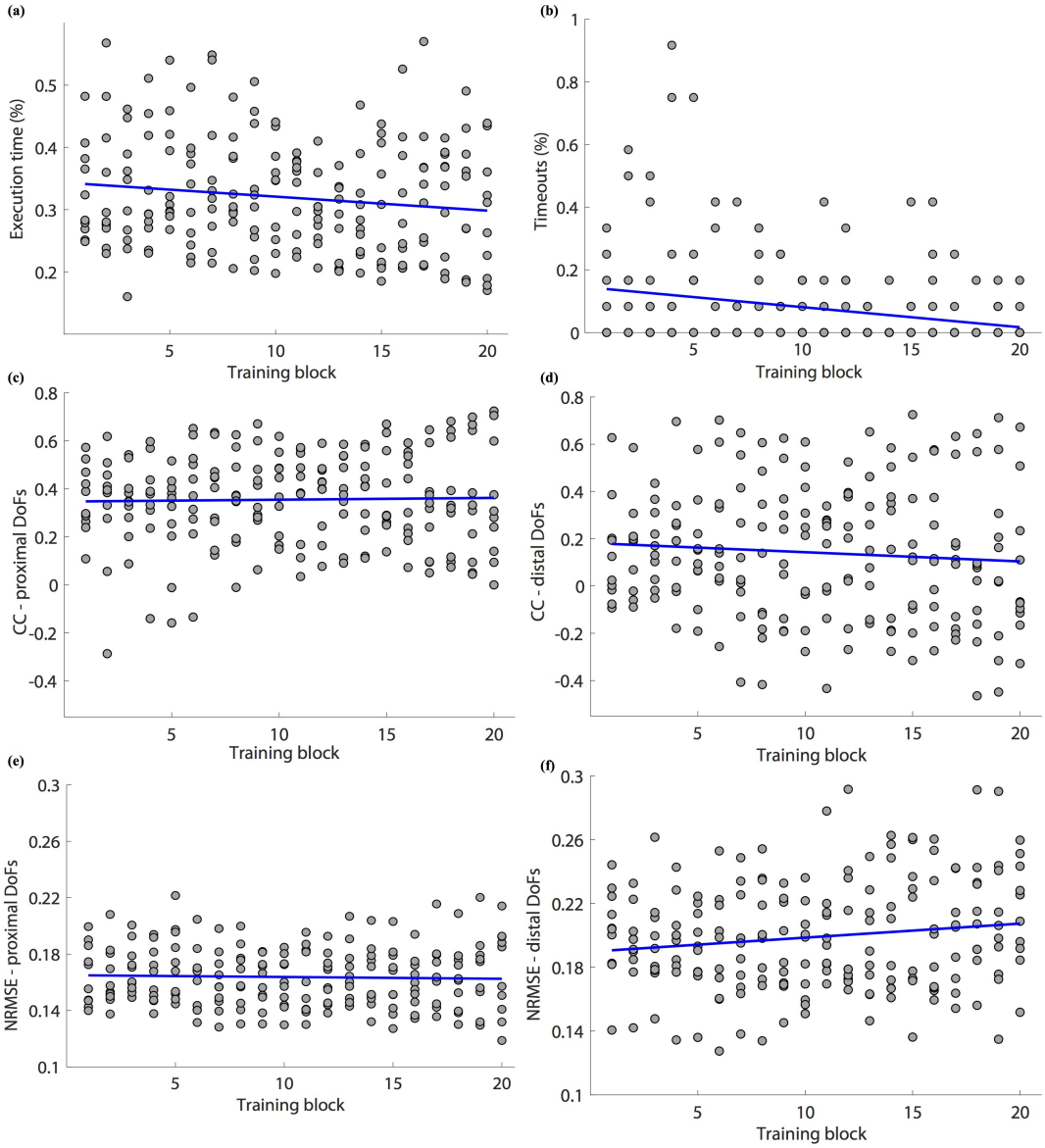

Figure 4.2: *Performance measured by Execution time (a), Timeouts (b), Correlation Coefficient ((c) and (d)) and the Normalized Root-Mean-Square-Error ((e) and (f)) metrics for the 20 training blocks from the closed-loop control session (TB1-TB5 of S2-S5), for all the participants. Correlation coefficient and normalized root-mean-square-error values are averaged across the proximal DoFs ((c) and (e)) and the distal DoFs ((d) and (f)). The polynomial model fitted to the outcome values (in blue) represents the learning trend.*

The results of the analysis of the TBs across sessions are illustrated in Figure 4.2. The linear model fitted to those values exhibits a significant negative slope for Execution time (p = 0.041, Figure 4.2(a)) and Timeouts (p = 3.35 $\cdot 10^{-4}$, Figure 4.2(b)). These negative correlations demonstrate the occurrence of a learning process characterized by shorter time periods needed to reach the target as well as fewer failures to reach the target over the course of the experiment. On the other hand, the CC and NRMSE values in Figure 4.2(c)-(f) show that the control of the distal DoFs was poorer towards the end, as reflected by the significant (p = 0.032) positive slope of NRMSE values. However, this did not happen for the proximal DoFs, noted that the ability of the participants to adapt the EMG activity was significantly (p_{CC} = 0.0098; p_{NRMSE} = 0.002) higher for the proximal DoFs than for the distal DoFs during the closed-loop myoelectric control (mean $CC_{proximal}$ = 0.355 ± 0.175; mean CC_{distal} = 0.141 ± 0.254; mean $NRMSE_{proximal}$ = 0.164 ± 0.020; mean $NRMSE_{distal}$ = 0.199 ± 0.028). Some participants produced progressively smoother paths over sessions (see Supplementary Figure 4.7), although the tendency was not significant when looking at all the subjects together (see supplementary Figure 4.6). In the within-session analysis, there were no learning trends or significant performance improvements for any of the metrics.

Albeit non-significant ($p_{CC-proximal}$ = 0.139; $p_{NRMSE-proximal}$ = 0.240), a trend towards higher performance (higher CC and lower NRMSE values) over the proximal DoFs can be discerned in the RBs across sessions (see Supplementary Figure 4.8). The negative slope of the regression lines for the distal DoFs indicates a non-significant ($p_{CC-distal}$ = 0.192; $p_{NRMSE-distal}$ = 0.345) trend towards a lower performance (lower CC and higher NRMSE values). No significant trends in the within session analysis of the RBs were found.

2) Perception

The correlation between the performance and the ratings given by the participants lay within the [0.1-0.7] range, as can be observed in Figure 4.3(a). The ANOVA shows a significant ($p < 10^{-6}$) difference between the correlation values of the metrics. Execution time happened to be the most intuitive metric for the participants to rate the difficulty of the trial, reflected in significantly higher mean correlation values (Execution time vs. Timeouts: $p = 0.024$; vs. SPARC-all: $p = 1 \cdot 10^{-6}$; vs. SPARC-proximal: $p = 4 \cdot 10^{-6}$; vs, SPARC-distal: $p = 1 \cdot 10^{-6}$) while Timeouts was the metric with the lowest correlation values (Timeouts vs. Execution time: $p = 0.024$; vs. SPARC-all: $p = 3 \cdot 10^{-6}$; vs. SPARC-proximal: $p = 6 \cdot 10^{-6}$; vs. SPARC-distal: $p = 3 \cdot 10^{-6}$).

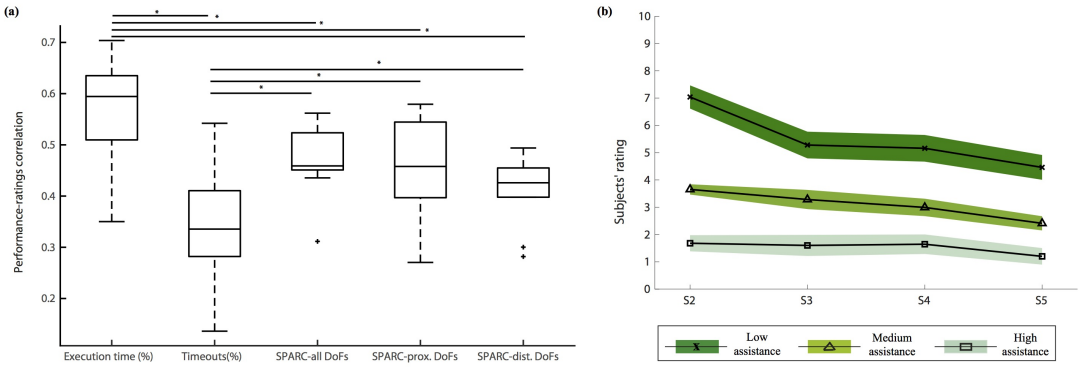

Figure 4.3: *Perception. Panel (a): Kendall tau correlations (including standard deviation and median) between the difficulty ratings given by the participants after each trial and the performance measured by the Execution time, Timeouts and SPARC metrics. Asterisks show significant differences ($p < 0.05$). Panel (b): Mean and standard error of the difficulty ratings given by all the participants after each trial for each closed-loop control session (S2-S5) and computed separately for each assistance level (high: light green and squares; medium: medium green and triangles; low: dark green and crosses). The higher the rating, the more difficult was for the participants to control the exoskeleton. Corrected pairwise comparisons show significant differences between the ratings given to the three assistance level trials.*

The mean ratings of the low, medium and high assistance level trials across all the participants for each session are presented in Figure 4.3(b). The two-

way ANOVA applied to these values confirms that the participants could perceive the different assistance levels, as reflected by the significantly different ratings given to the low, medium and high assistance trials (corrected pairwise comparisons: low vs. high: $p = 2.2 \cdot 10^{-5}$; low vs. medium: $p = 1.2 \cdot 10^{-4}$; medium vs. high: $p = 3.5 \cdot 10^{-5}$). Interestingly, the two-way ANOVA showed a significant ($p = 0.002$) session effect and significant pairwise differences between the ratings of sessions S2 and S5 ($p = 0.008$) and S3 and S5 ($p = 0.019$), meaning that participants found the various assistance level trials less difficult over sessions.

3) Assistance level - performance relationship

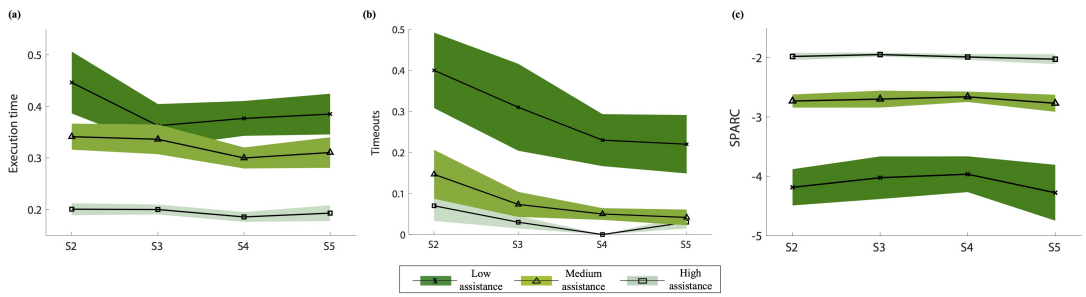

Figure 4.4: *Mean and standard error of the performance measured by the Execution time (a), Timeouts (b) and SPARC (c) for the different assistance levels (high: light green and squares; medium: medium green and triangles; low: dark green and crosses). The performance values for all the participants were averaged for each closed-loop control session (S2-S5).*

As can be seen in Figure 4.4, higher assistance values led to higher performance. Indeed, Assistance level had a significant effect on all the metrics, as reflected by the two-way ANOVA (Execution time: $p = 1.1 \cdot 10^{-5}$; Timeouts: $p = 4.9 \cdot 10^{-5}$; SPARC: $p < 10^{-6}$). The post-hoc comparisons show significant differences between the three assistance levels, except for the low vs. medium levels of Execution time and the medium vs. high level of Timeouts. A decrease of the timeouts over sessions for all the three assistance levels can also be noticed and was reflected by a significant ($p = 0.015$) effect of the

session factor in the two-way ANOVA, although post-hoc comparisons did not show any pairwise differences after Bonferroni correction.

4) Feedback questionnaire

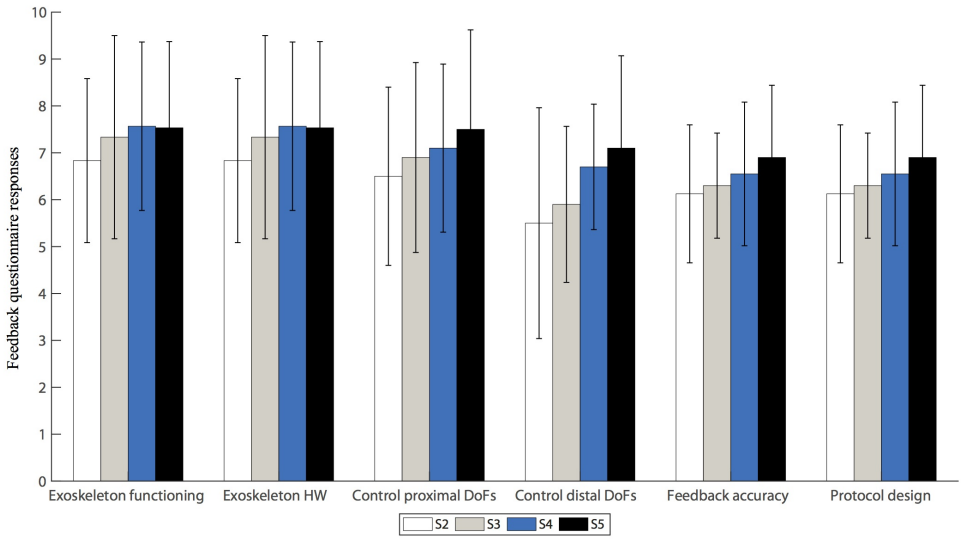

Figure 4.5: *Mean and standard deviation of the responses given by the participants to the feedback questionnaire after each closed-loop control session (S2-S5). The questions were grouped into five different categories: Exoskeleton functioning, Exoskeleton Hardware, Control of the exoskeleton (proximal and distal DoFs), Feedback accuracy and Protocol design. Higher values mean more positive feedback.*

Figure 4.5 illustrates the average responses of the participants to the questionnaires filled out at the end of each closed-loop control session. It shows satisfactory response values (in the range [6.3, 8.0]) that remained stable across sessions for the questions related to the exoskeleton functioning and hardware as well as the protocol design. Additionally, participants reported an increasing ease in controlling the exoskeleton over the sessions. From these values, a noticeable difference between the proximal and distal DoFs can be detected too, with the control over the proximal DoFs being apparently more intuitive than the distal DoFs. However, the responses about the control over the distal DoFs show that participants also found the control

of those DoFs easier towards the later sessions. The reason for this might be that participants were not told that the trial accomplishment depended only on the position of the proximal DoFs. Thus, they probably associated the reduction in execution time and number of timeouts over sessions with a better control of both proximal and distal DoFs. Finally, the ratings for the feedback accuracy were slightly more positive over sessions with mean values ranging from 6.1 to 6.9.

4.5 Discussion

In this study, we presented and validated a myoelectric interface intended for the upper limb rehabilitation of stroke patients. The system includes a ridge regression algorithm, a subject-specific myoelectric mirror model, fixed within and across sessions, and high-resolution EMG recordings. Our preliminary validation with healthy participants demonstrates that it is possible to achieve real-time, skillful and simultaneous control of a rehabilitation exoskeleton with multiple degrees of freedom using EMG activity and an EMG decoder trained on data from the contralateral arm. Furthermore, this myoelectric interface elicited motor learning in healthy individuals across five-sessions conducted over a 5-day period.

This is the first myoelectric system that has been successfully used to simultaneously control a 7-DoF exoskeleton in real-time, including proximal and distal joints. It has previously been demonstrated that training functional tasks, involving coordinated proximal and distal joint movements of the arm, might facilitate the activation of more affected distal muscles in patients with motor impairment, and ease the transfer of the acquired skills to activities of daily living [6, 47]. However, the existing non-invasive myoelectric systems do not offer the possibility of training coordinated multi-joint tasks, since they are restricted to the real-time simultaneous and proportional control of up to 4 DoFs (proximal or distal) of an external robot [124, 158–160], 2 DoFs of a prosthesis [41, 162] or 1-DoF (elbow or hand) of an upper-limb exoskeleton [163, 164]. The difficulty of continuously and accurately predicting users′ motion intention from EMG signals and of simultaneously controlling the velocity of several DoFs of an exoskeleton in real-time has

limited its clinical and commercial use. Our mirror myoelectric system goes a step further, as it allows safe, smooth and continuous multi-DoF control in real-time. Even more relevant for rehabilitation applications is that it can elicit motor learning in healthy subjects.

The results of the analysis across sessions demonstrate that the participants learned the mirror mapping and operated the myoelectric interface in a progressively more efficient way over the training period (see Figure 4.2). The kinematics predicted from the EMG activity defined a more direct and accurate movement towards the aimed position, reflected in higher speeds and in turn, lower time periods needed to reach a target. This was confirmed by the progressively more positive responses in subjects′ responses to the feedback questionnaire regarding feedback accuracy and ease in controlling the exoskeleton (see Figure 4.5) and the lower difficulty ratings over sessions (see Figure 4.3(b)). The performance also varied according to the assistance level. As expected, the higher the assistance, the shorter the execution time, the smaller the percentage of timeouts and the smoother the path. This difference could also be perceived by the participants, as revealed by the significantly different ratings given for the trials of each assistance level. More importantly, it was demonstrated that even during the trials with only 10% assistance, participants could successfully control the speed and direction of a 7-DoF exoskeleton with their EMG during a complex functional task. Indeed, they produced significantly ($p = 0.015$) fewer timeouts during the trials of any of the three assistance levels over the course of the experiment (see Figure 4.4(b)), and reported progressively less difficulty ($p = 0.002$) to perform the trials with any assistance level (see Figure 4.3(b)). Furthermore, the participants rated satisfactorily the usability and comfortability of the system and provided us with useful information to adapt and optimize the system for future experiments. Therefore, the results are encouraging and have relevant implications for its future application to a rehabilitation scenario with stroke patients.

There is a trend towards a degrading control (i.e., smaller CC and larger NRMSE values) of the distal DoFs over the course of the intervention (see Figure 4.2). Conversely, performance of the proximal DoFs improved over time. This

difference goes in line with the results found in previous offline studies in healthy and stroke patients [68, 71]. One reason for the difference between the proximal and distal DoFs performance could be that the movements of the distal DoFs were finer and more difficult to control than the proximal DoFs, as reported by the participants in the feedback questionnaire and by the significantly ($p_{CC} = 0.0098$; $p_{NRMSE} = 0.002$) lower mean performance of the distal DoFs compared to the proximal ones. In addition, the fact that the task completion condition was based only on the proximal DoF position could have influenced the performance. Despite the fact that participants could control and receive feedback on the distal DoFs, they were never informed whether the target position was successfully reached on those DoFs or not. This lack of information might have impeded the occurrence of a learning process (based on reinforcement learning, i.e. on reward), reflected in a more accurate control over the distal DoFs. This supports the importance of receiving contingent sensory feedback and reward (i.e., beep indicating task completion) of the DoFs being controlled for motor control [49, 81, 82]. Furthermore, there is a significant increase in variability in CC and NRMSE values in the distal DoFs during RBs (See Supplementary Figure 4.8(b) and (d)), which suggests implicit motor exploration or different motor control strategies.

The concepts of skill acquisition and motor adaptation and their relationship with motor recovery is still unclear [144]. Dipietro and colleagues suggested that an internal map of the trained task is built by the brain during motor recovery, following a process more similar to motor skill acquisition than motor adaptation [147]. Others have stated that repeated adaptation can lead to learning a new and more permanent motor skill that can cause long-lasting changes in the motor cortex and the cerebellum [168]. The results of our study demonstrate that four training sessions sufficed for healthy individuals to learn the imposed mapping and achieve proficient myoelectric control. However, from these results we cannot conclude whether the observed learning was the result of an adaptation or a skill acquisition process. The metrics assessing the myoelectric control (i.e., CC and NRMSE) during the RBs partially reflect the observed significant behavioral changes, indicating an intrinsically effective generalization and retention of the imposed mirror EMG-to-kinematics map. This is of great importance as this

might open a new door to efficient re-learning of correct EMG activation patterns. However, our results were not significant and in the distal DoFs, which were not rewarded during the training, the effects were mixed and inconclusive. A larger number of participants or sessions might be needed to find significant effects during the training. It should also be noticed that some of the participants may have partially or completely relied on strategies such as the reduction of interaction forces to accomplish the trials in a shorter time over blocks. The absence of sensors to measure such parameters is a limitation of the study that will be addressed in future experiments. It would also be necessary to assess the generalization of the gains to untrained tasks and the long-term effects of the training in order to determine which specific process occurred during the intervention. Nevertheless, the observed learning process and positive feedback from the healthy population encourage the transfer of this rehabilitation system to the clinical stage.

This mirror decoder has been designed for the rehabilitation of stroke patients, as they typically keep the motor abilities of one of their limbs intact or mostly intact. The system takes advantage of this characteristic by using the muscle activation patterns or synergies of their intact limb as a reference mapping for patients to learn to move their paretic limb through the recruitment of healthy synergies. Previous evidence suggests that the learning of a new neuromotor mapping is associated with the emergence of new muscle synergies. Moreover, these effects can persist after a week facilitating the generalization to new tasks while keeping the same mapping [159]. Other studies have also emphasized the importance of error strategies, guidance and feedback for muscle activation modulation and motor learning [169–174]. They demonstrated that guidance and feedback improves motor task learning and that errors should not be reduced or eliminated to induce learning, but instead they should be shown and in some cases, even amplified [173, 174]. Therefore, based on the results, we believe that training with this closed-loop system that provides the necessary assistance and the appropriate response stimuli (i.e., contingent feedback about the paretic EMG activity), patients will be able to learn the fixed mapping of healthy activity imposed by the mirror decoder. Whether this learning process leads to the formation of new and healthy muscle synergies in the paretic arm remains to be investigated in the

stroke population.

Many patients classified by standard scales as having completely paralyzed joints (i.e. no visually perceived movement) nevertheless retain significant residual muscle activity, which could be decoded and used to control external devices [35]. One of the limitations of the system presented here is that patients with no residual muscle activity could not benefit from it. However, patients without decodable muscle activity could initially train with brain-machine-interfaces (BMIs) until they recovered enough EMG activity [49,175] to profit from myoelectric interfaces or from hybrid-BMIs, with a shared brain and muscle control [71]. Despite its limitations, our approach opens the doors of rehabilitation to many stroke patients who retain minimal EMG activity but cannot benefit from other therapies such as constraint induced movement therapy and bilateral arm training [176] that require residual movement of the paretic limb.

4.6 Acknowledgements

This study was funded by the Fortüne-Program of the University of Tübingen (2422-0-1), the Bundes Ministerium für Bildung und Forschung BMBF MOTOR-BIC (FKZ 13GW0053) and AMORSA (FKZ 16SV7754) and the Ministry of Science of the Basque Country (Elkartek: EXOTEK).

4.7 Supplementary material

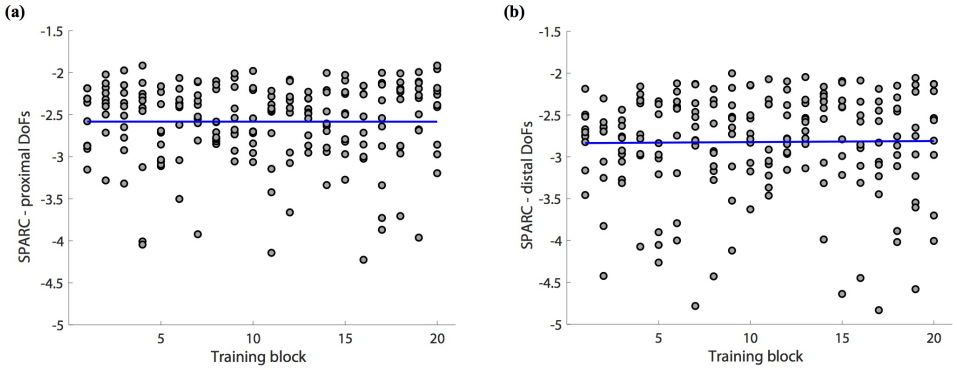

Figure 4.6: *Performance measured by the spectral arc length (SPARC) for the 20 training blocks from the closed-loop control session (TB1-TB5 of S2-S5), for all the participants. SPARC values are averaged across the proximal DoFs (a) and the distal DoFs (b). The polynomial model fit to the outcome values (in blue) represents the learning trend.*

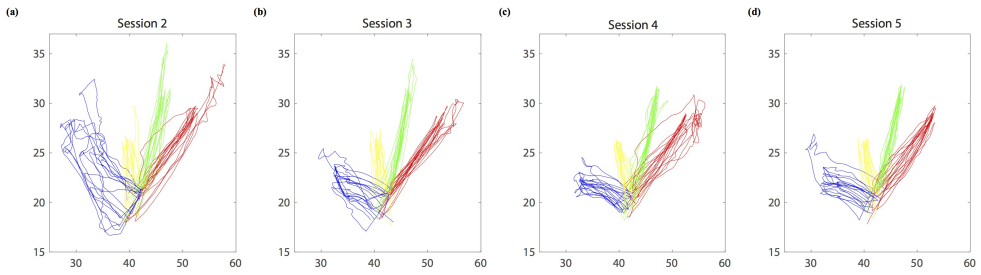

Figure 4.7: *Trajectories in x and y axes towards the four targets around the workspace, performed by one of the subjects during the closed-loop control session 2 (a), session 3 (b), session 4 (c) and session 5 (d). Values in x and y axes are in cm.*

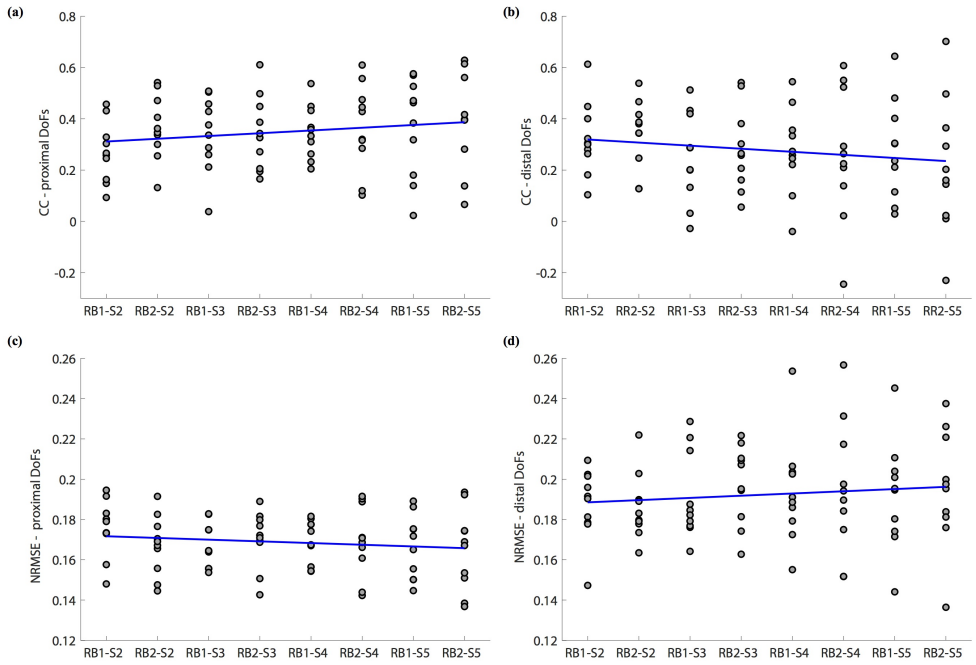

Figure 4.8: *Correlation coefficient ((a) and (b)) and normalized root-mean-square-error ((c) and (d)) metrics for each reference block (RB1-RB2) and closed-loop control session (S2-S5), for all the participants. Values are averaged across the proximal DoFs ((a) and (c)) and the distal DoFs ((b) and (d))). The polynomial model fit to the outcome values (in blue) represents the learning trend.*

5. Chapter 5: An EEG-based brain-machine interface to control a 7-degrees of freedom exoskeleton for stroke rehabilitation

This manuscript has been published as [70].

5.1 Abstract

Brain machine interfaces (BMIs) have previously been utilized to control rehabilitation robots with promising results. The design and development of more dexterous and user-friendly rehabilitation platforms is the next challenge to be tackled. We built a novel platform that uses an encephalograpy-based BMI to control a multi-degree of freedom exoskeleton in a rehabilitation framework. Its applicability to a clinical scenario is validated with six healthy subjects and a chronic stroke patient using motor imagery and attempt. Therefore, this study presents a potential system to carry out fully-featured motor rehabilitation therapies.

5.2 Introduction

Encephalographic (EEG)-brain machine interfaces (BMIs) have previously been used to control an external robot or exoskeleton in assistive and rehabilitation frameworks [177], [60], [49]. Several decoding methods and training protocols have been tested to find an efficient rehabilitation therapy that could increase cortical

plasticity and elicit motor recovery. Despite the limitations of EEG technology and the moderated decoding performance of the employed EEG-decoding methods, the aforementioned studies demonstrated the potentiality of EEG-based BMIs as a tool for post-stroke rehabilitation. The focus has lately turned towards the development of BMI-based rehabilitation platforms that allow a more natural and dexterous control of multiple degrees of freedom(DOFs), and boost motor recovery.

In this study we present an EEG-based BMI platform for the control of a multi-DOF exoskeleton (Tecnalia, Spain) in a rehabilitation framework. The platform combines EEG-decoding methods proven to induce significant motor recovery [49] with a control platform and a rehabilitation exoskeleton that allows the training of complex functional tasks, involving several DOFs of the arm, wrist and hand. The rehabilitation platform is validated with 6 healthy subjects and a chronic stroke patient, who followed a motor imagery and a motor attempt based protocol, respectively.

5.3 Methods

5.3.1 Experimental protocol

Six healthy subjects (3 female, age 24-30, all right handed) and a chronic stroke patient suffering from a right hemiparesis (male, 67 years old, 3 years from stroke) participated in the study. All of them were naive to motor imagery/attempt and gave written consent to the procedures as approved by the ethics committee of the Faculty of Medicine of the University of Tübingen, Germany.

They underwent a single session that consisted of two parts: a screening phase and a real-time BMI operation phase. The data collected during the initial phase was employed to select the electrodes and frequency bands that would constitute the input to the BMI. During the second part, the participants controlled a 7-DOF exoskeleton using an EEG-based BMI in real-time. The exoskeleton was placed over a mat and allowed the movement in 7-DOFs (details in [68]).

During the screening phase, the healthy subjects (the stroke patient) were asked

upon auditory and visual cues to either imagine their right hand opening (try to open and close his paretic hand) and closing or to relax for 5 seconds. Healthy subjects and the patient completed 5 and 3 blocks amounting to 55 and 33 trials of each condition, respectively. During the real-time phase, participants performed functional movements towards four different positions around the worskpace (see Fig. 5.1), while sitting and wearing the exoskeleton on their right upper limb. More precisely, they were instructed, by means of imperative auditory cues, to imagine/to attempt to reach a target while opening their hand and pronating their wrist and then back to a predefined rest position. Trials always started with a rest period of 3-5 seconds, followed by an auditory cue, a 2 second-long preparation time and a movement period. A timeout time of 7 seconds defined the maximum possible length of the movement period. If the target position was not reached within this time, the same target position was kept for the next trials until reaching it in all the DOFs. Otherwise, the trial ended as soon as the target was reached and subjects were instructed to head to the next position.

5.3.2 Data collection and processing

EEG data from 32 channels: FP1, FP2, F7, F3, Fz, F4, F8, FC5, FC1, FC2, FC6, T7, C3, Cz, C4, T8, TP9, CP5, CP1, CP2, CP6, TP10, P7, P3, Pz, P4, P8, PO9, PO10, O1, Oz, O2 and two EOG signals were collected at 1kHz (Brain Products GmbH, Germany). EEG signals were bandpass filtered (5-80Hz), notch-filtered at 50Hz and spatially filtered with a short-Laplacian filter. An autoregressive model of order 20 and its power was computed on the filtered signal, using 0.5sec-long windows and a step window of 50ms. Finally, the mean power on the chosen frequency bands and electrodes were used as input features for the classifier.

Kinematic activity of the above mentioned DOFs was recorded at 20Hz with an optical symbol recognition system and motor encoders.

Figure 5.1: *A hemiparetic stroke patient controlling the 7-DOF exoskeleton with the EEG-BMI. The patient's arm is at the initial rest position and the colored cylinders define the four target positions around the workspace.*

5.3.3 Real-time decoding and operation of the exoskeleton

The most discriminant electrodes and frequency bands were selected based on r-squared coefficients. Features were computed on those electrodes and bands, as described in Section 5.3.2) and fed to the classifier in real-time. Linear discriminant analysis was used to classify the input features as "Movement" or "Rest". The classifier was trained once using the screening data and then, retrained online at the end of each trial using the last two minutes of data from each condition. The outputs of the classifier were ignored during the rest and preparation periods, in which the exoskeleton remained still. However, during the movement period, the outputs classified as "Movement" triggered the autonomous movement of the exoskeleton towards the target position. On the other hand, outputs classified as "Rest" prevented the exoskeleton from moving. To achieve a more stable control and avoid flickering movements due to EEG signal noise, the current condition (i.e. exoskeleton in motion or in rest) was held as long as the decoder didn't classify 5 consecutive outputs of the other condition, following [49].

To measure the performance, we analyzed the percentage of time the robot was moving during the movement period, in which participants received feedback. Additionally, we compared this true positive rate (TPR) and the false positive rate (FPR: percentage of outputs classified as "Movement" during the rest period) offline.

5.4 Results

The mean percentage of time the robot was moving during the movement period for all the healthy subjects was 62.8% ±10.4% and for the stroke patient was 54.9%. The difference between the TPR and FPR (healthy subjects: mean = 39.8% ±7.3%; patient: 43.6%) was significant ($p = 0.018$). In addition, all the healthy subjects and the stroke patient could successfully operate the 7-DOF exoskeleton in real-time using the EEG-BMI and accomplished 40 and 24 trials, respectively.

5.5 Discussion and conclusions

This study presents and validates a novel control platform based on an EEG-BMI that links brain activity with the movement of a 7-DOF rehabilitation exoskeleton in real-time. Even if it is not possible to test it statistically, the results show that the TPR and FPR values of the healthy subjects were not noticeably different from ones of the stroke patient. Besides this, the number of times the decoder classified an output as "Movement" was significantly higher during the movement period than during the rest period. Although the performance of the decoder was not high, it should be taken into account that all the subjects were naive to motor imagery and a higher performance and more skillful control could be expected after several training sessions. Nevertheless, it is still not clear how strong the correlation between decoding performance and level of recovery is. In fact, Ramos-Murguialday et al. [49] demonstrated that this algorithm, albeit not the most accurate one, could serve to elicit certain degree of motor recovery, in combination with a dedicated BMI-based rehabilitation therapy. To the best of our knowledge, this is the only double-blinded study that showed an EEG-BMI based therapy that induced motor recovery in chronic stroke patients. Therefore,

although several algorithms could be used to decode EEG signals as part of a BMI system, we relied on this.

We have demonstrated that the participants were able to control the movement of the exoskeleton in real-time. Therefore, this whole system constitutes a potential rehabilitation platform for various reasons: i) it establishes a contingent link between the movement intention decoded from the brain activity and the actual movement of the paralyzed limb; ii) it provides a rehabilitation scenario in which functional movements towards various targets as well as the interaction with objects are considered; iii) it allows for the joint rehabilitation of distal and proximal joints, which has been proven to be beneficial [47]; iv) even patients with no residual movement at all could benefit from it; v) it can integrate other biosignals [68] and establish a hybrid control.

6. Chapter 6: Classification of different reaching movements from the same limb using EEG

This manuscript has been published as [53].

6.1 Abstract

Objective:
Brain-Computer-Interfaces (BCIs) have been proposed not only as assistive technologies but also as rehabilitation tools for lost functions. However, due to the stochastic nature, poor spatial resolution and signal to noise ratio from electroencephalography (EEG), multidimensional decoding has been the main obstacle to implement non-invasive BCIs in real-live rehabilitation scenarios. This study explores the classification of several functional reaching movements from the same limb using EEG oscillations in order to create a more versatile BCI for rehabilitation.
Methods:
Nine healthy participants performed four three-dimensional center-out reaching tasks in 4 different sessions while wearing a passive robotic exoskeleton at their right upper limb. Kinematics data were acquired from the robotic exoskeleton. Multiclass extensions of Filter Bank Common Spatial Patterns (FBCSP) and a linear discriminant analysis (LDA) classifier were used to classify the EEG activity into 4 forward reaching movements (from a starting position towards 4 target positions), a backward movement (from any of the targets to the starting position

and rest). Recalibrating the classifier using data from previous or the same session was also investigated and compared.
Results:
Average EEG decoding accuracy were significantly above chance with 67%, 62.75%, and 50.3% when decoding 3, 4 and 6 tasks from the same limb, respectively. Furthermore, classification accuracy could be increased when using data from the beginning of each session as training data to recalibrate the classifier.
Conclusion:
Our results demonstrate that classification from several functional movements performed by the same limb is possible with acceptable accuracy using EEG oscillations, especially if data from the same session are used to recalibrate the classifier. Therefore, an ecologically valid decoding could be used to control assistive or rehabilitation mutli-Degrees of Freedom (DoF) robotic devices using EEG data. These results have important implications towards assistive and rehabilitative neuroprostheses control in paralyzed patients.

6.2 Introduction

Brain-computer interface (BCI) systems can be used to decode brain activity into commands to control external devices [97, 178]. A recent double-blind controlled study has demonstrated for the first time that BCI control of a rehabilitation robot can promote motor recovery of severely paralyzed chronic stroke patients [49], being these results reproduced and confirmed [50, 60, 179]. BCIs can also function as an assistive device to restore a lost function, such as motor control. It is obvious that the number of DoFs that can be volitionally controlled is very relevant for assistive technologies and prosthetics. This has also been suggested to be of paramount importance in rehabilitation robotic therapies [180, 181]. Initial EEG-based BCI studies controlling several DoFs were achieved using motor imagery paradigms involving different limbs (e.g. 3D cursor control using hand vs feet vs tongue motor imagery) [182, 183]. This control strategy, albeit successful, is not based on "natural" or ecologically valid environments (i.e. based on EEG oscillations produced rapidly and without conscious effort when performing the task) and an extensive learning process is necessary to achieve acceptable control perfor-

mance. Recently, new strategies have been used to control multi-DoF robots based on EEG error potentials [184], steady state visual evoked potentials (SSVEPs) [185] and P300 potentials, even in ALS patients [186–188]. These strategies require attention but ignore motor descending corticospinal volleys, which seems to be key aspect in motor rehabilitation BCIs aiming at restoring natural corticomuscular connections [49]. Involvement on descending motor commands was suggested as key mechanism in motor rehabilitation because motor execution/attempt brain activity only was correlated with significant motor improvement compared to motor imagery related brain activity during a proprioceptive BCI rehabilitative intervention [49]. Other strategies like trajectory decoding [189] might offer a promising solution, albeit methodological challenges [190].

Neuronal population signals have been used to decode, with acceptable decoding performance, directional movement executions using non-invasive magnetoencephalographic (MEG) [86] and intracranial activity [84] from the motor cortex. Furthermore, intracortical activity has been succesfully used to control several degrees of freedom of robotic devices in primates [191, 192] and in humans [57, 193] decoding and/or encoding neural signals. Recently, control over functional electrical stimulation (FES) [194] in humans has been also achieved. Furthermore, intracranial EEG has also been used to continuously decode two-dimensional (2D) hand position [195], wrist movement trajectory [196] and seven different hand movement intentions in severely paralyzed chronic stroke patients [85]. However, invasive and MEG (nowadays too bulky and expensive to be considered as a practical option) data decoding are out of the scope of this paper.

Upper limb and especially hand movement decoding from electroencephalography (EEG) signals is still challenging mainly due to poor signal to noise ratio and spatial resolution [89]. Existing motor rehabilitation oriented BCI systems (i.e. decoding "natural" movement related EEG oscillations) decode two classes only using simple binary classification between rest and movement [49, 177, 179, 197–199]. These BCI systems only allow a user to control 1 DoF (e.g. orthosis for opening or closing the hand, a predefined functional electrical stimulation (FES) or visual feedback).

Recent studies have achieved classification of the same limb with acceptable performance using EEG data although many of these studies classify only two movements [87,89,200]. Liao et al. investigated the binary classification of ten different pairs of executed finger movements using 128-channel EEG signals achieving a promising average decoding performance of 77.1% [88]. In another study, six different wrist movement pairs (e.g. flexion vs extension or pronation vs supination) were decoded with average accuracy ranging from 60 to 80% [201]. A few other groups have reported some preliminary work on multi-class decoding using motor imagery and execution of movements from the same upper limb [68,87,202]. Yong et al. (2015) have shown a 3-class BCI system that discriminates EEG signals corresponding to rest, imaginary grasp, and elbow movement [87]. Furthermore, classification of hand movement directions from the same limb using EEG has not been sufficiently explored in the literature. Our previous work reported five class EEG decoding reported during multiclass classification of four movements directions and rest from the same limb [200].

We believe, discriminating different movements within the same limb would allow more intuitive control of neuroprostheses (e.g., brain controlled exoskeleton) without considering any artificial association between actual movement and neuroprosthetic movement. Therefore, in the here presented work, we aimed at discriminating 6 different functional movements from the same limb with acceptable accuracy levels using EEG data towards a more intuitive and natural control of rehabilitative devices like robotic exoskeletons and FES. Furthermore, we evaluated the impact of different recalibration strategies on the decoding to optimize system stability.

We hypothesize decoding accuracy levels allowing robotic control of rehabilitative devices of up to 6 functional movements from the same limb, could be achieved using EEG activity only.

6.3 Materials and Methods

6.3.1 Participants

Study participants included nine healthy right-handed subjects (6 male, age: 24±4 years) with no history of neurologic disease. Participants underwent four recording sessions (4 non-consecutive days) within eight days (average time between each session was 2 days). The experimental procedure was explained to the subjects and they were asked to sign a written consent form. Ethically permission was given by the ethical committee of the Faculty of Medicine, University of Tübingen, Germany.

6.3.2 Experimental Setup

Participants were seated in a comfortable chair in front of a desk (See Fig. A) especially designed for the experiment. Participants were asked to perform 4 different center-out functional reaching movements and move back to the initial starting position (see Fig. 6.1A) with their right upper limb attached to an IS-MORE 7-DoF robotic exoskeleton (Tecnalia, San Sebastian, Spain) upon imperative auditory cues (see Fig. 6.1A). All the participants were instructed to perform the outreaching movements in the same way, and rhythmic auditory cues were used to facilitate movements′ timing. The directional colored targets were named as Blue, Red, Green, and Brown. Participants were asked to reach a colored target and return to the rest position at a comfortable pace.

6.3.3 IS-MORE Robotic Exoskeleton

We decided to use an exoskeleton to record the kinematic data to simulate a realistic scenario condition in which a patient could brain-control the exoskeleton to produce functional movements like reach and grasp. For an optimal stroke rehabilitation paradigm, a realistic environment with different functional movements trained at the same time is very important. Training of reaching movements is key in stroke recovery, as it involves elbow-shoulder coordination [203]. The Exoskeleton was friction-free and motors were disengaged, although produced some mechanical restrictions (e.g. no vertical, or writs movement). Furthermore, the

haptics related to the use of the exoskeleton will be present during the real scenario and could also produce some brain activity from afferent origin, which could influence brain oscillatory signature of each motor task.

The exoskeleton can be moved in 7 DoFs including displacement and rotation of the forearm in a 2D horizontal plane (3 proximal DoFs: position in X, position in Y, and forearm orientation angle), pronation and supination of the wrist (1 distal DoF: wrist angle), flexion and extension of the thumb, index and the group of middle, ring and pinky fingers (3 distal DoFs: thumb angle; index angle; three fingers angle).

Kinematic data (position in X, position in Y, and forearm orientation angle) of the midpoint of the fore-arm was calculated and recorded via a camera attached to the bottom of the base of the device. The exoskeleton rolls on top of a map with micro optical symbols printed on it, which are used to calculate the instantaneous position (more details can be found in [68, 103]). The rest of the DoFs were recorded using motor encoders and potentiometers. Kinematic data was recorded at 18Hz. Participants also performed 4 hand grasping movements (pinch grip, key and cylindrical grasp and pointing with the index finger) and reach-and-grasp movements to the 4 targets described in the manuscript combining the different grasping movements using especially designed objects for that purpose. Although we have analyzed the data, we have not included neither the experimental procedure nor the classification results in this manuscript because we did not obtain "above chance level" classification results for the grasping movements.

6.3.4 Experimental Paradigm

Each experimental session was divided in 5 runs, each consisting of 40 trials (10 trials for each target). The experimental timing diagram for each trial is shown in Figure 6.1B. Each trial consisted of three phases separated by auditory cues: 1) resting interval (random length between 2-3 seconds); 2) an instructional cue regarding the target to be reached (2 sec); 3) "Go" cue to initiate reaching movements towards the indicated targets and come back to the starting position at a comfortable pace but always executed in less than 4 sec. In order to reduce ar-

tifacts, we asked subjects to keep the jaw and face muscles relaxed avoiding eye blinks or swallowing during data recording. Therefore, to increase participants′ awareness regarding artifacts, we performed a brief instruction task before the first session instructing subjects to perform face, neck, contralateral arm and eye movements, while raw data was shown to them.

6.3.5 Data acquisition

EEG was recorded according to the international 10-20 system from 32 active electrodes as FP1, FP2, F7, F3, Fz, F4, F8, FC5, FC1, FC2, FC6, T7, C3, Cz, C4, T8, TP9, CP5, CP1, CP2, CP6, TP10, P7, P3, Pz, P4, P8, PO9, O1, Oz, O2, and PO10 (ActiCap, Brain Products GmbH, Germany) and the cap was fixed by a chinstrap to avoid electrode shifts. EOG was recorded with passive electrodes. AFz and FCz were used as the ground and reference electrodes, respectively. The impedance of electrodes was kept below 5 kΩ. EEG data were sampled (BrainAmp, Brain Products GmbH, Germany) at a frequency of 2500Hz. BCI2000 software was used to record EEG data from the acquisition system and to present the auditory cues [204].

6.3.6 Data Analysis

Preprocessing

After offline visual inspection peripheral channels (Fp1, Fp2, T7, T8, TP9, TP10, P7, P8, O1, Oz, O2, PO9, and PO10) were removed from prospective data analysis due to excessive noise and/or artefacts. Blind Source Separation (BSS) algorithm [205] from the Automatic Artifact Removal (AAR) toolbox as an EEGLAB plug-in [206] was used to remove artifacts caused by eye-blinks and eye movements, and muscle activity from face, neck and shoulder movements. Live video streaming with a frontal view from the participants allowed the experimenter to control for systematic or random artifacts, which were reported to the participant if persistent and the correspondent experimental run was disregarded from the analysis. Data was downsampled to 250 Hz, band-pass filtered (0.1-70 Hz), and the power line noise was removed using a 50 Hz notch filter. An open-source

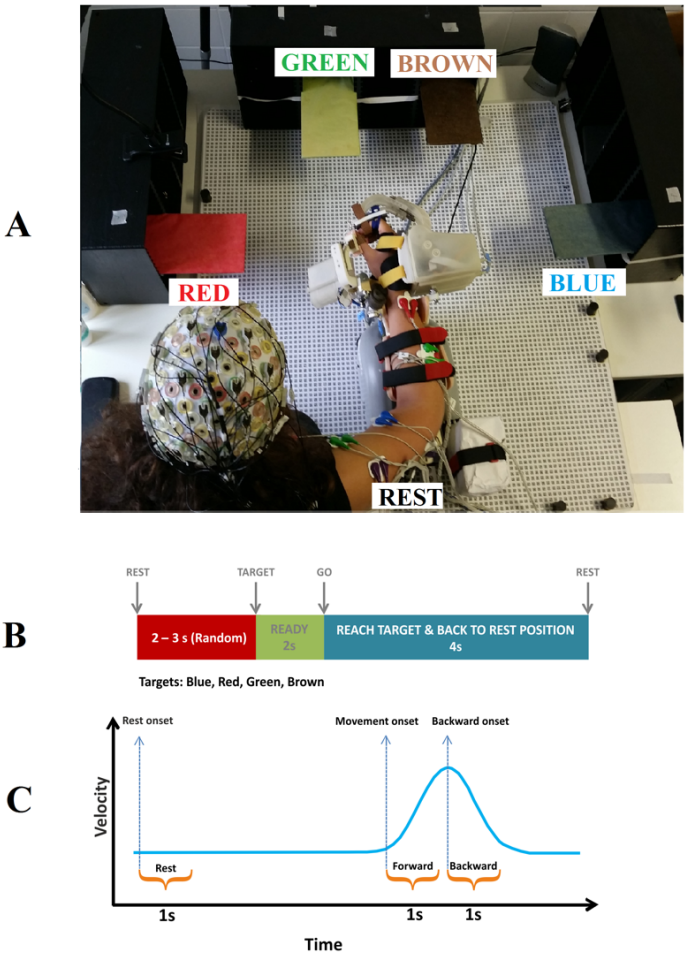

Figure 6.1: *A: Experimental situation. Participant performing a reaching movement from the starting rest position towards the green target. Reaching movements were executed towards the 4 different targets represented by rectangles coloured in blue, red, green and brown. B: Timing. To begin, an auditory "Rest" cue was presented indicating a random resting period between 2 to 3 sec. immediately after this period an instructional auditory cue indicated to which target the participant was asked to move (Blue, Red, Green, Brown). Two seconds afterwards a "GO" cue indicated the moment to start the active movement towards the targets at a comfortable pace, having a 4 seconds time out to perform the reaching movement and come back to the starting position. C: Movement onsets were identified for forward and backward movements into 1 second epoch for each trial by kinematics data. Rest class was also segmented into 1 second epoch from the beginning of each rest interval.*

MATLAB toolbox, BCILAB, was used to process the EEG data [207].

Time-Frequency Analysis

Time-frequency analysis for the investigation of spectral changes at distinct time points was performed using wavelet transforms even at the lowest frequency (1 Hz corresponding to 3 cycles during 1 s) as event-related spectral perturbations (ERSPs) [183]. The time window analyzed included 3 s before and 7 s after the auditory "Go" cue and the time course was obtained by averaging the power change of the frequency bands across all trials during the movement. The time window from -3 to -2 s before the "Go" cue was used as baseline (See Figure 6.2B).

Feature extraction and classification

The kinematics data (position in X, position in Y, and forearm orientation angle) of the base of the IS-MORE exoskeleton were only analyzed (up-sampled to 250Hz and synchronized with EEG data), and used to identify sub-movements within a task (forward and backward phases during reaching movements) and hence, to label EEG data. Every EEG trial for movements phase was segmented into two 1 second epochs (Fig 6.1C): a) starting from movement onset identified by kinematics data to forward movement towards the target); and b) starting movement after target was reached (backward movement towards the starting position). Rest class was also segmented into 1 second epochs from the beginning of each rest interval. Data from all trials for each class were appended and used to extract spatio-frequency features using Filter-Bank Common Spatial Patterns (FBCSP) [208], which is an extension of the standard Common Spatial Pattern (CSP) algorithm [209]. We applied FBCSP as feature extraction method because it uses frequency filtering into multiple frequency bands, which could benefit the decoding of different motor tasks as demonstrated previously [87]. Furthermore, CSP algorithm has been proven its efficacy calculating optimal spatial filters for motor related BCIs [87, 88, 195]. Spatial filters were created for three frequency windows: 7-15 Hz, 15-25 Hz, and 25-30 Hz. The log-variance of the filtered signal was used as feature for classification.

We set three as the number of spatial filters to use for the CSP algorithm in accordance to prior studies with CSP [87,208] resulting in 6 features per frequency band and 18 features per channel. The spatial patterns used in feature extraction representing the areas involved in each movement EEG activity were obtained with the help of FCSP patterns (Figure 6.2A). We obtained the topographical distribution of the difference in EEG activity during 2 different movement conditions (e.g. reaching towards Blue vs Rest) in specific frequency bands. As depicted with data from a representative participant in Figure 6.2A, the EEG activity difference is prominent when comparing each movement direction and Rest. However, the difference is not obvious when comparing EEG activity produced during reaching movements towards 2 different targets (e.g. Blue vs Red). Therefore, FCSP patterns of ERD of the mu and beta rhythms were needed to extract distinct features for the different execution movements.

The resulting feature vector was then fed to the Linear Discriminant Analysis (LDA) classifier as multi class classifier. Taking into account the similar performance of LDA and SVM for multiclass classification [87], we chose LDA as our preferred method. It is basically a two-class classifier extended to more classes by one-vs-one voting. For the one-vs-one voting scheme, the classifier was trained for a K(K-1)/2 binary classifiers in a K-way multiclass problem [210]. Validation performance was estimated using five-fold blockwise cross-validation with 5 trials safety margin. Thus, each session was split up into five folds, with each fold being used for testing and used the remaining four folds to train the classifier. Decoding accuracy was estimated according to the average over all folds for each session.

To evaluate the statistical significance thresholds for decoding accuracy, we used the chance levels ($p<0.05$) for an infinite number of trials and classes using the binomial cumulative distribution [211]. From now on, we will refer to this significance level when reporting classification accuracy results.

The collected EEG data contained nine different states: REST, and 8 actual directional movements: 4 forward (F) (towards BLUE, RED, GREEN, and BROWN

Table 6.1: *Decoding schemes: different sessions were used for training and testing to investigate re-calibration effects on classification performance. If the same session was used for training and testing (in scheme 1 and 2 indicated by *), it was evaluated using a 5-fold cross-validation to ensure that training and test set do not overlap. Scheme 3 trained with previous ìcalibrationî sessions and tested on current session.*

Scheme 1 (within session)		Scheme 2 (recalibrated between-sessions)		Scheme 3 (between sessions)	
Training	Testing	Training	Testing	Training	Testing
S1	S1*				
S2	S2*	**S1-S2**	S2*	**S1**	S2
S3	S3*	**S1-S2-S3**	S3*	**S1-S2**	S3
S4	S4*	**S1-S2-S3-S4**	S4*	**S1-S2-S3**	S4

targets) and 4 backward (B) (coming back from each target to the starting position) that we combined in one movement only (coming back to the starting position from any target (BACKWARD)) to reduce the number of classes. In this manuscript, we described the classification of three different complexity cases, decoding 3, 4 and 6 movement classes:

1) 3 class (RED, BLUE, REST)

2) 4 class (RED, BLUE, BACKWARD, REST)

3) 6 class (RED, BLUE, GREEN, BROWN, BACKWARD, REST)

Recalibration

In order to investigate how the recalibration could affect the classification results, we first divided each session in 5 data blocks that were used later as folds for the cross-validation of the classification and tested three decoding schemes using data from the different four sessions (see Table 6.1):

Scheme 1 (within session): We used each session for both training and testing with five-fold cross-validation. The within session decoding accuracy was averaged over all folds.

Scheme 2 (recalibrated between-sessions): Previous and current session data (four folds) were used for training, and only one fold of current session (S2* or S3* or S4*) was used for testing. The recalibrated between sessions decoding accuracy was averaged over all folds.

Scheme 3 (between sessions): All previous session data were used for training and current session was used for testing in between sessions.

Statistical analysis

We performed two separate statistical analyses to evaluate: (i) changes in performance over sessions, and (ii), if any factor (scheme, class, and session) had a significant effect in performance.

- To check for learning effects over sessions, we compared classification accuracy differences between the different sessions using a repeated measures ANOVA separately for the 3-class, 4-class, and 6-class problems. The time (four sessions for scheme 1, and three sessions for schemes 2 and 3; see Table1) was considered the independent variable and the classification accuracy the dependent variable.

- A three-way ANOVA was performed to study the influence of the three factors (Scheme, Class, Session) in classification accuracy (dependent variable). Factor scheme consisted of 3 levels (Scheme 1, Scheme 2, Scheme 3); factor classification problem included 3 levels (3-, 4-, and 6-classes); and factor session had also 3 levels (S2, S3, S4). Notice that session S1 was removed from this analysis to facilitate comparisons, as it was only tested in Scheme 1 (within session). When these factors or their interactions reached significance ($p < 0.05$), subsequent post-hoc t-tests were performed, applying a Bonferroni correction for multiple comparisons. These post-hoc comparisons were considered significant if the p-value was below 0.05 after correction.

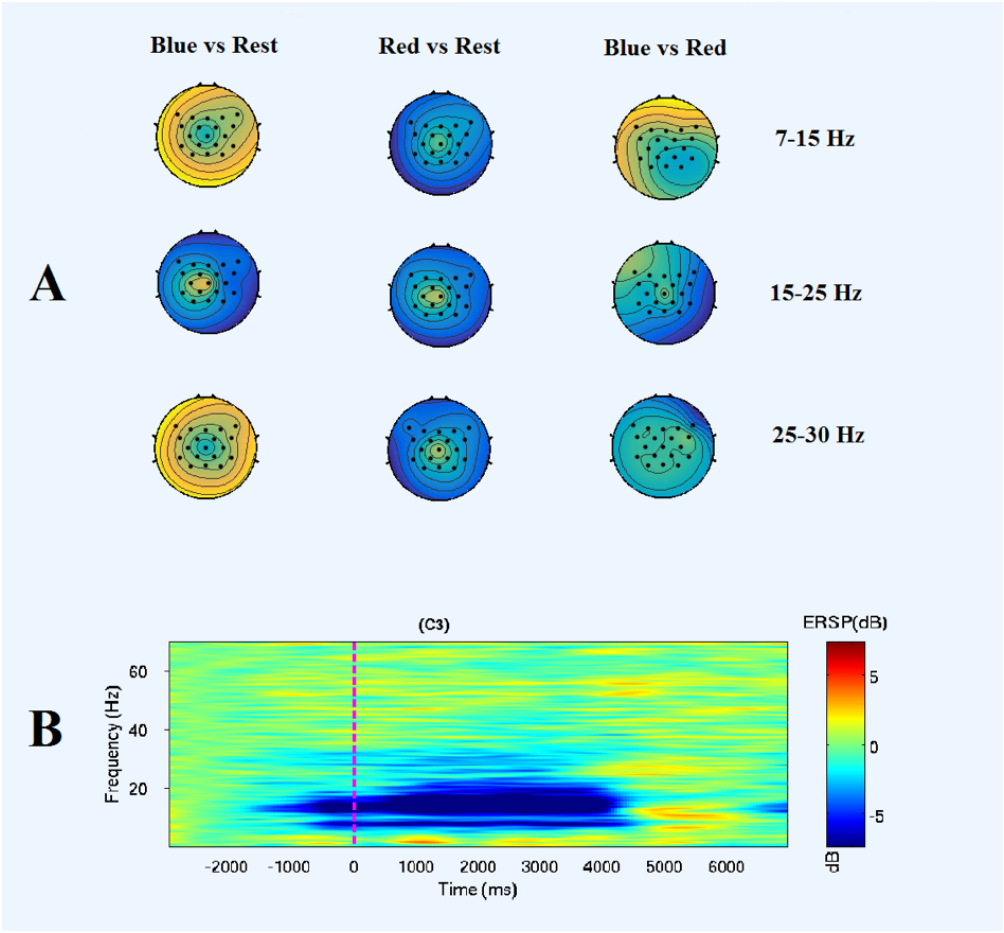

Figure 6.2: *Filter Bank Common Spatial Pattern (FBCSP) and Time-Frequency analysis: EEG data from a representative participant transformed into spatio-frequency topographical maps and into one selected channel time-frequency domain. A: Highest-ranking common spatial patterns for each pair of movements within the specific frequency band (Black dots represent the 19 channels used for classification). BLUE and RED stand for reaching movement towards the blue and red target respectively. B: Channel C3 time-frequency event-related spectral perturbation (ERSP) during reaching towards the blue target. The vertical dashed line shows the time when the Go cue was presented to the participant.*

Table 6.2: *Within session classification results for 3-class (left), 4-class (middle), and 6-class (right) classification accuracy for all participants and sessions. For each participant, average and SD is shown in the last column of the table. In the lower cell of the table significance level of the decoding is shown. Five-fold cross-validation was used to estimate the accuracy. "P" indicates participant and "S" for the session.*

	3-class					4-class					6-class				
	S1 (%)	S2 (%)	S3 (%)	S4 (%)	Average (%)	S1 (%)	S2 (%)	S3 (%)	S4 (%)	Average (%)	S1 (%)	S2 (%)	S3 (%)	S4 (%)	Average (%)
P1	70	86	81	64	75.25 ± 10	59	64	69	59	62.75 ± 4.7	47	54	67	49	54.25 ± 8.9
P2	69	72	78	80	74.75 ± 5.1	72	71	77	75	73.75 ± 2.7	64	53	70	69	64 ± 7.7
P3	65	62	62	73	65.5 ± 5.1	59	62	60	70	62.75 ± 4.9	54	63	49	55	55.25 ± 5.8
P4	64	72	62	65	65.75 ± 4.3	59	60	65	58	60.5 ± 3.1	43	51	53	41	47 ± 5.8
P5	52	60	58	65	58.75 ± 5.3	58	59	55	69	60.25 ± 6	44	41	40	42	41.75 ± 1.7
P6	56	53	49	55	53.25 ± 3	47	51	46	48	48 ± 2.1	38	36	28	32	33.5 ± 4.4
P7	71	61	78	78	72 ± 8	66	62	65	68	65.25 ± 2.5	50	55	58	52	53.75 ± 3.5
P8	64	63	82	75	71 ± 9.1	65	67	74	64	67.5 ± 4.5	49	52	54	47	50.5 ± 3.1
P9	66	65	69	67	66.75 ± 1.7	61	66	67	62	64 ± 2.9	53	52	58	50	53.25 ± 3.4
Average	64.1 ± 6.3	66 ± 9.5	68.7 ± 11.6	69.1 ± 7.9	67 ±7.33	60.6 ± 6.8	62.4 ± 5.6	64.2 ± 9.5	63.6 ± 8	62.75 ± 6.8	49.1 ± 7.5	50.7 ± 7.9	53 ± 12.9	48.5 ± 10.3	50.3 ± 8.76
Significance level	**40%**					**30%**					**20.33%**				

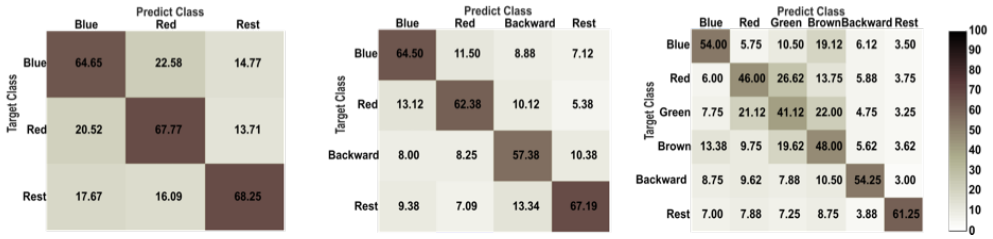

Figure 6.3: *Within session classification results. Confusion matrices showing the mean classification accuracy (%) of all participants for different combination of movements (BLUE, RED, GREEN, BROWN, backward, and Rest).*

6.4 Results

Regardless of the number of movements to be classified and the calibration strategy, the classification results were above significance level in all participants. For clarity, the results section was categorized into three sections according to different decoding schemes (calibration strategy) and complexity of the classification (number of movements to be classified).

Scheme 1 (within session classification): Each session was used for training and testing with five-fold cross-validation.

3-Movements Classification

We obtained an average accuracy of 67±7.33% (significance level 40%) for classifying 3-classes (Blue vs Red vs Rest) as can be seen in detail from Table 2. The maximum classification accuracy over all sessions was observed in Participant1 (75.25±10) and the minimum for Participant 6 (53.25±3). The maximum and minimum classification accuracy for one session was observed in Participant1 (Session 2; 86%) and Participant6 (Session 3; 49%) respectively. The mean average accuracy across participants increased from the first session (64%) to the fourth session (69%) being this difference non-significant (p=0.61). The confusion matrix demonstrated that the 3 classes were similarly classified with no clear confusion between classes.

4-Movements Classification

Table 6.2 (in the middle) shows a mean classification accuracy of 62.75±6.89% (significance level 30%) for all participants when classifying 4-classes (Blue, Red, Backward, and Rest). Maximum classification accuracy over all sessions was observed in Participant2 (73.75±2.7) and the minimum in Participant6 (48±2.1). Same as for the 3-class classification, the maximum and minimum classification in one session was achieved by Participant1 (Session 3; 77%) and Participant6 (Session 3; 46%) respectively. The Average accuracy increased from the first session for 60.6% compared to the fourth-session for 63.6% (See Table 6.2 in the middle), being this difference non-significant (p=0.76).

6-Movements Classification

Table 2 (in the right) shows an average accuracy of 50.3±8.76% (significance level 20.33%) for all participants when classifying 5 movements towards different targets (Blue, Red, Green, Brown, and Backward) and Rest. Maximum classification accuracy over all sessions was observed in Participant2 (64±7.7) and the minimum in Participant6 (33.5±4.4). The maximum and minimum classification in one session was observed in Participant2 (Session 3; 70%) and Participant6 (Session 3; 28%) respectively. In the Confusion matrix (Fig 3. in the right) can be seen that in contrast to the targets more separated from each other (Blue and Red), neighbor targets are confused by the classifier. Average accuracy did not

change significantly between sessions (p=0.77).

Scheme 2 (recalibrated between-sessions classification): In this scheme, previous and current sessions were used for training and only the current session was used for testing with five-fold cross-validation.

Table 6.3 shows the mean decoding performance of multiclass combinations of 3-class, 4-class, and 6-class during 3 different recalibration using different combinations of sessions: a) two sessions were used for training (S1, S2) and tested on unseen data of S2; b) three sessions were used for training (S1, S2, S3) and tested on unseen data of S3; and c) four sessions (S1, S2, S3, S4) were used for training and tested on unseen data of S4. In each recalibration of sessions (Table 3.) the previous and the current session were used as the training sets, and the current session was used as the testing set.

As shown in Table 6.3, mean classification accuracies for the first recalibration of sessions (S1 and S2 for training; S2* for testing) were 67.2±11.4%, 61.5±13%, and 47.5±11.54% for 3-class, 4-class, and 6-class respectively. The maximum classification accuracy in the 3-, 4- and 6-class paradigm was 80% (Participant9), 74.4% (Participant9) and 65.2% (Participant2) respectively. The minimum classification accuracy in the 3-, 4- and 6-class paradigm was obtained always for Participant6 and was 49.3%, 35.6%, and 27%, respectively.

During the second recalibration of sessions in Table 6.3, mean classification accuracies (S1, S2, S3 for training; S3* for testing) were 69.2±12.13%, 62.7±15.27%, and 47.15±11.38%. The maximum average accuracy in the 3-, 4- and 6-class paradigm was 87.5% (Participant9), 86.1% (Participant2) and 63.1% (Participant9), respectively. The minimum classification accuracy in the 3-, 4- and 6-class paradigm was obtained for Participant6 and was 48.6%, 42.7%, and 28.7%, respectively.

During the third recalibration of sessions, mean classification accuracies (S1, S2, S3, S4 for training; S4* for testing) were 67.1±15.86, 59.7±18.9, and 46.8±13.23.

Table 6.3: *Mean classification accuracy (%) for the offline analysis of multiclass combination during different session calibration and current session with testing on current session. If the same session was used for training and testing (in scheme 1 and 2 indicated by *), it was evaluated using a 5-fold cross-validation to ensure that training and test set do not overlap. First recalibration: two sessions were used for training (S1, S2) and tested on unseen data of S2*. Second recalibration: three sessions were used for training (S1, S2, S3) and tested on unseen data of S3*. Third recalibration: four sessions (S1, S2, S3, S4) were used for training and tested on unseen data of S4*. "P" indicates participant.*

	3-class			4-class			6-class		
	S1-S2* (%)	S1-S2-S3* (%)	S1-S2-S3-S4* (%)	S1-S2* (%)	S1-S2-S3* (%)	S1-S2-S3-S4* (%)	S1-S2* (%)	S1-S2-S3* (%)	S1-S2-S3-S4* (%)
P1	79	73.7	48.1	73.6	60.4	33.6	57.2	52.6	44.8
P2	79.6	84.9	84.8	73.7	86.1	82.2	65.2	58.5	67.1
P3	55.3	60.5	62	51.3	48	48.8	38.1	37.5	36.2
P4	66.5	63.2	59.9	68.4	65	54.6	53.8	46	38.2
P5	59	64.2	60.5	62	61.5	64.5	52.5	55.4	56.5
P6	49.3	48.6	45.4	35.6	42.7	34.2	27	28.7	25.7
P7	63.2	67.6	76.4	62.7	49.3	69.8	42.8	36.2	49.4
P8	73.7	72.9	76.5	52.6	66.5	63.1	40.2	46.4	42.1
P9	80	87.5	91	74.4	85	87	50.6	63.1	62
Average	67.2 ± 11.4	69.2 ± 12.13	67.1 ± 15.86	61.5 ± 13	62.7 ± 15.27	59.7 ± 18.9	47.5 ± 11.54	47.15 ± 11.38	46.8 ± 13.23
Significance level	38	37.11	36.5	28.5	28	27.5	19.16	18.77	18.41

The maximum classification accuracy was also observed for 3-, 4- and 6-class 91% (Participant9), 87% (Participant9), and 67.1% (Participant2), respectively. The minimum classification accuracy for 3-, 4- and 6-class was obtained for 45.4% (Participant6), 33.6% (Participant 1), and 25.7% (Participant6), respectively. For all combinations the significance level is shown in Table 6.3. Furthermore, we also analyzed the difference in performance for scheme 2 depending on how many sessionsí data were included in the recalibration of the classifier (See Table 6.3). Although there was an overall increase in classification accuracy, our ANOVA analysis resulted in not significant results, (3-class p-value= 0.93; 4-class p-value= 0.92; 6-class p-value= 0.98).

Scheme 3 (between-sessions classification): In this scheme, previous sessions were used for training and only current session was used for testing.

Table 4 shows the mean classification accuracy of multiclass combination for 3-class, 4-class, and 6-class for three different combinations (see Table 6.1). We

analyzed 3 different recalibration of sessions using the previous session as training set and the current session as test set. a) one session was used for training (S1) and tested on session S2; b) two sessions were used for training (S1, S2) and tested on session S3; c) three sessions (S1, S2, S3) were used for training and tested on session S4.

For the first recalibration in Table 6.4, the mean classification accuracies (S1 for training; S2 for testing) were 52.1±8.34%, 54±9.98%, and 42.5±9.88% for 3-class, 4-class, and 6-class, respectively (Table 6.4). The maximum classification accuracy was observed for 3-, 4-, and 6-class 68.4% (Participant9), 72.4% (Participant2), and 55.9% (Participant2). The minimum classification accuracy in 3-, 4- and 6-class paradigm was obtained 41.4% (Participant6), 37.5% (Participant6), and 29% (Participant9), respectively.

In the second recalibration in Table 6.4, mean classification accuracies (S1 and S2 for training; S3 for testing) were 58.3±13.93%, 57.7±13.86%, and 44.4±11.79%. The maximum average accuracy was observed for 3-, 4-, and 6-class 77% (Participant8), 81.6% (Participant9), and 63.2% (Participant9), respectively. The minimum classification accuracy in the 3-, 4- and 6-class was obtained for 38.8% (Participant7), 41.4% (Participant3), and 27% (Participant6), respectively. In the third recalibration in Table 4, mean classification accuracies (S1, S2, S3 for training; S4 for testing) were 58.5±12.2, 55.7±16.03, and 44.2±13.5, respectively. The maximum classification accuracy was observed for 3-, 4- and 6-class 71.7% (Participant7), 75.7% (Participant9), and 68.4% (Participant2). The minimum classification accuracy in the 3-, 4- and 6-class was obtained for 41.4% (Participant1), 32.2% (Participant1), and 25.7% (Participant6). ANOVA analysis to test session effect resulted in not significant results for scheme 3 (See Table 6.4) in the recalibration of the classifier (3-class p-value= 0.43; 4-class p-value= 0.83; 6-class p-value= 0.93).

Comparison of recalibration schemes:

A 3-way ANOVA was used to assess the influence of the three calibration schemes (within session, recalibrated between sessions, and between sessions),

Table 6.4: *Mean classification accuracy (%) of the offline analysis of multiclass combination during session calibration and testing on current session. First recalibration: one session was used for training (S1) and tested on session S2. Second recalibration: two sessions were used for training (S1, S2) and tested on session S3. Third recalibration: three sessions (S1, S2, S3) were used for training and tested on session S4. "P" indicates participant.*

	3-class			4-class			6-class		
	S1-S2 (%)	**S1-S2-S3** (%)	**S1-S2-S3-S4** (%)	**S1-S** (%)	**S1-S2-S3** (%)	**S1-S2-S3-S4** (%)	**S1-S2** (%)	**S1-S2-S3** (%)	**S1-S2-S3-S4** (%)
P1	42.8	62.5	41.4	55.3	58.6	32.2	48.7	55.3	37.1
P2	49.3	69.7	71.1	72.4	71.1	74.3	55.9	50	68.4
P3	46.1	51.3	53.9	46.7	41.4	46.1	34.9	39.5	33.6
P4	54.6	46.7	53.9	61.2	58.6	48	50	38.2	32.2
P5	57.2	62.3	65.4	53.5	57.5	60.5	50.2	53.5	52
P6	41.4	42.8	42.8	37.5	40.8	35.5	34	27	25.7
P7	55.3	38.8	71.7	55.3	44.7	67.8	48	32.2	46.7
P8	54	77	73	46.1	65.8	61.2	32.2	40.8	46.1
P9	68.4	73.7	53.9	58	81.6	75.7	29	63.2	56.6
Average	52.1 ± 8.34	58.3 ± 13.93	58.5 ± 12.2	54 ± 9.98	57.7 ± 13.86	55.7 ± 16.03	42.5 ± 9.88	44.4 ± 11.79	44.2 ± 13.5
Significance level	40	38	37.11	300	28.5	28	20.33	19.6	18.77

classification problems (3-, 4-, and 6-classes), testing sessions, and the interaction between factors (see Table 6.5). As can be seen in Table 6.5, the factors scheme and class had a significant effect on the classification accuracy (Scheme, $F=11.71$; $p<0.0001$ and class, $F=43.71$; $p<0.0001$). The factor sessions, as well as all the interactions between factors were not significant. All the post-hoc comparisons can be seen in Table 6.6. For the factor scheme, significant differences were found between Schemes 1 and 3 (i.e., calibration within session vs between sessions, $p<0.0001$), and between Schemes 2 and 3 (i.e., recalibrated between sessions vs between sessions, $p=0.001$). For the factor classification problem, significant differences were found between the 3-class and 6-class problems ($p<0.0001$), and between the 4-class and 6-class problems ($p<0.0001$). Figure 6.4 shows the interaction plot between the two significant factors and the dependent variable (classification accuracy).

6.5 Discussion

In this study, multiple decoding schemes and algorithms for the continuous mapping of EMG signals into upper limb kinematics were tested. The analysis included

Table 6.5: *Results of 3-way Anova between the three recalibration schemes. Significant difference was tested for the main factors with recalibration scheme (3 levels: Scheme1, Scheme2, Scheme3), classification problem (3 levels: 3-, 4- and 6-classes), test sessions (3 levels: S2, S3, S4) and interaction factor. * P < .05.*

	3-way ANOVA scheme × class × session		
	df	*F*-value	*p*-value
Class	2	43.71	$p < 0.0001$[a]
Scheme	2	11.71	$p < 0.0001$[a]
Session	2	0.72	0.484
Scheme × class	4	0.88	0.475
Scheme × session	4	0.22	0.923
Class × session	4	0.17	0.951
Scheme × class × session	8	0.08	0.999
Error	216		

[a] $p < 0.05$.

Table 6.6: *Results of the multiple comparisons for scheme and class. Significant difference was tested for the calibration schemes pair-wise (Scheme1 vs Scheme2, Scheme1 vs Scheme3, and Scheme2 vs Scheme3) and classification problem pair-wise (3-class vs 4-class, 3-class vs 6-class, 4-class vs 6-classes). * P < .05, Bonferroni corrected.*

Scheme	**Sch1 Sch2**	**Sch1 Sch3**	**Sch2 Sch3**
p-value	0.876	$p < 0.0001$[a]	0.001[a]
Class	**3-class 4-class**	**3-class 6-class**	**4-class 6-class**
p-value	0.130	$p < 0.0001$[a]	$p < 0.0001$[a]

[a] $p < 0.05$, Bonferroni corrected.

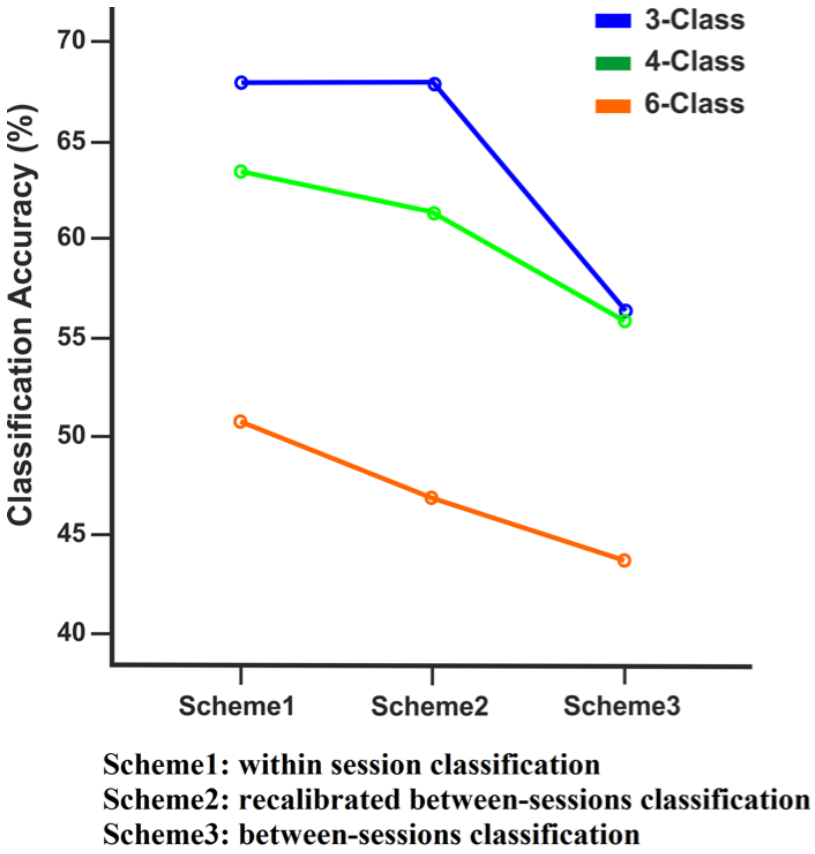

Figure 6.4: *Classification accuracy of three class combination between three schemes. The graph shows the mean classification accuracy for three classification problem (3-, 4- and 6-classes) between three recalibration schemes (Scheme1: within session classification, Scheme2: recalibrated between sessions, and Scheme3: between-sessions classification).*

the decoding of distal and proximal DOFs during complex functional movements involving coordinated upper-arm and fore-arm muscle activity. Kalman filter and ridge regression techniques were compared across different decoding scenarios in order to test their ability to overcome the EMG non-stationarity as well as the variability in the performed movements. All these aspects are of great importance and have a direct impact on the clinical applications of EMG decoding.

The Kalman filter model has been extensively used before for myoelectric control applications. However, simple algorithms like ridge regression are often underestimated and therefore excluded from EMG decoding studies. Regularization methods impose a constraint to the model coefficients (i.e. control how large the coefficients are). This introduces the advantage of preventing overfitting and thus, of having a model with good generalization characteristics. This is highly desirable, especially in situations in which the decoder should be able to generalize to movements from which sufficient training data is not available. The results of the work presented here confirm our hypothesis that ridge regression generalizes to new EMG data better than the Kalman filter. Therefore, ridge regression constitutes a desirable algorithm for the continuous EMG decoding of upper limb kinematics.

Factors such as external interference, electrode shift and lift, electrode impedance changes, muscle fatigue, sweat and varying upper-limb positions alter the EMG signal distribution. Sources of variation like external interference can be mostly suppressed by filtering or electromagnetic shielding techniques. However, the remaining sources constitute a persistent issue in clinical practice and severely affect the performance of myoelectric decoders. In fact, we believe that in this particular study, one of the main factors affecting the performance stability could have been the variable positioning of the EMG electrodes from session-to-session since they were just placed within the general vicinity. A daily re-calibration phase was proposed as a solution to alleviate the effects of such non-stationarities. The additional time of re-calibrating the decoder and the cost of recording new data at the beginning of each session could be a concern for certain applications. Nevertheless, the performance comparisons between the three developed decoding schemes showed that there was a significant improvement in performance (a 14% increase

in CC and a 8% reduction in NRMSE with respect to SS) when a re-calibration of the decoder was carried out. Moreover, the NRMSE values of the re-calibrated decoder were not significantly different from those achieved when training and testing the decoder with data from the same session (WS2 decoder). This implies that a re-calibration phase could reduce the error to the extent that the values would be just as low as if the decoder was trained using a larger amount of data only from the current session. It should also be mentioned that the calibration data length was 5 min, 1.5 min and 3 min for each task respectively and that it took a negligible amount of time to build the decoding model and choose the optimal regularization parameter, as opposed to other more complex algorithms. Therefore, the proposed approach was not very time and computationally demanding and served to significantly raise the performance. Nonetheless, the benefits and disadvantages of including a daily re-calibration phase should be carefully considered in order to choose the most suitable approach for each particular scenario.

The majority of recent studies in the field of myoelectric control interfaces are constrained to the decoding of a few distal or proximal DOFs. These devices could be employed for those cases in which impaired function of a few specific DOFs is present. However, the ability for interfaces to control multiple DOFs of the upper limb during dexterous and functional movements is necessary, especially for patients who are undergoing rehabilitation therapies for motor impairment of an entire extremity. Our protocol included the decoding of coordinated multi-joint movements. While the NRMSE was stable at a very low value for all the DOFs, the lower CC values achieved for the distal DOFs might be due to the limited number of electrodes used for the decoding of distal DOFs. Extensors and flexor muscles of the forearm are often more difficult to target and it is usually hard to isolate the EMG activity from each recorded muscle. This makes the discrimination and decoding of individual finger movements more challenging. The minimum number of electrodes on the forearm that are necessary to attain an accurate decoding of distal DOF movements has been extensively investigated before [42, 72, 105, 212]. From the results presented in these previous studies, it can be concluded that a minimum of 12-16 electrodes are necessary to distinguish between multiple individual finger and wrist movements. Therefore, future studies should be performed with additional

electrodes placed over the fore-arm in order to improve the decoding accuracy of distal DOFs.

6.6 Conclusion

This study addressed important aspects for the use of myoelectric control interfaces in clinical practice, which were: (*i*) the choice of a decoding algorithm with good generalization characteristics; (*ii*) the training procedure to follow in order to develop a decoder, which is robust to non-stationarities; and (*iii*) the decoding of coordinated distal and proximal DOF movements during complex functional tasks. From the results presented here, we concluded that a simple regularized algorithm such as ridge regression has good generalization characteristics for the EMG-based continuous decoding of multiple DOFs of the upper limb. Moreover, we demonstrated that by introducing a daily re-calibration phase the effects of the session-to-session non-stationarities could be significantly mitigated. Further studies including additional electrodes over the fore-arm should be performed in order to more accurately discriminate individual finger movements. Nevertheless, this pilot study is an important step towards the development of a robust myoelectric interface for the online control of coordinated multi-joint movements in robot-aided rehabilitation therapies.

6.7 Acknowledgements

This study was funded by the Baden-Württemberg Stiftung (GRUENS), the Indian-European collaborative research and technological development projects (INDIGO-DTB2-051), the Natural Science Fundation of China (NSFC 31450110072), EU COST action TD1006, Deutsche Forschungsgemeinschaft (DFG, Koselleck), Eva und Horst Köhler Stiftung, Volkswagen Stiftung and Bundes Ministerium für Bildung und Forschung BMBF MOTOR-BIC (FKZ 13GW0053). A. Sarasola-Sanz's work is supported by La Caixa-DAAD scholarship, E. López-Larraz's work by the Spanish projects HYPER-CSD2009-00067 and DGA-FSE (grupo T04) and N. Irastorza-Landa's work by the Basque Government and IKERBASQUE, Basque Foundation for Science, Bilbao, Spain.

7. Chapter 7: A Hybrid Brain-Machine Interface based on EEG and EMG activity for the Motor Rehabilitation of Stroke Patients

This manuscript has been published as [71].

7.1 Abstract

Including supplementary information from the brain or other body parts in the control of brain-machine interfaces (BMIs) has been recently proposed and investigated. Such enriched interfaces are referred to as hybrid BMIs (hBMIs) and have been proven to be more robust and accurate than regular BMIs for assistive and rehabilitative applications. Electromyographic (EMG) activity is one of the most widely utilized biosignals in hBMIs, as it provides a quite direct measurement of the motion intention of the user. Whereas most of the existing non-invasive EEG-EMG-hBMIs have only been subjected to offline testings or are limited to one degree of freedom (DoF), we present an EEG-EMG-hBMI that allows the simultaneous control of 7-DoFs of the upper limb with a robotic exoskeleton. Moreover, it establishes a biologically-inspired hierarchical control flow, requiring the active participation of central and peripheral structures of the nervous system. Contingent visual and proprioceptive feedback about the user's EEG and EMG activity

is provided in the form of velocity modulation during functional task training. We believe that training with this closed-loop system may facilitate functional neuroplastic processes and eventually elicit a joint brain and muscle motor rehabilitation. Its usability is validated during a real-time operation session in a healthy participant and a chronic stroke patient, showing encouraging results for its application to a clinical rehabilitation scenario.

7.2 Introduction

Hybrid brain machine interfaces (hBMI), understood as systems that directly decode the user's intention from brain and possibly other type of signals (electromyogram (EMG), electrooculogram (EOG), kinematics, force, etc) to control an actuator, are recently getting more attention in the field of assistive and rehabilitative technologies for motor-disabled people.

Despite conventional non-invasive BMI therapies have shown noteworthy results in rehabilitative [49, 50, 59, 60, 199] applications, they have limitations such as low reliability and accuracy when it comes to complex functional task training. Although the inclusion of additional non-physiological information such as kinematics, may improve BMI performance, it is not a direct link to the nervous system and might be less efficient producing functional neuroplasticity in a rehabilitative solution. On the other hand, EMG has been widely employed to control prostheses, rehabilitation exoskeletons or functional electrical stimulation systems, as it provides a more direct and robust measurement of the user's motion intention than brain signals. However, issues such as the absence of sufficient residual EMG activity or muscle fatigue may hinder the exploitation of myoelectric interfaces. Thus, hBMIs have emerged as systems that build on the advantages and alleviate the restraints of each of the single signal-based approaches, resulting in a more robust system.

A few studies have already demonstrated that introducing supplementary input information coming from the muscles can lead to a higher decoding accu-

racy [61–66] or the inclusion of more degrees of freedom (DoFs) [67], reflected in a richer and smoother control of assistive or rehabilitation devices. Nonetheless, the way in which the control is shared between the input signals is not trivial and varies among applications. Although numerous input processing methods (sequential or simultaneous) and fusion algorithms (e.g. outputs of the EMG- and EEG-classifiers are fused with equally balanced weights or using a Bayesian approach [61]) have been proposed, it still remains a challenge to find a fusion strategy that takes into account all the variables playing a role on the control.

We present a hBMI system that consists of an EEG-based binary classifier and an EMG-based continuous decoder of trajectories. To the best of our knowledge, the only study that carried out a real-time testing of a similar hBMI is [213], in which 4 able-bodied subjects and a spinal cord injury patient operated a hBMI to control the elbow joint angle (1 DoF) during a functional task with an exoskeleton. Our approach goes a step further and allows the real-time control of 7 DoFs of the upper limb. Moreover, it follows a biologically-inspired hierarchical control flow involving both central and peripheral structures of the nervous system. Additionally, it puts emphasis on the correction of pathological muscle activity, which is of paramount importance to ensure an effective transfer to activities of daily living and hence, a proper motor rehabilitation [34]. The usability of the hBMI is evaluated in a real-time operation session with a healthy individual and a chronic stroke patient.

7.3 Methods

7.3.1 Experimental design

One healthy subject (male, age: 26) and a chronic stroke patient (male, age: 62, 2 years from stroke, severe left hemiparesia, modified upper limb Fugl-Meyer Assessment (mFMA) = 59/114 and combined hand and arm FMA = 7/54) volunteered to participate in the study. Both of them were naive to the operation of BMIs and gave written consent to the procedures as approved by the Ethics Committee of the Faculty of Medicine of the University of Tübingen, Germany. The partici-

pants underwent a calibration session and a real-time hBMI operation session on separate days. Notice that since the protocol that we designed includes the use of both upper limbs, for simplicity we will refer to the non-dominant side of the healthy participant as the paretic side and to the dominant one as the healthy side.

The actuator of the hBMI was the IS-MORE exoskeleton (Tecnalia-San Sebastian, Spain). It is a 7-DoF upper limb robotic exoskeleton (see Fig. 7.1), which allowed the displacement and rotation of the forearm on a 2D horizontal plane parallel to the mat's plane (3 proximal DoFs : (i) p_x position; (ii) p_y position; (iii) θ_{xy} angle), the pronation and supination of the wrist (1 distal DoF: (iv) ϕ_{wrist} angle) and the flexion and extension of the thumb, the index and the group of middle, ring and pinky fingers measured as the angle of rotation with respect to the metacarpophalangeal joints (3 distal DoFs: (v) δ_{thumb}; (vi) ψ_{index}; (vii) $\alpha_{3fingers}$. The exoskeleton was placed over a 70 x 50cm mat surrounded by three shelves marked with different colors, which constituted the three targets the participants had to reach during the experiments (see Fig. 7.1).

Participants started the real-time operation task with their paretic arm and hand relaxed in a comfortable rest position. Then participants were asked, upon auditory cues, to reach one of the three targets around the workspace (see Fig. 7.1), while supinating the wrist and opening their hand. They were given 7 seconds to reach the final configuration. If the target was not reached, the trial was considered unaccomplished and an inter-trial interval of 3-5 seconds started, followed by a 2 second-preparation time. After this, a new trial from the current position towards the same target began. Once the target was reached, participants were instructed to go back to the initial rest position following the same procedure. In each block, participants had to reach each target twice. The healthy subject completed 5 blocks while the patient was able to operate the hBMI during 3 blocks.

The calibration session was divided into an EEG screening and an EMG calibration. The reason for this was that the EMG calibration was performed with the healthy upper limb. This implied that no EEG activity that reflected the movement volition of the paretic upper limb was available in order to select the

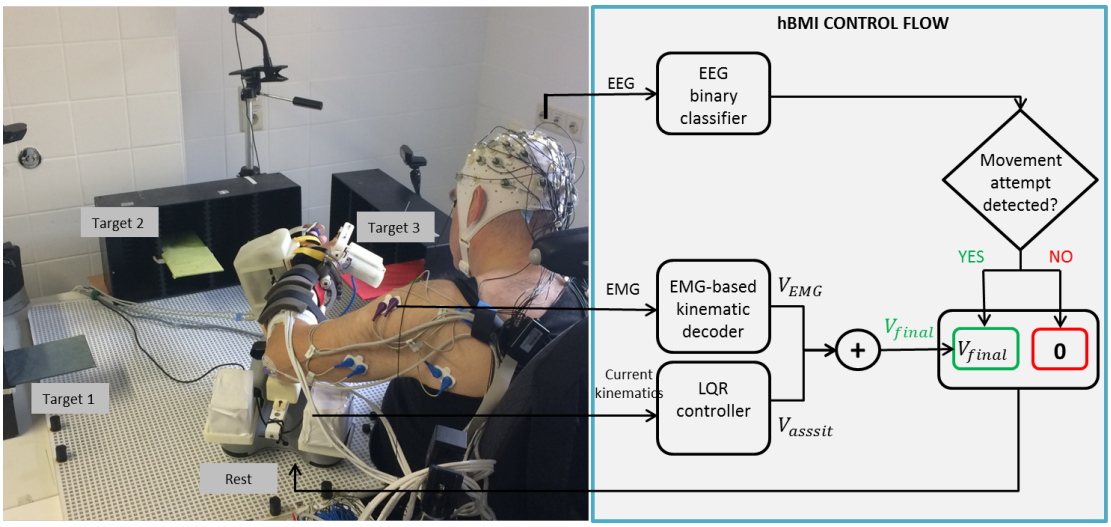

Figure 7.1: *(Left): workspace where the experiments were performed, showing the three targets the participants had to reach and the initial "Rest" position. (Right): hBMI hierarchical control flow employed during the hBMI operation session.*

electrodes on the ipsilesional hemisphere that would control the hBMI.

In the EEG screening, participants were presented with two auditory and visual cues indicating to relax or to (try to) open and close their paretic hand for 5 seconds. Participants completed 4 blocks of 8 repetitions of each condition.

In the EMG calibration, the participants performed the same task explained above but in this case, with their healthy arm. Both participants completed 5 blocks during this calibration phase.

During both phases, the motors of the exoskeleton were on, which means that the subjects had to actively follow the movement driven by the robot. Although this condition avoided that factors such as weight and friction had an impact on the EMG activity, the risk that the patients remained passive existed too. That's why participants were repetitively reminded that the movement had to be followed actively and as naturally as possible. Finally, whereas the speed and direction of the calibration movements were predefined and fully-assisted, during the real-time operation, the movement was partially influenced by their paretic EMG activity.

It is important to clarify that even if the exoskeleton allowed the movement in 7 DoFs and the healthy participant controlled all of them during the hBMI operation, he had to reach the target position only in the 3 proximal DoFs in order to accomplish the trial and move on to the next target. In the case of the stroke patient, instead, the control of the exoskeleton was done only in the three proximal DoFs because the motors of the exoskeleton didn't have enough torque to overcome the high spasticity in the distal DoFs, being the movements of these joints unreliable. Therefore, for both participants, only the performance of the control of the 3 proximal DoFs is reported in this paper.

7.3.2 Data acquisition and processing

A set of 32 EEG channels with a high density of electrodes over the motor cortex (FP1, FP2, F7, F3, Fz, F4, F8, FC3, FC1, FC2, FC4, C5, C3, C1, Cz, C2, C4, C6, CP5, CP3, CP1, CPz, CP2, CP4, CP6, P7, P3, Pz, P4, P8, O1, O2) and two EOG channels were collected at 1KHz (Brain Products GmbH, Germany). Additionally, EMG data from several upper and forearm muscles were acquired with the same system and sampling frequency. Six bipolar electrodes (Myotronics-Noromed, USA) were placed over the Abductor Pollicis Longus, the Biceps, the Triceps and the Frontal, Middle and Back portions of the Deltoid while two high-density arrays of 24 channels each (Tecnalia-Serbia, Serbia) were utilized to record the activity from the extensor and flexor muscles of the forearm. The reference and ground electrodes were located over the olecranon and the clavicle, respectively. Kinematic data of the 7-DOFs was recorded at 20Hz with a camera attached to the bottom of the exoskeleton and motor encoders (more details in [68]).

EEG signals were bandpass filtered (4^{th} order Butterworth filter at 5-48Hz), down-sampled to 100Hz and spatially filtered with a short-Laplacian filter. The resulting signals were modelled as an autoregressive process of order 20 using 0.5sec-long windows and a step window of 50ms and then the mean power spectral density was computed. The most discriminative perilesional channels and frequency bands were identified offline and used as input features to the decoder. EEG features were normalized using the last 4 minutes of data during the real-time

operation.

EMG data was filtered using a 4^{th} order Butterworth bandpass filter (10-500Hz) and a 50Hz comb filter. Five time-domain features (Mean of absolute value, Variance, Waveform Length, Root-mean-square error and the Logarithm of the Variance) were extracted from each of the selected EMG channels during the calibration process. Features were normalized to zero mean and unit variance using the mean and standard deviation computed on the last minute of EMG data during the online operation phase.

Kinematic data was low-pass filtered with a 4^{th} order Butterworth filter (1.5Hz).

7.3.3 hBMI calibration

As explained in Section 7.3.1, the calibration session consisted of the following two parts:

i) An EEG screening phase, in which participants either relax or (try to) open and close their paretic hand. R-squared values comparing the EEG activity during the movement execution (attempt) and the relax conditions were computed offline. The frequency band and the two electrodes on the ipsilesional motor area with highest r-squared values were selected. Features were extracted on those electrodes and bands, as explained in Section 7.3.2, and used as input to the EEG-decoder to control the hBMI. The collected data and a linear discriminant analysis were employed to build a binary classifier that would classify the EEG activity either as "Movement" or "Rest".

ii) An EMG calibration phase, during which the participants wore the exoskeleton on their healthy arm and performed the same functional task that would be trained during the hBMI operation session. For each participant, the channels with highest amount of information were selected offline from the high-density arrays as follows: First, channels were bipolarized along the straight direction and both diagonals. The decoding performance (measured by the correlation coefficient (CC)) was computed iteratively, starting with all the possible channels and getting rid of the channel with the lowest regression coefficient in each loop.

Finally, the minimum amount of channels, up to a maximum of 50, that would suffice to achieve a CC = max(CC) - 5% * (max(CC) - min(CC)) were selected. After this dimensionality reduction process, an EMG decoder was trained using all the bipolar electrode channels and the selected subset of the high-density array channels. In order to have a decoder based on non-compensatory EMG activity only, it was trained with data from the healthy arm and then used to decode the activity from the paretic arm. A ridge regression algorithm with a regularization parameter $\lambda = 10^4$ chosen experimentally was used to build such a decoder and thereby, to continuously map the input EMG signals into the predicted kinematics in real-time during the hBMI operation.

7.3.4 hBMI operation

The control strategy of our hBMI followed a top-down approach by establishing an "EEG-gated EMG control" type. Both decoders worked continuously and simultaneously and a hierarchical control based on the natural motor command flow was implemented (see Fig. 7.1). First of all, to ensure the active participation of the patient, the movement volition detection from the EEG signal was required to initiate the movement. Thus, the output of the EEG decoder would determine at all times whether the control of the hBMI was handed over to the muscles or not. For example, outputs of the EEG decoder classified as "Rest" during a trial period would prevent the exoskeleton from moving, independently of the EMG decoder output. However, if during the trial time the subject was desynchronizing the sensorimotor rhythms (i.e. output classified as "Movement"), the movement of the exoskeleton would be triggered. In this case, the final direction and speed of the exoskeleton would be partially determined by the kinematics predicted by the EMG decoder (50% for the case of the healthy participant and 40% for the patient, chosen experimentally) and by an assistive component, which would always redirect the exoskeleton towards the target position. Written mathematically, the fusion formula of the assistive and the predicted components into the final kinematic command sent to the exoskeleton in each DoF i = 1:7 would be the following:

$$V_{final_i} = \gamma * V_{EMG_i} + (1 - \gamma) * V_{assistive_i} \quad (1)$$

where for each DoF i, V_{final_i} is the final velocity sent to the exoskeleton, V_{EMG_i} the velocity predicted from the EMG activity, $V_{assistive_i}$ the assistive component computed using a linear-quadratic regulator (LQR) and $\gamma \epsilon$ [0,1] the weight determining the amount of influence of the EMG activity in the control of the direction and the speed of the movement.

Additional filtering measures were applied to the output of the EEG and EMG decoders in order to achieve a smoother and more stable real-time control: First of all, the movement of the exoskeleton was not triggered (or stopped) until the EEG-decoder output was classified five consecutive times as "Movement" (or "Rest"), following the procedure in [49]. On top of that, a weighted moving average filter with a backwards window of 180ms and linearly decaying weights starting from the most recent value was applied to the kinematics predicted by the EMG decoder. The outputs of the decoders were ignored for the control during the rest and the preparation periods, in which the movement of the exoskeleton was blocked.

An adaptive strategy was followed for the EEG decoder, which was retrained at the end of each trial with the last two minutes of data collected from each condition period ("Rest" and "Movement"). A supervised approach was followed by utilizing the ground-truth labels marked by the experimental design. However, regardless of the performance drop due to the session-to-session and arm-to-arm transfers, the EMG decoder was kept fixed during the whole intervention since the aim was to provide the participants with feedback about how correct and natural their muscle activation patterns were, based on the EMG recorded from the healthy arm during the calibration.

7.3.5 Performance evaluation

We utilized several metrics to evaluate the performance of the subjects when operating the hBMI in real-time. Five metrics previously reported in [49] were computed to assess the ability of the participants to modulate their SMR rhythms to control the hBMI:

- *Percentage of time the exoskeleton was moving during a trial.* This perfor-

mance metric reflects the ability of the subject to decrease the SMR power during a trial.

- *Percentage of maximum consecutive time the exoskeleton moved during a trial.* This metric reflects the longest time period the participant was able to maintain a SMR desynchronization within a trial.

- *Number of movement onsets or transitions from the "Rest" to the "Movement" condition.* This measures how many times the participant lost control over the SMR modulation.

- *Latency to the first movement onset.* This represents the reaction time of the participant in producing the necessary SMR modulation to trigger the movement for the first time at the beginning of a trial.

- *True positive rate (TPR) and false positive rate (FPR)*, being the TPR the percentage of outputs classified as "Movement" during a trial and the FPR the percentage of outputs classified as "Movement" during a resting period.

Regarding the evaluation of the control based on the EMG activity modulation, the performance metrics that we used for such analysis are the following:

- *Number of trials needed to reach a target*, which reflects the number of unaccomplished trials that the participant performed before reaching the target.

- *Spectral Arc Length (SPARC)*, which is a measurement of how smooth the movement of the exoskeleton was in each DoF. It was presented in [167] and the closer to zero the values, the smoother the trajectory was.

- *Correlation coefficient (CC)* between the assistive velocity component and the EMG-based predicted velocity during the periods in which the exoskeleton was in motion.

- *Normalized root-mean-squared-error (NRMSE)* computed by comparing the assistive velocity component and the EMG-based predicted velocity component during the intervals in which the exoskeleton was moving.

Despite the SPARC, CC and NRMSE were computed for each of the DoFs individually, the mean across the proximal DoFs are reported in the results.

The values of all the aforementioned metrics were computed for each of the participants and blocks of the hBMI operation session. Finally, a Wilcoxon test was applied to each metric to compare the performance of the two participants in each category.

7.4 Results

Due to the low number of blocks performed by the participants, motor skill learning was not expected to happen. Nevertheless, both participants were able to modulate their brain and muscle activity to successfully operate the hBMI and hence, reach the presented targets.

The EEG-based control performances of the healthy participant (black) and the stroke patient (white) are presented in Figs. 7.2 and 7.3. Fig.7.2 shows the first four metrics evaluating the EEG performance. Despite the stroke, the patient's performance was non-significantly different from the one of the healthy participant (Percentage of mov-time: $p = 0.213$; Percentage of max-consec-mov-time: $p = 0.957$; Number of onsets: $p = 0.173$; Latency: $p = 0.327$). The mean values for each of the metrics across all the blocks are: 1) percentage of movement time per trial = 68.09% (healthy) and 61.20% (patient); 2) percentage of maximum consecutive movement time/trial = 45.57% (healthy) and 45.59% (patient); 3) Number of onsets = 2.731 (healthy) and 2.350 (patient); 4) Latency to first movement onset = 0.614sec (healthy) and 0.836sec (patient). During the first block, the patient needed more time to start the brain control and produce the first movement of the exoskeleton than the healthy participant. However, this latency difference was reduced in later blocks, in which the patient ended up needing a lower number of onsets to achieve a percentage of time moving the exoskeleton similar to the healthy participant as well as a larger consecutive time moving the exoskeleton per trial.

Fig.7.3 represents the mean of the instantaneous output (blue) from the EEG-

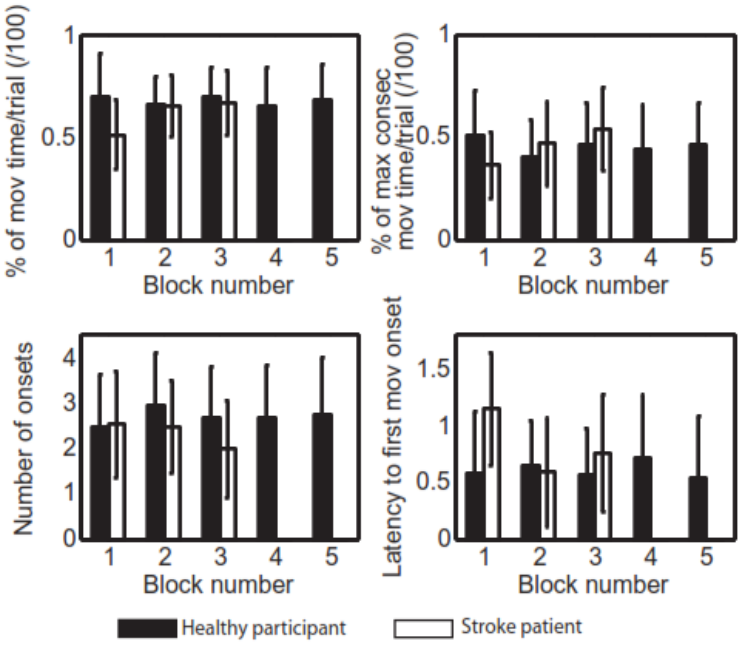

Figure 7.2: *Mean and standard deviation of the EEG-based control performance values achieved by the healthy participant (black) and the stroke patient (white), measured by the percentage of time the exoskeleton was moving during a trial (top left), the percentage of maximum consecutive time the exoskeleton was moving within a trial (top right), the number of movement onsets per trial (bottom left) and the latency to the first movement onset (bottom right).*

decoder across all the trials and blocks as well as that same output mean after applying the smoothing measure (red). Therefore, the TPR and FPR can be derived from the values achieved during the "Trial" and "Rest" periods, respectively, which resulted in a TPR = 0.725 and a FPR = 0.307 in the case of the healthy participant, and a TPR = 0.642 and a FPR = 0.201 for the patient. The healthy participant presented a steadier control of the SMR desynchronization resulting in a larger percentage of time in motion per trial. Instead, the patient presented more difficulties to trigger the initial movement of the exoskeleton and to keep the concentration to desynchronize his SMR during the whole trial, as reflected in the late performance raise at the beginning of the trial and the clear drops around seconds 4 and 6.

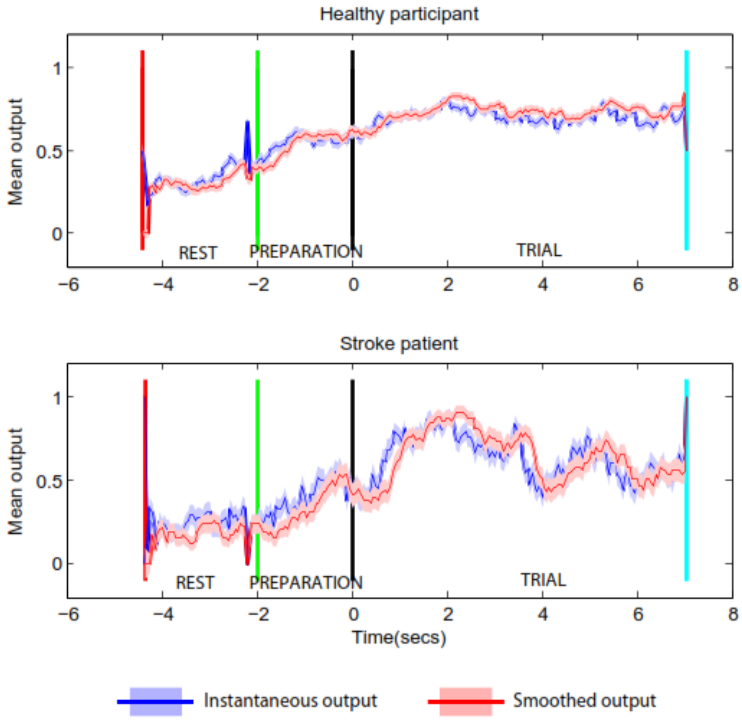

Figure 7.3: *Mean and standard error of the instantaneous output (blue) and the smoothed output (red) from the EEG decoder during the "Rest", "Preparation" and "Trial" periods across all the trials and blocks performed by the healthy participant (top) and the stroke patient (bottom).*

Finally, the results from the EMG performance evaluation are presented in Fig.7.4. The mean number of trials needed to reach a target was 3.455 for the healthy participant and 3.833 for the patient. The mean SPARC values across blocks were -2.637 (healthy) and -2.778 (patient), while the mean CC values were 0.308 (healthy) and -0.107 (patient) and the mean NRMSE resulted in 0.109 (healthy) and 0.159 (patient). In spite of the significantly lower (CC: $p = 0.0001$; NRMSE: $p = 0.014$) decoding accuracy achieved by the stroke patient due to the pathological EMG activity, the higher assistance level given to the patient during the hBMI operation helped him to achieve scores for the SPARC and number of trials per target metrics similar to the healthy participant.

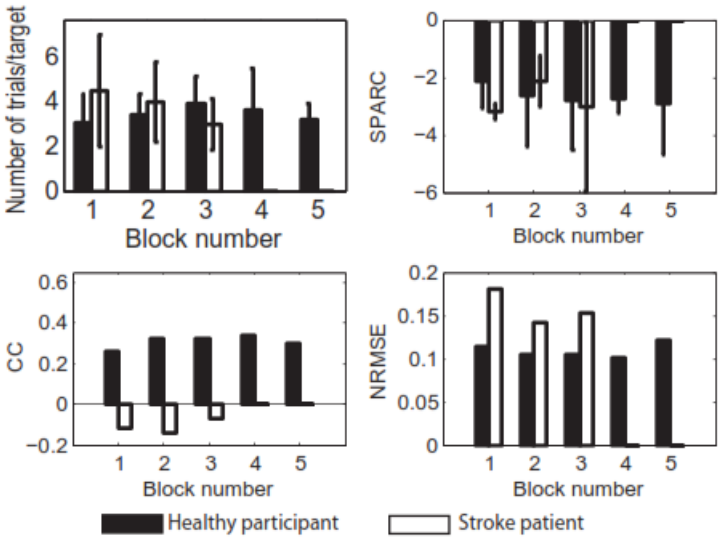

Figure 7.4: *Mean and standard deviation of the EMG-based control performance values achieved by the healthy participant (black) and the stroke patient (white), measured by the number of trials needed to reach a target (top left), the mean SPARC (top right), CC (bottom left) and NRMSE (bottom right) across the three proximal DoFs.*

7.5 Discussion

This study presents and validates the usability of a novel hBMI system that follows a top-down approach. The hierarchical control strategy was inspired by the biologically natural motor command flow. In a healthy individual, motor commands are initiated at the brain level and then they travel through the spinal cord to reach the peripheral nerves and finally the muscles, whose fibers are activated by the motor units to produce the desired movement. Therefore, it seems natural to think that an effective hBMI control strategy should constantly require an initial command from the brain to later on transfer the control to the muscles. In this way, the active participation of the brain is necessary at all times for the movement to occur, which prevents the patient from remaining passive (i.e. no desynchronization happening in the brain) while the exoskeleton assists the movement of his/her limb. Moreover, by including the muscles in the control of the hBMI, various problems generally present in stroke patients such as muscle weakness and the existence of abnormal muscle synergies are tackled. Therefore, thanks to the

supplementary information coming from the muscles, the proposed hBMI not only offers the possibility of achieving a higher decoding accuracy and a more dexterous and smoother control of the actuator, but it also envisages the possibility of a joint brain and muscle rehabilitation.

The same EEG decoder algorithm as the presented here was utilized before in a double blind sham-controlled clinical trial in 32 chronic stroke patients [49] and it was proven to be a valid algorithm to induce motor recovery. Although initially the stroke patient had some trouble to trigger the movement of the exoskeleton at the beginning of the trial, he rapidly learned and got better, eventually achieving a performance equal to or even better than that of the healthy participant. Therefore, in this preliminary study, both participants could control the onset of the movement with notable ease and the results confirm a high EEG modulation performance, which is encouraging for its use in future clinical trials.

The employed EMG decoder enabled the continuous and real-time control of the speed and direction of the movement in 7 DoFs concurrently, which constitutes an advance over previous classification or decoding approaches of a few DoFs. The lower EMG decoding performance achieved by the stroke patient can be explained by the existence of pathological EMG activity in the paretic limb. Thus, the kinematics predicted by the EMG decoder trained with healthy activity didn't correlate with the assistive component, which constantly redirected the movement towards the target. However, since the weight of the assistive component on the control of the exoskeleton was set at a higher value for the stroke patient (60%) than for the healthy participant (50%), the former could successfully reach the targets and achieve scores of path smoothness and number of trials per target comparable to the healthy individual. Hence, in spite of the modest performance values of the EMG-based control, both participants were able to bring the exoskeleton to the desired final position. Continuously controlling a 7-DoF myoelectric interface during functional tasks might not be intuitive even for healthy subjects and especially at the beginning. A longer training period is necessary for the participants to adapt to the EMG model and achieve a skillful control of the exoskeleton.

Finally, it should be mentioned that in these experiments, all the DoFs were controlled following the same control strategy. However, in case a patient didn't have any residual EMG at all in some or all the involved muscles, the control could start being based solely on EEG activity and would progressively shift towards a hybrid control, as the muscles recovered certain degree of activity as a result of the training. Alternative strategies that would take factors such as muscle fatigue into account could be developed too.

7.6 Conclusion

A new hBMI rehabilitation system was presented and its usability was validated with one healthy participant and a chronic stroke patient in a real-time operation session. This hBMI rehabilitation system establishes a hierarchical EEG- and EMG-based control strategy with the goal of evoking a joint brain and muscle rehabilitation in stroke patients. Therefore, by being built upon neurophysiological principles and by constantly requiring the active participation of central and peripheral structures of the nervous system, this hBMI constitutes a potential tool to boost the recovery of lost motor function at proximal and distal segments of the upper limb. Nevertheless, further experiments with a large population of stroke patients are necessary to assess the effectiveness of the presented hBMI in eliciting motor rehabilitation.

7.7 Acknowledgements

This study was funded by the Baden-Württemberg Stiftung (GRUENS ROB-1), the Deutsche Forschungsgemeinschaft (DFG, Koselleck), the Fortüne-Program of the University of Tübingen (2422-0-0), and the Bundes Ministerium für Bildung und Forschung BMBF MOTORBIC (FKZ 13GW0053) and AMORSA (FKZ 16SV7754). A. Sarasola-Sanz's work is supported by La Caixa-DAAD and N. Irastorza-Landa's work by the Basque Government and IKERBASQUE.

8. References

[1] World Health Organization Atlas of Heart Disease and Stroke. Technical report, 2004.

[2] Cristina Martínez, Barandalla Codirector, Miguel Ángel, and Ciga Lozano. ICTUS: Incidencia, factores de riesgo y repercusión. Technical report.

[3] Henk T. Hendricks, Jacques van Limbeek, Alexander C. Geurts, and Machiel J. Zwarts. Motor recovery after stroke: A systematic review of the literature. *Archives of Physical Medicine and Rehabilitation*, 83(11):1629–1637, nov 2002.

[4] Vincent C K Cheung, Andrea Turolla, Michela Agostini, Stefano Silvoni, Caoimhe Bennis, Patrick Kasi, Sabrina Paganoni, Paolo Bonato, and Emilio Bizzi. Muscle synergy patterns as physiological markers of motor cortical damage.

[5] Eliana García-Cossio, Doris Broetz, Niels Birbaumer, and Ander Ramos-Murguialday. Cortex integrity relevance in muscle synergies in severe chronic stroke. *Frontiers in human neuroscience*, 8(September):744, 2014.

[6] Naoyuki Takeuchi and Shin-Ichi Izumi. Maladaptive Plasticity for Motor Recovery after Stroke: Mechanisms and Approaches. *Neural Plasticity*, 2012:1–9, jun 2012.

[7] E Bizzi, V C K Cheung, A D'Avella, P Saltiel, and M Tresch. Combining modules for movement. *Brain research reviews*, 57(1):125–33, jan 2008.

[8] Andrea D'avella, Alessandro Portone, Laure Fernandez, and Francesco Lacquaniti. Behavioral/Systems/Cognitive Control of Fast-Reaching Movements by Muscle Synergy Combinations. 2006.

[9] Tamar Flash and Binyamin Hochner. Motor primitives in vertebrates and invertebrates. *Current Opinion in Neurobiology*, 15(6):660–666, 2005.

[10] Matthew C Tresch, Philippe Saltiel, Andrea D'Avella, and Emilio Bizzi. Coordination and localization in spinal motor systems. *Brain Research Reviews*, 40(1):66–79, 2002.

[11] Julius P. A. Dewald, Vikram Sheshadri, Michelle L. Dawson, and Randall F. Beer. Upper-Limb Discoordination in Hemiparetic Stroke: Implications for Neurorehabilitation. *Topics in Stroke Rehabilitation*, 8(1):1–12, apr 2001.

[12] Timothy H. Murphy and Dale Corbett. Plasticity during stroke recovery: from synapse to behaviour. *Nature Reviews Neuroscience*, 10(12):861–872, dec 2009.

[13] John W Krakauer. Motor learning: its relevance to stroke recovery and neurorehabilitation. *Current Opinion in Neurology*, 19(1):84–90, feb 2006.

[14] K. Jacobs and J. Donoghue. Reshaping the cortical motor map by unmasking latent intracortical connections. *Science*, 251(4996):944–947, feb 2006.

[15] Dora YL Chan, Chetwyn CH Chan, and Derrick KS Au. Motor relearning programme for stroke patients: a randomized controlled trial. *Clinical Rehabilitation*, 20(3):191–200, mar 2006.

[16] Jeffrey A. Kleim and Theresa A. Jones. Principles of Experience-Dependent Neural Plasticity: Implications for Rehabilitation After Brain Damage. *Journal of Speech, Language, and Hearing Research*, 51(1), feb 2008.

[17] B.T. Volpe, H.I. Krebs, N. Hogan, L. Edelstein, C. Diels, and M. Aisen. Neurology. *Neurology*, 53(8):1874–1874, may 2000.

[18] C G Burgar, P S Lum, P C Shor, and H F Machiel Van der Loos. Development of robots for rehabilitation therapy: the Palo Alto VA/Stanford

experience. *Journal of rehabilitation research and development*, 37(6):663–73, 2000.

[19] Peter S. Lum, Charles G. Burgar, Peggy C. Shor, Matra Majmundar, and Machiel Van der Loos. Robot-assisted movement training compared with conventional therapy techniques for the rehabilitation of upper-limb motor function after stroke. *Archives of Physical Medicine and Rehabilitation*, 83(7):952–959, 2002.

[20] Susan E Fasoli, Hermano I Krebs, Joel Stein, Walter R Frontera, Richard Hughes, and Neville Hogan. Robotic therapy for chronic motor impairments after stroke: follow-up results. *Archives of Physical Medicine and Rehabilitation*, 85(7):1106–1111, jul 2004.

[21] CD Takahashi, L Der-Yeghiaian, V Le, and RR Motiwala. Robot-based hand motor therapy after stroke. *Brain*, 2008.

[22] Albert C. Lo, Peter D. Guarino, Lorie G. Richards, Jodie K. Haselkorn, George F. Wittenberg, Daniel G. Federman, Robert J. Ringer, Todd H. Wagner, Hermano I. Krebs, Bruce T. Volpe, Christopher T. Bever, Dawn M. Bravata, Pamela W. Duncan, Barbara H. Corn, Alysia D. Maffucci, Stephen E. Nadeau, Susan S. Conroy, Janet M. Powell, Grant D. Huang, and Peter Peduzzi. Robot-Assisted Therapy for Long-Term Upper-Limb Impairment after Stroke. *New England Journal of Medicine*, 362(19):1772–1783, may 2010.

[23] Gert Kwakkel, Carel GM Meskers, Erwin E van Wegen, Guus J Lankhorst, Alexander CH Geurts, Annet A van Kuijk, Eline Lindeman, Anne Visser-Meily, Erwin de Vlugt, and J Hans Arendzen. Impact of early applied upper limb stimulation: The EXPLICIT-stroke programme design. *BMC Neurology*, 8(1):49, dec 2008.

[24] Gerdienke B Prange, Michiel J A Jannink, Catharina G M Groothuis-Oudshoorn, Hermie J Hermens, and Maarten J IJzerman. Systematic review of the effect of robot-aided therapy on recovery of the hemiparetic arm after stroke. *JRRD*, 43(2):171–184, 2006.

[25] A Jackson, J B Zimmermann, Andrew Jackson, Jonas B Zimmermann, and A & Jackson. Neural interfaces for the brain and spinal cord-restoring motor function. *Nature Publishing Group*, 8:690–699, 2012.

[26] A R Fugl-Meyer, L Jääskö, I Leyman, S Olsson, and S Steglind. The post-stroke hemiplegic patient. 1. a method for evaluation of physical performance. *Scandinavian journal of rehabilitation medicine*, 7(1):13–31, 1975.

[27] Steven L Wolf, Pamela A Catlin, Michael Ellis, Audrey Link Archer, Bryn Morgan, and Aimee Piacentino. Stroke Assessing Wolf Motor Function Test as Outcome Measure for Research in Patients After Assessing Wolf Motor Function Test as Outcome Measure for Research in Patients After Stroke. 2013.

[28] Douglas Carroll. A quantitative test of upper extremity function. *Journal of Chronic Diseases*, 18(5):479–491, may 1965.

[29] Gitendra Uswatte, ; Edward Taub, David Morris, Mary Vignolo, and Karen Mcculloch. Reliability and Validity of the Upper-Extremity Motor Activity Log-14 for Measuring Real-World Arm Use. 2005.

[30] ASHWORTH and B. Preliminary trial of carisoprodol in multiple sclerosis. *Practitioner*, 192:540–542, 1964.

[31] Thomas J. Kiresuk and Robert E. Sherman. Goal attainment scaling: A general method for evaluating comprehensive community mental health programs. *Community Mental Health Journal*, 4(6):443–453, dec 1968.

[32] Sang Wook Lee, Kristin M Wilson, Blair A Lock, and Derek G Kamper. Subject-specific myoelectric pattern classification of functional hand movements for stroke survivors. *IEEE transactions on neural systems and rehabilitation engineering : a publication of the IEEE Engineering in Medicine and Biology Society*, 19(5):558–66, oct 2011.

[33] Xu Zhang and Ping Zhou. High-Density Myoelectric Pattern Recognition. *IEEE transactions on Biomedical Engineering*, 59(6):1649–1657, 2012.

[34] Benedetta Cesqui, Peppino Tropea, Silvestro Micera, and Hermano Krebs. EMG-based pattern recognition approach in post stroke robot-aided rehabilitation: a feasibility study. *Journal of NeuroEngineering and Rehabilitation*, 10(1):75, 2013.

[35] Ander Ramos-Murguialday, Eliana García-Cossio, Armin Walter, Woosang Cho, Doris Broetz, Martin Bogdan, Leonardo G. Cohen, and Niels Birbaumer. Decoding upper limb residual muscle activity in severe chronic stroke. *Annals of Clinical and Translational Neurology*, 2(1):1–11, jan 2015.

[36] A Irastorza-Landa, N., Sarasola-Sanz, A., López-Larraz, E., Bibián, C., Shiman, F., Birbaumer, N., & Ramos-Murguialday. Design of Continuous EMG Classification approaches towards the Control of a Robotic Exoskeleton in Reaching Movements. In *IEEE International Conference on Rehabilitation Robotics*, 2017.

[37] Denise J. Berger and Andrea D'Avella. Effective force control by muscle synergies. *Frontiers in Computational Neuroscience*, 8:46, apr 2014.

[38] Jimson G. Ngeo, Tomoya Tamei, and Tomohiro Shibata. Continuous and simultaneous estimation of finger kinematics using inputs from an EMG-to-muscle activation model. *Journal of NeuroEngineering and Rehabilitation*, 11(1), 2014.

[39] Samuel Farmer, M Barbara Silver-Thorn, Philip A Voglewede, Scott A Beardsley, Barbara Silver-Thorn, and Philip Voglewede. Within-socket Myoelectric Prediction of Continuous Ankle Kinematics for Control of a Powered Transtibial Prosthesis. *Journal of Neural Engineering DOI. Journal of Neural Engineering DOI. Journal of Neural Engineering*, 11(5):56027–56027, 2014.

[40] Ali Ameri and Kevin Englehart. Support Vector Regression for Improved Real-Time, Simultaneous Myoelectric Control Invasive myoelectric control View project. 2014.

[41] Anders L Fougner, Øyvind Stavdahl, and Peter J Kyberd. System training and assessment in simultaneous proportional myoelectric prosthesis control. *Journal of NeuroEngineering and Rehabilitation*, 11(1):75, apr 2014.

[42] Janne M. Hahne, Felix Biessmann, Ning Jiang, Hubertus Rehbaum, Dario Farina, Frank C. Meinecke, Klaus-Robert Muller, and Lucas C. Parra. Linear and Nonlinear Regression Techniques for Simultaneous and Proportional Myoelectric Control. *IEEE Transactions on Neural Systems and Rehabilitation Engineering*, 22(2):269–279, 2014.

[43] Denise J. Berger and Andrea D'Avella. Towards a Myoelectrically Controlled Virtual Reality Interface for Synergy-Based Stroke Rehabilitation. pages 965–969. Springer, Cham, 2017.

[44] Mohammad Ghassemi, Rajiv Ranganathan, Alex Barry, K. Triandafilou, and Derek Kamper. Introduction of an EMG-Controlled Game to Facilitate Hand Rehabilitation After Stroke. pages 451–455. Springer, Cham, 2017.

[45] Jie Liu, Sang Hoon Kang, Dali Xu, Yupeng Ren, Song Joo Lee, and Li-Qun Zhang. EMG-Based Continuous and Simultaneous Estimation of Arm Kinematics in Able-Bodied Individuals and Stroke Survivors. *Frontiers in Neuroscience*, 11:480, aug 2017.

[46] Ivan Vujaklija, Vahid Shalchyan, Ernest N Kamavuako, Ning Jiang, Hamid R Marateb, and Dario Farina. Online mapping of EMG signals into kinematics by autoencoding.

[47] E. Garcia-Cossio, N. Birbaumer, and A. Ramos-Murguialday. Facilitation of completely paralyzed forearm muscle activity in chronic stroke patients. *International IEEE/EMBS Conference on Neural Engineering, NER*, pages 1545–1548, 2013.

[48] Niels Birbaumer. Breaking the silence: Brain-computer interfaces (BCI) for communication and motor control. *Psychophysiology*, 43(6):517–532, nov 2006.

[49] Ander Ramos-Murguialday, Doris Broetz, Massimiliano Rea, Leonhard Läer, Ozge Yilmaz, Fabricio L Brasil, Giulia Liberati, Marco R Curado, Eliana Garcia-Cossio, Alexandros Vyziotis, Woosang Cho, Manuel Agostini, Ernesto Soares, Surjo Soekadar, Andrea Caria, Leonardo G Cohen, and Niels Birbaumer. Brain-machine interface in chronic stroke rehabilitation: a controlled study. *Annals of neurology*, 74(1):100–8, jul 2013.

[50] Takashi Ono, Keiichiro Shindo, Kimiko Kawashima, Naoki Ota, Mari Ito, Tetsuo Ota, Masahiko Mukaino, Toshiyuki Fujiwara, Akio Kimura, Meigen Liu, and Junichi Ushiba. Brain-computer interface with somatosensory feedback improves functional recovery from severe hemiplegia due to chronic stroke. *Frontiers in Neuroengineering*, 7:19, jul 2014.

[51] Sam Darvishi, Michael C. Ridding, Brenton Hordacre, Derek Abbott, and Mathias Baumert. Investigating the impact of feedback update interval on the efficacy of restorative brain-computer interfaces. *Royal Society Open Science*, 4(8):170660, aug 2017.

[52] Patrick Ofner, Andreas Schwarz, Joana Pereira, and Gernot R. Müller-Putz. Upper limb movements can be decoded from the time-domain of low-frequency EEG. *PLOS ONE*, 12(8):e0182578, aug 2017.

[53] Farid Shiman, Eduardo López-Larraz, Andrea Sarasola-Sanz, Nerea Irastorza-Landa, Martin Spüler, Niels Birbaumer, and Ander Ramos-Murguialday. Classification of different reaching movements from the same limb using EEG. *Journal of Neural Engineering*, 14(4):046018, aug 2017.

[54] Karunesh Ganguly, Dragan F Dimitrov, Jonathan D Wallis, and Jose M Carmena. Reversible large-scale modification of cortical networks during neuroprosthetic control. *Nature neuroscience*, 14(5):662–7, may 2011.

[55] Aaron C Koralek, Xin Jin, John D Long, Rui M Costa, Jose M Carmena, and Jose M. Carmena. Corticostriatal plasticity is necessary for learning intentional neuroprosthetic skills. *Nature*, 483(7389):331–5, mar 2012.

[56] Leigh R Hochberg, Mijail D Serruya, Gerhard M Friehs, Jon A Mukand, Maryam Saleh, Abraham H Caplan, Almut Branner, David Chen, Richard D

Penn, and John P Donoghue. Neuronal ensemble control of prosthetic devices by a human with tetraplegia. *Nature*, 442(7099):164–71, 2006.

[57] Jennifer L Collinger, Brian Wodlinger, John E Downey, Wei Wang, Elizabeth C Tyler-Kabara, Douglas J Weber, Angus J C McMorland, Meel Velliste, Michael L Boninger, and Andrew B Schwartz. High-performance neuroprosthetic control by an individual with tetraplegia. *Lancet (London, England)*, 381(9866):557–64, feb 2013.

[58] A Bolu Ajiboye, Francis R Willett, Daniel R Young, William D Memberg, Brian A Murphy, Jonathan P Miller, Benjamin L Walter, Jennifer A Sweet, Harry A Hoyen, Michael W Keith, P Hunter Peckham, John D Simeral, John P Donoghue, Leigh R Hochberg, and Robert F Kirsch. Restoration of reaching and grasping movements through brain-controlled muscle stimulation in a person with tetraplegia: a proof-of-concept demonstration. *Lancet (London, England)*, 389(10081):1821–1830, 2017.

[59] Kai Keng Ang, Cuntai Guan, Karen Chua, Tan Tock, and Seng Hospital. Clinical study of neurorehabilitation in stroke using EEG-based motor imagery brain-computer interface with robotic feedback Deep Learning for Brain-Computer Interfaces View project Brain-Computer Interface and Stroke View project. *IEEE Engineering in Medicine and Biology Society*, 2010.

[60] Floriana Pichiorri, Giovanni Morone, Manuela Petti, Jlenia Toppi, Iolanda Pisotta, Marco Molinari, Stefano Paolucci, Maurizio Inghilleri, Laura Astolfi, Febo Cincotti, and Donatella Mattia. Brain-computer interface boosts motor imagery practice during stroke recovery. *Annals of Neurology*, 77(5):851–865, may 2015.

[61] Robert Leeb, Hesam Sagha, Ricardo Chavarriaga, José Del, and R Millán. A hybrid brain-computer interface based on the fusion of electroencephalographic and electromyographic activities. *J. Neural Eng*, 8:25011–5, 2011.

[62] Kazuo Kiguchi and Yoshiaki Hayashi. A study of EMG and EEG during perception-assist with an upper-limb power-assist robot. In *2012 IEEE Inter-*

national Conference on Robotics and Automation, pages 2711–2716. IEEE, may 2012.

[63] Tom Carlson, Luca Tonin, Serafeim Perdikis, Robert Leeb, José Del, and R Millán. A Hybrid BCI for Enhanced Control of a Telepresence Robot.

[64] Ke Lin, Andrea Cinetto, Yijun Wang, Xiaogang Chen, Shangkai Gao, and Xiaorong Gao. An online hybrid BCI system based on SSVEP and EMG. 2016.

[65] Angela Riccio, Elisa Mira Holz, Pietro Aricò, Francesco Leotta, Fabio Aloise, Lorenzo Desideri, Matteo Rimondini, Andrea Kübler, Donatella Mattia, and Febo Cincotti. Hybrid P300-Based Brain-Computer Interface to Improve Usability for People With Severe Motor Disability: Electromyographic Signals for Error Correction During a Spelling Task. *Archives of Physical Medicine and Rehabilitation*, 96(3):S54–S61, mar 2015.

[66] Xiangxin Li, Oluwarotimi Williams Samuel, Xu Zhang, Hui Wang, Peng Fang, and Guanglin Li. A motion-classification strategy based on sEMG-EEG signal combination for upper- limb amputees. *Journal of NeuroEngineering and Rehabilitation*, 14(2), 2017.

[67] Kazuo Kiguchi, Thilina Dulantha LALITHARATNE, and Yoshiaki Hayashi. Estimation of Forearm Supination/Pronation Motion Based on EEG Signals to Control an Artificial Arm *. *Journal of Advanced Mechanical Design, Systems, and Manufacturing*, 7(1), 2013.

[68] Andrea Sarasola-Sanz, Nerea Irastorza-Landa, Farid Shiman, Eduardo Lopez-Larraz, Martin Spuler, Niels Birbaumer, and Ander Ramos-Murguialday. EMG-based multi-joint kinematics decoding for robot-aided rehabilitation therapies. In *2015 IEEE International Conference on Rehabilitation Robotics (ICORR)*, pages 229–234. IEEE, aug 2015.

[69] Andrea Sarasola-Sanz, Nerea Irastorza-Landa, Eduardo López-Larraz, Farid Shiman, Martin Spüler, Niels Birbaumer, and Ander Ramos-Murguialday. Design and effectiveness evaluation of mirror myoelectric interfaces: a novel

method to restore movement in hemiplegic patients. *Scientific Reports*, 8(1):16688, dec 2018.

[70] A. Sarasola-Sanz, E. López-Larraz, N. Irastorza-Landa, J. Klein, D. Valencia, A. Belloso, F. O. Morin, M. Spüler, N. Birbaumer, and A. Ramos-Murguialday. An EEG-Based Brain-Machine Interface to Control a 7-Degrees of Freedom Exoskeleton for Stroke Rehabilitation. pages 1127–1131. Springer, Cham, 2017.

[71] Andrea Sarasola-Sanz, Nerea Irastorza-Landa, Eduardo Lopez-Larraz, Carlos Bibian, Florian Helmhold, Doris Broetz, Niels Birbaumer, and Ander Ramos-Murguialday. A hybrid brain-machine interface based on EEG and EMG activity for the motor rehabilitation of stroke patients. In *2017 International Conference on Rehabilitation Robotics (ICORR)*, pages 895–900. IEEE, jul 2017.

[72] Francesco Tenore, Ander Ramos, Amir Fahmy, Soumyadipta Acharya, Ralph Etienne-cummings, and Nitish V Thakor. Decoding of individuated finger movements using surface Electromyography Decoding of individuated finger movements using surface Electromyography. pages 0–24.

[73] Elaine Corbett, Eric Perreault, and Konrad Koerding. Mixture of time-warped trajectory models for movement decoding. *Advances in Neural Information Processing Systems*, pages 433–441, 2010.

[74] Minas V. Liarokapis, Panagiotis K. Artemiadis, Kostas J. Kyriakopoulos, and Elias S. Manolakos. A Learning Scheme for Reach to Grasp Movements: On EMG-Based Interfaces Using Task Specific Motion Decoding Models. *IEEE Journal of Biomedical and Health Informatics*, 17(5):915–921, sep 2013.

[75] Ryan J. Smith, Francesco Tenore, David Huberdeau, Ralph Etienne-Cummings, and Nitish V. Thakor. Continuous decoding of finger position from surface EMG signals for the control of powered prostheses. In *2008 30th Annual International Conference of the IEEE Engineering in Medicine and Biology Society*, pages 197–200. IEEE, aug 2008.

[76] Nicholas A. Sachs, Elaine A. Corbett, Lee E. Miller, and Eric J. Perreault. Continuous movement decoding using a target-dependent model with EMG inputs. *Proceedings of the Annual International Conference of the IEEE Engineering in Medicine and Biology Society, EMBS*, pages 5432–5435, 2011.

[77] Panagiotis Artemiadis, Kostas Kyriakopoulos, Panagiotis K Artemiadis, and Kostas J Kyriakopoulos. A Switching Regime Model for the EMG-Based Control of a Robot Arm Special Issue on Muscle Synergies View project DIAGNOR: fault DIAGnosis and accommodation of wheeled mObile Robots View project A Switching Regime Model for the EMG-Based Control of a Robot. 2011.

[78] Panagiotis K Artemiadis and Kostas J Kyriakopoulos. A bio-inspired filtering framework for the EMG-based control of robots The MIT Faculty has made this article openly available . Please share Citation Accessed Citable Link Detailed Terms A Bio-inspired Filtering Framework for the EMG-based Control of Robo. 2014.

[79] Jinsook Roh, William Z. Rymer, Eric J. Perreault, Seng Bum Yoo, and Randall F. Beer. Alterations in upper limb muscle synergy structure in chronic stroke survivors. *Journal of Neurophysiology*, 109(3), 2013.

[80] O. Urra, A. Casals, and R. Jane. Synergy analysis as a tool to design and assess an effective stroke rehabilitation. In *2014 36th Annual International Conference of the IEEE Engineering in Medicine and Biology Society*, pages 3550–3553. IEEE, aug 2014.

[81] Stephen H. Scott. Optimal feedback control and the neural basis of volitional motor control. *Nature Reviews Neuroscience*, 5(7):532–545, jul 2004.

[82] Emanuel Todorov and Michael I. Jordan. Optimal feedback control as a theory of motor coordination. *Nature Neuroscience*, 5(11):1226–1235, nov 2002.

[83] E. López-Larraz, A. Sarasola-Sanz, N. Irastorza-Landa, N. Birbaumer, and A. Ramos-Murguialday. Brain-machine interfaces for rehabilitation in stroke: A review. *NeuroRehabilitation*, 43(1):77–97, jul 2018.

[84] Apostolos P. Georgopoulos, Andrew B. Schwartz, and Ronald E. Kettner. Neuronal population coding of movement direction. *Science*, 1986.

[85] Martin Spüler, Armin Walter, Ander Ramos-Murguialday, Georgios Naros, M Spüler, A Walter, A Ramos-Murguialday, G Naros, N Birbaumer, A Gharabaghi, W Rosenstiel, and M Bogdan. Decoding of motor intentions from epidural ECoG recordings in severely paralyzed chronic stroke patients Acoustocerebrography View project Improving the Instructional Efficiency of Motor-Imagery driven Restorative Brain-Computer-Interfaces View project De. *Article in Journal of Neural Engineering*, 2014.

[86] Stephan Waldert, Hubert Preissl, Evariste Demandt, Christoph Braun, Niels Birbaumer, Ad Aertsen, and Carsten Mehring. Behavioral/Systems/Cognitive Hand Movement Direction Decoded from MEG and EEG. 2008.

[87] Xinyi Yong and Carlo Menon. EEG Classification of Different Imaginary Movements within the Same Limb. *PLOS ONE*, 10(4):e0121896, apr 2015.

[88] Ke Liao, Ran Xiao, Jania Gonzalez, and Lei Ding. Decoding Individual Finger Movements from One Hand Using Human EEG Signals. *PLoS ONE*, 9(1):e85192, jan 2014.

[89] J. Sanes, J. Donoghue, V Thangaraj, R. Edelman, and S Warach. Shared neural substrates controlling hand movements in human motor cortex. *Science*, 268(5218):1775–1777, jun 1995.

[90] Philip Parker, Bernard Hudgins, P Parker, K Englehart, and B Hudgins. Myoelectric signal processing for control of powered prostheses Invasive myoelectric control View project Confidence-Based Rejection Threshold and User Error View project Myoelectric signal processing for control of powered limb prostheses. *Article in Journal of Electromyography and Kinesiology*, 2007.

[91] Yuxuan Zhou. A frequency and pulse-width co-modulation strategy for transcutaneous neuromuscular electrical stimulation based on sEMG time-domain features. 2016.

[92] Eduardo López-Larraz, Andreas M Ray, Thiago C Figueiredo, Carlos Bibián, Niels Birbaumer, and Ander Ramos-Murguialday. *Stroke lesion location influences the decoding of movement intention from EEG*. 2017.

[93] Wanjoo Park, Gyu Hyun Kwon, Yun-Hee Kim, Jong-Hwan Lee, and Laehyun Kim. EEG response varies with lesion location in patients with chronic stroke. *Journal of NeuroEngineering and Rehabilitation 2016 13:1*, 13(1):21, mar 2016.

[94] Magdalena Stępień, Jan Conradi, Gunnar Waterstraat, Friederike U. Hohlefeld, Gabriel Curio, and Vadim V. Nikulin. Event-related desynchronization of sensorimotor EEG rhythms in hemiparetic patients with acute stroke. *Neuroscience Letters*, 488(1):17–21, jan 2011.

[95] Claudia Sannelli, Carmen Vidaurre, Klaus-Robert Müller, and Benjamin Blankertz. A large scale screening study with a SMR-based BCI: Categorization of BCI users and differences in their SMR activity. *PLOS ONE*, 14(1):e0207351, jan 2019.

[96] Ning Jiang, Johnny Lg Vest-Nielsen, Silvia Muceli, and Dario Farina. EMG-based simultaneous and proportional estimation of wrist/hand dynamics in uni-Lateral trans-radial amputees. *Journal of NeuroEngineering and Rehabilitation*, 9(1):42, 2012.

[97] Ander Ramos-Murguialday, Markus Sch??rholz, Vittorio Caggiano, Moritz Wildgruber, Andrea Caria, Eva Maria Hammer, Sebastian Halder, and Niels Birbaumer. Proprioceptive Feedback and Brain Computer Interface (BCI) Based Neuroprostheses. *PLoS ONE*, 7(10), 2012.

[98] John W. Krakauer, S. Thomas Carmichael, Dale Corbett, and George F. Wittenberg. Getting Neurorehabilitation Right. *Neurorehabilitation and Neural Repair*, 26(8):923–931, oct 2012.

[99] N N Johnson, J Carey, B J Edelman, A Doud, A Grande, K Lakshminarayan, and B He. Combined rTMS and virtual reality brain,Äìcomputer interface training for motor recovery after stroke. *Journal of Neural Engineering*, 15(1):016009, feb 2018.

[100] Martin Spüler, Wolfgang Rosenstiel, and Martin Bogdan. Adaptive SVM-based classification increases performance of a MEG-based Brain-Computer Interface (BCI). 2012.

[101] Arthur E. Hoerl and Robert W. Kennard. Ridge Regression: Biased Estimation for Nonorthogonal Problems. *Technometrics*, 12(1):55–67, feb 1970.

[102] R. E. Kalman. A New Approach to Linear Filtering and Prediction Problems. *Journal of Basic Engineering*, 82(1):35, mar 1960.

[103] H. Zabaleta, D. Valencia, J. Perry, J. Veneman, and T. Keller. Absolute position calculation for a desktop mobile rehabilitation robot based on three optical mouse sensors. In *2011 Annual International Conference of the IEEE Engineering in Medicine and Biology Society*, pages 2069–2072. IEEE, aug 2011.

[104] M. Zecca, Silvestro Micera, M. C. Carrozza, and P. Dario. Control of Multifunctional Prosthetic Hands by Processing the Electromyographic Signal. *Critical Reviews? in Biomedical Engineering*, 30(4-6):459–485, 2002.

[105] Heather Daley, Kevin Englehart, Levi Hargrove, and Usha Kuruganti. High density electromyography data of normally limbed and transradial amputee subjects for multifunction prosthetic control. *Journal of Electromyography and Kinesiology*, 22(3):478–484, 2012.

[106] Matthew C Tresch, Philippe Saltiel, Andrea D'Avella, and Emilio Bizzi. Coordination and localization in spinal motor systems. *Brain Research Reviews*, 40(1-3):66–79, oct 2002.

[107] Vincent C K Cheung, Andrea Turolla, Michela Agostini, Stefano Silvoni, Caoimhe Bennis, Patrick Kasi, Sabrina Paganoni, Paolo Bonato, and Emilio Bizzi. Muscle synergy patterns as physiological markers of motor cortical damage. *Proceedings of the National Academy of Sciences of the United States of America*, 109(36):14652–6, sep 2012.

[108] Gert Kwakkel, Robert C. Wagenaar, Tim W. Koelman, Gustaaf J. Lankhorst, and Johan C. Koetsier. Effects of Intensity of Rehabilitation After Stroke. *Stroke*, 28(8), 1997.

[109] R. Riener, T. Nef, and G. Colombo. Robot-aided neurorehabilitation of the upper extremities. *Medical & Biological Engineering & Computing*, 43(1):2–10, feb 2005.

[110] B. Corteville, E. Aertbelien, H. Bruyninckx, J. De Schutter, and H. Van Brussel. Human-inspired robot assistant for fast point-to-point movements. In *Proceedings 2007 IEEE International Conference on Robotics and Automation*, pages 3639–3644. IEEE, apr 2007.

[111] Etienne Burdet, Gowrishankar Ganesh, Chenguang Yang, and Alin Albu-Schäffer. Interaction Force, Impedance and Trajectory Adaptation: By Humans, for Robots. pages 331–345. Springer Berlin Heidelberg, 2014.

[112] Vijaykumar Rajasekaran, Eduardo López-Larraz, Fernando Trincado-Alonso, Joan Aranda, Luis Montesano, Antonio J. Del-Ama, and Jose L. Pons. Volition-adaptive control for gait training using wearable exoskeleton: preliminary tests with incomplete spinal cord injury individuals. *Journal of NeuroEngineering and Rehabilitation*, 15(1):4, dec 2018.

[113] M. DiCicco, L. Lucas, and Y. Matsuoka. Comparison of control strategies for an EMG controlled orthotic exoskeleton for the hand. In *IEEE International Conference on Robotics and Automation, 2004. Proceedings. ICRA '04. 2004*, pages 1622–1627 Vol.2. IEEE, 2004.

[114] Rong Song, Kai-yu Tong, Xiaoling Hu, and Wei Zhou. Myoelectrically controlled wrist robot for stroke rehabilitation. *Journal of NeuroEngineering and Rehabilitation*, 10(1):1, 2013.

[115] Ander' Chaudhary, Ujwal; Birbaumer, Niels; Ramos-Murguialday. Brain,Äìcomputer interfaces for communication and rehabilitation. *Nature Reviews Neurology*, 12:513–525, 2016.

[116] N. S. K. Ho, K. Y. Tong, X. L. Hu, K. L. Fung, X. J. Wei, W. Rong, and E. A. Susanto. An EMG-driven exoskeleton hand robotic training device on chronic stroke subjects: Task training system for stroke rehabilitation. In *2011 IEEE International Conference on Rehabilitation Robotics*, pages 1–5. IEEE, jun 2011.

[117] Rong Song, Kai-yu Tong, Xiaoling Hu, and Le Li. Assistive Control System Using Continuous Myoelectric Signal in Robot-Aided Arm Training for Patients After Stroke. *IEEE Transactions on Neural Systems and Rehabilitation Engineering*, 16(4):371–379, aug 2008.

[118] X.L. Hu, K.Y. Tong, R. Song, X.J. Zheng, K.H. Lui, W.W.F. Leung, S. Ng, and S.S.Y. Au-Yeung. Quantitative evaluation of motor functional recovery process in chronic stroke patients during robot-assisted wrist training. *Journal of Electromyography and Kinesiology*, 19(4):639–650, 2009.

[119] Michelle L. Woodbury, Craig A. Velozo, Lorie G. Richards, and Pamela W. Duncan. Rasch Analysis Staging Methodology to Classify Upper Extremity Movement Impairment After Stroke. *Archives of Physical Medicine and Rehabilitation*, 94(8):1527–1533, 2013.

[120] Ning Jiang, Ivan Vujaklija, Hubertus Rehbaum, Bernhard Graimann, and Dario Farina. Is accurate mapping of EMG signals on kinematics needed for precise online myoelectric control? *IEEE Transactions on Neural Systems and Rehabilitation Engineering*, 22(3):549–558, 2014.

[121] Neville Hogan, Hermano I Krebs, Brandon Rohrer, Jerome J Palazzolo, Laura Dipietro, Susan E Fasoli, Joel Stein, Richard Hughes, Walter R Frontera, Daniel Lynch, and Bruce T Volpe. Motions or muscles? Some behavioral factors underlying robotic assistance of motor recovery. *JRRD*, 43(5):605–618, 2006.

[122] Hermano Krebs, Bruce Volpe, and Neville Hogan. A working model of stroke recovery from rehabilitation robotics practitioners. *Journal of NeuroEngineering and Rehabilitation*, 6(1):6, 2009.

[123] Silvia Muceli, Ning Jiang, and Dario Farina. Extracting Signals Robust to Electrode Number and Shift for Online Simultaneous and Proportional Myoelectric Control by Factorization Algorithms. *IEEE Transactions on Neural Systems and Rehabilitation Engineering*, 22(3):623–633, may 2014.

[124] Mark Ison, Ivan Vujaklija, Bryan Whitsell, Dario Farina, and Panagiotis Artemiadis. High-Density Electromyography and Motor Skill Learning for Robust Long-Term Control of a 7-DoF Robot Arm. *IEEE Transactions on Neural Systems and Rehabilitation Engineering*, 24(4):424–433, apr 2016.

[125] R Jacobs and J M Macpherson. Two functional muscle groupings during postural equilibrium tasks in standing cats. *Journal of neurophysiology*, 76(4):2402–11, oct 1996.

[126] MC Tresch, P Saltiel, E Bizzi Nature Neuroscience, and undefined 1999. The construction of movement by the spinal cord. *nature.com*.

[127] E. Bizzi, A. D'Avella, P. Saltiel, and M. Tresch. Book Review: Modular Organization of Spinal Motor Systems. *The Neuroscientist*, 8(5):437–442, oct 2002.

[128] Andrea D'Avella, Philippe Saltiel, and Emilio Bizzi. Combinations of muscle synergies in the construction of a natural motor behavior. *Nature neuroscience*, 6(3):300–308, 2003.

[129] Simon Giszter, Vidyangi Patil, and Corey Hart. Primitives, premotor drives, and pattern generation: a combined computational and neuroethological perspective. *Progress in Brain Research*, 165:323–346, jan 2007.

[130] Jo Anne Ting, Aaron D'Souza, Kenji Yamamoto, Toshinori Yoshioka, Donna Hoffman, Shinji Kakei, Lauren Sergio, John Kalaska, Mitsuo Kawato, Peter Strick, and Stefan Schaal. Variational Bayesian least squares: An application to brain-machine interface data. *Neural Networks*, 21(8):1112–1131, 2008.

[131] Andrea D'Avella and Dinesh K. Pai. Modularity for Sensorimotor Control: Evidence and a New Prediction. *Journal of Motor Behavior*, 42(6):361–369, oct 2010.

[132] Francesco Lacquaniti, Yuri P. Ivanenko, and Myrka Zago. Patterned control of human locomotion. *The Journal of Physiology*, 590(10):2189–2199, may 2012.

[133] Emilio Bizzi and Vincent C. K. Cheung. The neural origin of muscle synergies. *Frontiers in Computational Neuroscience*, 7:51, apr 2013.

[134] Andrea D'Avella and Francesco Lacquaniti. Control of reaching movements by muscle synergy combinations. *Frontiers in Computational Neuroscience*, 7:42, apr 2013.

[135] Lior Shmuelof and John†W. Krakauer. Are We Ready for a Natural History of Motor Learning? *Neuron*, 72(3):469–476, nov 2011.

[136] H. Aizawa, M. Inase, H. Mushiake, K. Shima, and J. Tanji. Reorganization of activity in the supplementary motor area associated with motor learning and functional recovery. *Experimental Brain Research*, 84(3):668–671, apr 1991.

[137] Hermano I. Krebs, Thomas Brashers-Krug, Scott L. Rauch, Cary R. Savage, Neville Hogan, Robert H. Rubin, Alan J. Fischman, and Nathaniel M. Alpert. Robot-aided functional imaging: Application to a motor learning study. *Human Brain Mapping*, 6(1):59–72, jan 1998.

[138] I Toni, M Krams, R Turner, RE Passingham Neuroimage, and undefined 1998. The time course of changes during motor sequence learning: a whole-brain fMRI study. *Elsevier*.

[139] C. Weiller and Michel Rijntjes. Learning, plasticity, and recovery in the central nervous system. *Experimental Brain Research*, 128(1-2):134–138, sep 1999.

[140] Jonas A Hosp and Andreas R Luft. Cortical plasticity during motor learning and recovery after ischemic stroke. *Neural plasticity*, 2011:871296, oct 2011.

[141] Reza. Shadmehr and Steven P. Wise. *The computational neurobiology of reaching and pointing : a foundation for motor learning*. MIT Press, 2005.

[142] John W Krakauer and Pietro Mazzoni. Human sensorimotor learning: adaptation, skill, and beyond. *Current Opinion in Neurobiology*, 21(4):636–644, aug 2011.

[143] Daniel M. Wolpert, Jörn Diedrichsen, and J. Randall Flanagan. Principles of sensorimotor learning. *Nature Reviews Neuroscience*, 12(12):739–751, dec 2011.

[144] Tomoko Kitago and John W Krakauer. Motor learning principles for neurorehabilitation. 110, 2013.

[145] Lamberto Piron, Andrea Turolla, Michela Agostini, Carla Silvana Zucconi, Laura Ventura, Paolo Tonin, and Mauro Dam. Motor Learning Principles for Rehabilitation: A Pilot Randomized Controlled Study in Poststroke Patients. *Neurorehabilitation and Neural Repair*, 24(6):501–508, jul 2010.

[146] Kamal Narayan Arya, Shanta Pandian, Rajesh Verma, and R.K. Garg. Movement therapy induced neural reorganization and motor recovery in stroke: A review. *Journal of Bodywork and Movement Therapies*, 15(4):528–537, oct 2011.

[147] L. Dipietro, H. I. Krebs, B. T. Volpe, J. Stein, C. Bever, S. T. Mernoff, S. E. Fasoli, and N. Hogan. Learning, Not Adaptation, Characterizes Stroke Motor Recovery: Evidence From Kinematic Changes Induced by Robot-Assisted Therapy in Trained and Untrained Task in the Same Workspace. *IEEE Transactions on Neural Systems and Rehabilitation Engineering*, 20(1):48–57, jan 2012.

[148] John W Krakauer. The applicability of motor learning to neurorehabilitation. Technical report, 2015.

[149] David J. Reinkensmeyer, Etienne Burdet, Maura Casadio, John W. Krakauer, Gert Kwakkel, Catherine E. Lang, Stephan P. Swinnen, Nick S. Ward, and Nicolas Schweighofer. Computational neurorehabilitation: modeling plasticity and learning to predict recovery. *Journal of NeuroEngineering and Rehabilitation*, 13(1):42, dec 2016.

[150] David J. Reinkensmeyer, Jeremy L. Emken, and Steven C. Cramer. Robotics, Motor Learning, and Neurologic Recovery. *Annual Review of Biomedical Engineering*, 6(1):497–525, aug 2004.

[151] Laura Marchal-Crespo and David J Reinkensmeyer. Review of control strategies for robotic movement training after neurologic injury. *Journal of neuroengineering and rehabilitation*, 6(1):20, 2009.

[152] Erik Scheme and Kevin Englehart. Electromyogram pattern recognition for control of powered upper-limb prostheses: State of the art and challenges for clinical use. *The Journal of Rehabilitation Research and Development*, 48(6):643, jun 2011.

[153] Ann M Simon, Levi J Hargrove, Blair A Lock, Todd A Kuiken, and Ann Simon. The Target Achievement Control Test: Evaluating real-time myoelectric pattern recognition control of a multifunctional upper-limb prosthesis. *J Rehabil Res Dev. J Rehabil Res Dev*, 48(6):619–627, 2011.

[154] Matthew R Williams and Robert F Kirsch. Evaluation of head orientation and neck muscle EMG signals as command inputs to a human-computer interface for individuals with high tetraplegia. *IEEE transactions on neural systems and rehabilitation engineering : a publication of the IEEE Engineering in Medicine and Biology Society*, 16(5):485–96, oct 2008.

[155] Mark Ison, Chris Wilson Antuvan, and Panagiotis Artemiadis. Learning efficient control of robots using myoelectric interfaces. In *2014 IEEE International Conference on Robotics and Automation (ICRA)*, pages 2880–2885. IEEE, may 2014.

[156] T. Itou, M. Terao, J. Nagata, and M. Yoshida. Mouse cursor control system using EMG. In *2001 Conference Proceedings of the 23rd Annual International Conference of the IEEE Engineering in Medicine and Biology Society*, pages 1368–1369. IEEE.

[157] Saritha M. Radhakrishnan, Stuart N. Baker, and Andrew Jackson. Learning a Novel Myoelectric-Controlled Interface Task. *Journal of Neurophysiology*, 100(4):2397–2408, oct 2008.

[158] Tobias Pistohl, Christian Cipriani, Andrew Jackson, and Kianoush Nazarpour. Abstract and proportional myoelectric control for multi-fingered hand prostheses. *Annals of Biomedical Engineering*, 41(12), 2013.

[159] Mark Ison, Ivan Vujaklija, Bryan Whitsell, Dario Farina, and Panagiotis Artemiadis. High-Density Electromyography and Motor Skill Learning for Robust Long-Term Control of a 7-DoF Robot Arm. *IEEE transactions on neural systems and rehabilitation engineering : a publication of the IEEE Engineering in Medicine and Biology Society*, 4320(c):1–10, 2015.

[160] Aymar de Rugy, Gerald E. Loeb, and Timothy J. Carroll. Are muscle synergies useful for neural control? *Frontiers in Computational Neuroscience*, 7:19, mar 2013.

[161] Massimo Sartori, Guillaume Durandau, Strahinja Došen, and Dario Farina. Robust simultaneous myoelectric control of multiple degrees of freedom in wrist-hand prostheses by real-time neuromusculoskeletal modeling. *Journal of Neural Engineering*, 15(6):066026, dec 2018.

[162] Sebastian Amsuess, Ivan Vujaklija, Peter Goebel, Aidan D. Roche, Bernhard Graimann, Oskar C. Aszmann, and Dario Farina. Context-Dependent Upper Limb Prosthesis Control for Natural and Robust Use. *IEEE Transactions on Neural Systems and Rehabilitation Engineering*, 24(7):744–753, jul 2016.

[163] Z Tang, K Zhang, S Sun, Z Gao, L Zhang, Z Yang Sensors, and undefined 2014. An upper-limb power-assist exoskeleton using proportional myoelectric control. *mdpi.com*.

[164] Zhiyuan Lu, Xiang Chen, Xu Zhang, Kay-Yu Tong, and Ping Zhou. Real-Time Control of an Exoskeleton Hand Robot with Myoelectric Pattern Recognition. *International Journal of Neural Systems*, 27(05):1750009, aug 2017.

[165] Mark Ison, Panagiotis Artemiadis. The role of muscle synergies in myoelectric control: trends and challenges for simultaneous multifunction control. *Journal of Neural Engineering*, 11(5):051001, oct 2014.

[166] Chris Wilson Antuvan, Mark Ison, and Panagiotis Artemiadis. Embedded Human Control of Robots Using Myoelectric Interfaces. *IEEE Transactions on Neural Systems and Rehabilitation Engineering*, 22(4):820–827, jul 2014.

[167] Sivakumar Balasubramanian, Alejandro Melendez-Calderon, Agnes Roby-Brami, and Etienne Burdet. On the analysis of movement smoothness. *Journal of neuroengineering and rehabilitation*, 12:112, dec 2015.

[168] Amy J Bastian. Understanding sensorimotor adaptation and learning for rehabilitation. *Current opinion in neurology*, 21(6):628–33, dec 2008.

[169] J.L. Emken and D.J. Reinkensmeyer. Robot-Enhanced Motor Learning: Accelerating Internal Model Formation During Locomotion by Transient Dynamic Amplification. *IEEE Transactions on Neural Systems and Rehabilitation Engineering*, 13(1):33–39, mar 2005.

[170] Jeremy L Emken, Raul Benitez, and David J Reinkensmeyer. Human-robot cooperative movement training: Learning a novel sensory motor transformation during walking with robotic assistance-as-needed. *Journal of NeuroEngineering and Rehabilitation*, 4(1):8, mar 2007.

[171] James L. Patton, Mary Ellen Stoykov, Mark Kovic, and Ferdinando A. Mussa-Ivaldi. Evaluation of robotic training forces that either enhance or reduce error in chronic hemiparetic stroke survivors. *Experimental Brain Research*, 168(3):368–383, jan 2006.

[172] Roland Sigrist, Georg Rauter, Laura Marchal-Crespo, Robert Riener, and Peter Wolf. Sonification and haptic feedback in addition to visual feedback enhances complex motor task learning. *Experimental Brain Research*, 233(3):909–925, mar 2015.

[173] Laura Marchal-Crespo, Peter Wolf, Nicolas Gerig, Georg Rauter, Lukas Jaeger, Heike Vallery, and Robert Riener. The role of skill level and motor task characteristics on the effectiveness of robotic training: first results. In *2015 IEEE International Conference on Rehabilitation Robotics (ICORR)*, pages 151–156. IEEE, aug 2015.

[174] Laura Marchal-Crespo, Lars Michels, Lukas Jaeger, Jorge López-Olóriz, and Robert Riener. Effect of Error Augmentation on Brain Activation and Motor Learning of a Complex Locomotor Task. *Frontiers in Neuroscience*, 11:526, sep 2017.

[175] Sivakumar Balasubramanian, Eliana Garcia-Cossio, Niels Birbaumer, Etienne Burdet, and Ander Ramos-Murguialday. Is EMG a Viable Alternative to BCI for Detecting Movement Intention in Severe Stroke? *IEEE Transactions on Biomedical Engineering*, 65(12):2790–2797, dec 2018.

[176] Niels Birbaumer, Ander Ramos Murguialday, and Leonardo Cohen. Brain-computer interface in paralysis. *Current opinion in neurology*, 21(6):634–8, 2008.

[177] Ethan Buch, Cornelia Weber, Leonardo G. Cohen, Christoph Braun, Michael A. Dimyan, Tyler Ard, Jurgen Mellinger, Andrea Caria, Surjo Soekadar, Alissa Fourkas, and Niels Birbaumer. Think to move: A neuromagnetic brain-computer interface (BCI) system for chronic stroke. *Stroke*, 39(3):910–917, 2008.

[178] Jonathan R Wolpaw, Niels Birbaumer, Dennis J Mcfarland, Gert Pfurtscheller, and Theresa M Vaughan. Brain-computer interfaces for communication and control. Technical report, 2002.

[179] Kai Keng Ang, Cuntai Guan, Kok Soon Phua, Chuanchu Wang, Longjiang Zhou, Ka Yin Tang, Gopal J Ephraim Joseph, Christopher Wee Keong Kuah, and Karen Sui Geok Chua. Brain-computer interface-based robotic end effector system for wrist and hand rehabilitation: results of a three-armed randomized controlled trial for chronic stroke. *Frontiers in neuroengineering*, 7(July):30, 2014.

[180] Duncan L. Turner, Ander Ramos-Murguialday, Niels Birbaumer, Ulrich Hoffmann, and Andreas Luft. Neurophysiology of robot-mediated training and therapy: A perspective for future use in clinical populations. *Frontiers in Neurology*, 4 NOV(November):1–11, 2013.

[181] Karim G Oweiss and Islam S Badreldin. Neuroplasticity subserving the operation of brain-machine interfaces. *Neurobiology of disease*, 83:161–71, nov 2015.

[182] Jonathan R Wolpaw and Dennis J Mcfarland. Control of a two-dimensional movement signal by a noninvasive brain-computer interface in humans. Technical report, 2004.

[183] Dennis J McFarland, William A Sarnacki, and Jonathan R Wolpaw. Electroencephalographic (EEG) control of three-dimensional movement. *Journal of neural engineering*, 7(3):036007, jun 2010.

[184] Iñaki Iturrate, Ricardo Chavarriaga, Luis Montesano, Javier Minguez, and José del R. Millán. Teaching brain-machine interfaces as an alternative paradigm to neuroprosthetics control. *Scientific Reports*, 5(1):13893, nov 2015.

[185] R Ortner, B Z Allison, G Korisek, H Gaggl, and G Pfurtscheller. An SSVEP BCI to Control a Hand Orthosis for Persons With Tetraplegia. *IEEE Transactions on Neural Systems and Rehabilitation Engineering*, 19(1):1–5, feb 2011.

[186] Lynn M McCane, Susan M Heckman, Dennis J McFarland, George Townsend, Joseph N Mak, Eric W Sellers, Debra Zeitlin, Laura M Tenteromano, Jonathan R Wolpaw, and Theresa M Vaughan. P300-based brain-computer interface (BCI) event-related potentials (ERPs): People with amyotrophic lateral sclerosis (ALS) vs. age-matched controls. *Clinical neurophysiology : official journal of the International Federation of Clinical Neurophysiology*, 126(11):2124–31, nov 2015.

[187] Eric W Sellers and Emanuel Donchin. A P300-based brain-computer interface: Initial tests by ALS patients. *Clinical Neurophysiology*, 117:538–548, 2006.

[188] Carlos Escolano, Ander Ramos Murguialday, Tamara Matuz, Niels Birbaumer, and Javier Minguez. A telepresence robotic system operated with a

P300-based brain-computer interface: Initial Tests with ALS patients. *2010 Annual International Conference of the IEEE Engineering in Medicine and Biology Society, EMBC'10*, (Figure 1):4476–4480, 2010.

[189] Trent J Bradberry, Rodolphe J Gentili, and José L Contreras-Vidal. Reconstructing Three-Dimensional Hand Movements from Noninvasive Electroencephalographic Signals. 2010.

[190] Javier M. Antelis, Luis Montesano, Ander Ramos-Murguialday, Niels Birbaumer, and Javier Minguez. On the Usage of Linear Regression Models to Reconstruct Limb Kinematics from Low Frequency EEG Signals. *PLoS ONE*, 8(4), 2013.

[191] Jose M Carmena, Mikhail A Lebedev, Roy E Crist, Joseph E O'Doherty, David M Santucci, Dragan F Dimitrov, Parag G Patil, Craig S Henriquez, and Miguel A. L Nicolelis. Learning to Control a Brain,ÄìMachine Interface for Reaching and Grasping by Primates. *PLoS Biology*, 1(2):e42, oct 2003.

[192] Andrew B. Schwartz, X. Tracy Cui, Douglas†J. Weber, and Daniel W. Moran. Brain-Controlled Interfaces: Movement Restoration with Neural Prosthetics. *Neuron*, 52(1):205–220, oct 2006.

[193] Leigh R Hochberg, Daniel Bacher, Beata Jarosiewicz, Nicolas Y Masse, John D Simeral, Joern Vogel, Sami Haddadin, Jie Liu, Sydney S Cash, Patrick van der Smagt, and John P Donoghue. Reach and grasp by people with tetraplegia using a neurally controlled robotic arm. *Nature*, 485(7398):372–5, may 2012.

[194] Chad Bouton, Ammar Shaikhouni, Marcie Bockbrader, and David Friedenberg. Restoring cortical control of functional movement in a human with quadriplegia. 2016.

[195] Tobias Pistohl, Tonio Ball, Andreas Schulze-Bonhage, Ad Aertsen, and Carsten Mehring. Prediction of arm movement trajectories from ECoG-recordings in humans. *Journal of Neuroscience Methods*, 167(1):105–114, jan 2008.

[196] Martin Spüler, Wolfgang Rosenstiel, and Martin Bogdan. Predicting Wrist Movement Trajectory from Ipsilesional ECoG in Chronic Stroke Patients.

[197] Keiichiro Shindo, Kimiko Kawashima, Junichi Ushiba, Naoki Ota, Mari Ito, Tetsuo Ota, Akio Kimura, and Meigen Liu. Effects of Neurofeedback Training with an Electroencephalogram-based Brain-Computer Interface for Hand Paralysis in Patients with Chronic Stroke: A Preliminary Case Series Study.. *J Rehabil Med*, 43:951–957, 2011.

[198] Eduardo López-Larraz, Luis Montesano, Ángel Gil-Agudo, and Javier Minguez. Continuous decoding of movement intention of upper limb self-initiated analytic movements from pre-movement EEG correlates. *Journal of NeuroEngineering and Rehabilitation*, 11(1):153, nov 2014.

[199] Eduardo López-Larraz, Fernando Trincado-Alonso, Vijaykumar Rajasekaran, Soraya Pérez-Nombela, Antonio J. Del-Ama, Joan Aranda, Javier Minguez, Angel Gil-Agudo, and Luis Montesano. Control of an Ambulatory Exoskeleton with a Brain,ÄìMachine Interface for Spinal Cord Injury Gait Rehabilitation. *Frontiers in Neuroscience*, 10:359, aug 2016.

[200] Farid Shiman, Nerea Irastorza-Landa, Andrea Sarasola-Sanz, Martin Spuler, Niels Birbaumer, and Ander Ramos-Murguialday. Towards decoding of functional movements from the same limb using EEG. In *Proceedings of the Annual International Conference of the IEEE Engineering in Medicine and Biology Society, EMBS*, volume 2015-Novem, pages 1922–1925. Institute of Electrical and Electronics Engineers Inc., 2015.

[201] Aleksandra Vuckovic and Francisco Sepulveda. Delta band contribution in cue based single trial classification of real and imaginary wrist movements. *Medical & Biological Engineering & Computing*, 46(6):529–539, jun 2008.

[202] Jaime Ibáñez, J. I. Serrano, M. D. del Castillo, J. Minguez, and J. L. Pons. Predictive classification of self-paced upper-limb analytical movements with EEG. *Medical & Biological Engineering & Computing*, 53(11):1201–1210, nov 2015.

[203] M C Cirstea and M F Levin. Compensatory strategies for reaching in stroke. *Brain : a journal of neurology*, 123 (Pt 5:940–53, may 2000.

[204] Gerwin Schalk, Dennis J Mcfarland, Thilo Hinterberger, Niels Birbaumer, Jonathan R Wolpaw, D J Mcfarland, N Birbaumer, and J R Wolpaw. BCI2000: A General-Purpose Brain-Computer Interface (BCI) System. *IEEE TRANSACTIONS ON BIOMEDICAL ENGINEERING*, 51(6), 2004.

[205] Arie Yeredor. Blind Separation of Gaussian Sources via Second-Order Statistics with Asymptotically Optimal Weighting. Technical Report 7, 2000.

[206] Germán Gómez-Herrero. Automatic Artifact Removal (AAR) toolbox v1.3 (Release 09.12.2007) for MATLAB. Technical report, 2007.

[207] Arnaud Delorme, Tim Mullen, Christian Kothe, Zeynep Akalin Acar, Nima Bigdely-Shamlo, Andrey Vankov, and Scott Makeig. EEGLAB, SIFT, NFT, BCILAB, and ERICA: New Tools for Advanced EEG Processing. *Computational Intelligence and Neuroscience*, 2011:1–12, 2011.

[208] Kai Keng Ang, Zheng Yang Chin, Haihong Zhang, and Cuntai Guan. Filter Bank Common Spatial Pattern (FBCSP). pages 2390–2397, 2008.

[209] H. Ramoser, J. Muller-Gerking, and G. Pfurtscheller. Optimal spatial filtering of single trial EEG during imagined hand movement. *IEEE Transactions on Rehabilitation Engineering*, 8(4):441–446, dec 2000.

[210] Christopher M. Bishop. *Pattern Recognition and Machine Learning*, volume 60. 1965.

[211] Etienne Combrisson and Karim Jerbi. Exceeding chance level by chance: The caveat of theoretical chance levels in brain signal classification and statistical assessment of decoding accuracy. *Journal of Neuroscience Methods*, 250:126–136, 2015.

[212] Sebastian Maier and Patrick Van Der Smagt. Surface EMG suffices to classify the motion of each finger independently.

[213] Toshihiro Kawase, Takeshi Sakurada, Yasuharu Koike, and Kenji Kansaku. A hybrid BMI-based exoskeleton for paresis: EMG control for assisting arm movements. *Journal of Neural Engineering*, 14(1):016015, feb 2017.